

THESIS FOR THE DEGREE OF DOCTOR OF PHILOSOPHY

**Effects of Corona and Ozone Exposure on
Properties of Polymeric Materials for High
Voltage Outdoor Applications**

BIN MA



High Voltage Engineering
Department of Materials and Manufacturing Technology
CHALMERS UNIVERSITY OF TECHNOLOGY
Göteborg, Sweden 2011

Effects of Corona and Ozone Exposure on Properties of Polymeric Materials for
High Voltage Outdoor Applications

BIN MA

ISBN 978-91-7385-565-5

©BIN MA, 2011.

Doktorsavhandlingar vid Chalmers tekniska högskola

Ny serie nr. 3246

ISSN 0346-718X

High Voltage Engineering

Department of Materials and Manufacturing Technology

Chalmers University of Technology

SE-412 96 Göteborg

Sweden

Telephone +46 (0)31 772 1000

Chalmers Bibliotek, Reproservice

Göteborg, Sweden 2011

谨献给 光阴的故事——

无悔的青春

Effects of Corona and Ozone Exposure on Properties of Polymeric Materials for High Voltage Outdoor Applications

Bin Ma

Division of High Voltage Engineering

Department of Materials and Manufacturing Technology

Chalmers University of Technology

Abstract

Despite the past four decades of service experiences with polymeric insulators in power systems all over the world, an adequate standard allowing for proper selection of polymeric materials for applications in high voltage outdoor environments has still been lacking. Therefore CIGRE Working Group D1.14 concentrated during recent years numerous activities aiming at defining all the physical parameters important for the use of polymeric materials in outdoor insulation and on checking if relevant test methods for their evaluation are available. Among the twelve parameters identified, the resistance to corona/ozone belongs to the group of remaining four parameters which still need to be standardized.

In this context, the investigations reported in this thesis concentrated on elaborating adequate test methodology for evaluating the resistance of housing materials to AC corona/ozone treatments. The work contributed this way to an international effort to check the effectiveness of the proposed methodology by participating in a CIGRE round robin test (RRT) activities. The test procedure has been based on a use of multi-needle corona source for treatment of polymeric material samples in a dry and ventilated discharge chamber. The treatment conditions were thoroughly investigated and set; the elaborated procedure was thereafter checked by performing treatments and measuring resulting changes of electrical and mechanical properties on five different types of housing material samples delivered by collaborating industrial partners. Results obtained from the study showed that the mostly affected parameter, on nearly all the materials investigated, was surface resistivity. At the same time, the effects of the treatment on volume resistivity, dielectric permittivity and dissipation factor, all being the properties of the materials bulk, remained rather weak. Apart from that, the changes in mechanical properties, including breakdown strength and elongation at break, were also noticeable. These could mainly be attributed to surface oxidation, as revealed by scanning electron microscopy (SEM) as well as Fourier transform infrared spectroscopy (FTIR) analyses. Surface cracking that appeared

Abstract

during the treatment on some of the materials as well as the accompanying it reduction of mechanical strength allow believing that the presence of corona and ozone in the vicinity of polymeric insulators may especially influence their mechanical integrity when continuously remaining under tension.

In the second group of investigations the elaborated in this thesis test methodology was applied for determining differences and similarities in the effects of AC and DC corona/ozone treatments on housing polymeric materials. The tests were in this case performed on two types of commercially available high temperature vulcanized (HTV) silicone rubber materials. Less pronounced effects of the treatment were found during DC corona/ozone exposure. This is a result of DC corona intensity reduction, attributed to electrostatic charging of the polymeric surfaces and subsequent reduction of electric field strength in the discharge regions. Among the investigated dielectric properties, surface resistivity still remained the mostly affected parameter. At the same time, the polymer matrix in the bulk remained practically untouched. The results of tensile tests did not exhibit clear regularities and the observed reduction of the mechanical performance was weak. Furthermore, the intensity of surface oxidation, as revealed by FTIR and X-ray photoelectron spectroscopy (XPS) analyses, could in turn be correlated with the measured during the treatments ozone concentrations. The AC corona exposure, with higher discharge intensity than under the DC treatment, produced higher doses of ozone and yielded a more severe surface oxidation. Hydrophilic groups (e.g. OH), formed on the oxidized surfaces of the HTV silicone rubber samples, determine therefore the loss of hydrophobic property and the rate of its recovery. One may conclude that the less pronounced degradation of silicone rubber materials during DC corona/ozone exposure provides positive indication for successful service of polymeric insulators in HVDC installations.

The investigations presented in this thesis included also evaluation of the resistance to corona/ozone treatment of two batches of model nanocomposite materials, e.g. epoxy and silicone (PDMS) nanocomposites. The obtained results were, in general, similar to those found on the commercial materials. It was clearly observed that the introduction of the nano-filler had retarded deeper degradation on the surface of the nanocomposites.

Keywords: Outdoor insulation, composite insulation, silicone rubber, corona treatment, ozone treatment, nanocomposite, surface resistivity, volume resistivity, dielectric response, mechanical strength, hydrophobicity, ageing.

Acknowledgement

First and foremost, I would like to express my deepest gratitude to my supervisor and examiner Prof. Stanislaw M. Gubanski for his strict military-like training, patient guidance, continuous support, valuable discussions as well as encouragement throughout the Ph.D. program during the past four years. Also, I wish to sincerely thank my co-supervisor Dr. Henrik Hillborg of ABB Corporate Research, Västerås, for his guidance and assistance in sample preparations, usage of instrumentation and support in interpretation of chemical analysis data performed within this project.

The entire work has been carried out within the Elforsk's ELECTRA program, project number 36054, with financial support from ABB and Swedish Energy Agency, which is gratefully acknowledged. I am thankful for the input provided during the reference group meetings by Lars Palmqvist, Uno Gäfvert and Yuriy Serdyuk. Financial support from Schneider Electric's fund in memorial of Erik Feuk, providing possibilities for participation in scientific conferences is acknowledged as well. I also thank China Scholarship Council (CSC) for partially financing my stay in Sweden when performing the first part of this project.

Members of the CIGRE WG D1.14 are acknowledged for their contributions when discussing the main ideas behind the proposed test methodology. Manufacturers and users of housing materials (Huntsman, Dow Corning, Wacker, Tyco Electronics and Sediver) are also acknowledged for supplying material samples, for performing some of the mechanical property testing, as well as for agreeing to publish the results.

I also appreciate the work done by Dr. Christine Leuci of Bluestar Silicones, Saint Fons, France, who carried out the structural and chemical analysis related to the content of Chapter 4. Dr. Andrej Krivda and his co-workers of ABB Corporate Research, Dättwil, Switzerland are thanked for supplying and characterizing epoxy nanocomposite samples. As well, Prof. Josef Kindersberger of Laboratory for High Voltage Technology and Power Transmission of Technische Universität München, München, Germany, is appreciated for providing the nano-PDMS samples for the investigations reported in Chapter 5. Besides, my department colleagues Urban Paul Einar Jelvestam and Henrik Persson are acknowledged for their assistance with the

Acknowledgement

XPS experiments as well as the tensile tests described in this chapter. Ms. Sevil Atarijabarzadeh, a Ph.D. student at the School of Chemical Science and Engineering of the Royal Institute of Technology in Stockholm is acknowledged for assistance in preparing the HTV silicone rubber samples for the investigations presented in Chapter 5 also.

Many thanks go to the Department of Materials and Manufacturing Technology, especially all the colleagues, former and present, at the Division of High Voltage Engineering, for creating a very comfortable and friendly working environment. I hereby wish to particularly thank Dr. Johan Andersson, a former PhD student at the division, for his big brother-like concern, encouragement, enthusiasm, as well as inspiration and discussions at the early stage of this project. Dr. Jörgen Blennow is thanked for his valuable suggestions and comments when designing a surge protection device for an oscilloscope. Dr. Yuriy Serdyuk is appreciated for some short but inspiring discussions regarding corona discharge mechanisms.

Finally, I am grateful to my parents Ma En'ning, Hou Jinfang, and my wife Na Na. Without your permanent love, support, encouragement, and delicious foods every day, the work presented in this thesis would be a mission impossible.

Bin Ma

Göteborg, Sweden

2011

Table of contents

Abstract.....	v
Acknowledgement.....	vii
Table of contents.....	ix
1 Introduction	1
1.1 Thesis outline	4
1.2 List of publications	5
1.3 Author's contribution	6
2 Literature review.....	7
2.1 Polymeric HV outdoor insulation	7
2.1.1 Polymeric materials for HV outdoor environments	7
2.1.2 Polymeric micro- and nanocomposites	9
2.2 Corona and ozone	12
2.2.1 Corona discharges.....	12
2.2.2 Ozone production in corona discharges	17
2.3 Corona discharges and polymeric insulators.....	18
2.3.1 Field experiences	18
2.3.2 Laboratory investigations	20
3 Material testing and characterization techniques	25
3.1 Corona ageing test development.....	25
3.1.1 General assumption.....	25
3.1.2 Components	25
3.1.3 Evaluation of corona test arrangement	29

Table of contents

3.2	Material characterization techniques	40
3.2.1	Volume and surface resistivities/charging currents	40
3.2.2	Frequency domain dielectric response	41
3.2.3	Temperature dependency of dielectric response	43
3.2.4	Scanning electron microscopy	43
3.2.5	Infrared spectroscopy	44
3.2.6	X-ray photoelectron spectroscopy	45
3.2.7	Tensile tests	46
3.2.8	Dynamic contact angles	46
3.3	Concluding remarks	48
4	AC corona ageing tests	49
4.1	Testing procedure	49
4.1.1	Procedure for the samples involved in RRT	49
4.1.2	Procedure for the model nano-epoxy samples	50
4.2	CIGRE Round Robin Test	52
4.2.1	Material description	52
4.2.2	Ozone concentration	52
4.2.3	Dielectric properties	53
4.2.4	Mechanical properties	58
4.2.5	Physical and chemical characteristics	58
4.3	Tests upon epoxy micro- and nano-composites	64
4.3.1	Preparation and characterization of specimens	64
4.3.2	Dielectric properties	64
4.4	Concluding remarks	72
5	Material performance under AC and DC corona ageing tests	73
5.1	Specimens and testing procedure	73
5.2	AC and DC corona/ozone treatments	74
5.2.1	Corona discharge intensities	74
5.2.2	Ozone concentration	75

5.3	Effects upon HTV silicone rubber properties	77
5.3.1	Dielectric properties	77
5.3.2	Mechanical properties	82
5.3.3	FTIR studies	84
5.3.4	XPS studies	86
5.3.5	Hydrophobicity variations.....	92
5.4	Tests upon model nano-PDMS samples	92
5.4.1	Material description	92
5.4.2	Dielectric properties	93
5.5	Concluding remarks.....	97
6	Conclusions	99
6.1	Test methodology and conditions	99
6.2	Resistance to AC corona ageing	100
6.3	Performance changes induced by AC/DC coronas	100
6.4	Performance of nanocomposites under corona ageing	101
7	Future work.....	103
	Bibliography.....	105
	Appendix A: Abbreviations	119
	Appendix B: Charging currents for nano-PDMS samples.....	121

Table of contents

1 Introduction

Nowadays, the flourishing development of power systems all over the world, especially in developing countries like China, forces manufacturers of high voltage equipment for power generation, transmission and distribution to develop better and more reliable components, with a life time spanning over a few decades. High voltage insulators belong to this group. Insulators made of porcelain and glass have been used for a long time. Porcelain insulators were first introduced in telegraph lines around 1835 and later used in power transmission applications around 1880 [1]. Insulators evolved rapidly from up-scaled versions of the telegraph pin insulators to what we have been familiar with as traditional insulators – cap-pin insulators made of porcelain or glass and long-rod insulators made of porcelain. Glass and ceramic insulators had long been the only insulators on the market until the late 1950's and early 1960's, when the first modern non-ceramic insulator (NCI) was introduced. They are often also called polymeric insulators, with advantages over traditional counterparts of low weight, vandalism resistance, hydrophobic surface properties, etc., showing a steadily increasing share of the insulator market. Over four decades passed afterwards, by the end of last century, it was reported that 60-70 % of the installed insulators in the USA had been already of polymeric type [2]. It was estimated that in 1999, 0.6 million polymeric insulators had been installed in the Chinese national grid operating at voltage levels between 35-500 kV [3], while in 1990 this number was 3,000 only. Associated with the fast development of the Chinese networks, typically reflected by new constructions of ultra high voltage (UHV) transmission lines, application of polymeric insulators takes place at extraordinarily high pace. In 2009 Liang, et al. [4] reported that, by 2008, about 4.5 million silicone rubber (SIR) insulators had been serving in Chinese power systems, among which 7,200 were adopted for the UHV 1000 kV AC project as well as 35,000 were planned for the UHV 800 kV DC projects. From a worldwide perspective, already in 2005, the estimated share of silicone polymeric insulators was equal to about 25 %, whereas porcelain insulators accounted for 50 % and glass insulators for 25 % [5]. For comparison, in 1990 the share was estimated to only 2 % for SIR based polymeric insulators.

Chapter 1. Introduction

In the struggle on the way of polymeric insulators becoming broadly accepted on the market as an alternative solution to the traditional porcelain and glass counterparts, researchers and engineers tested numerous ideas and solutions. Many of these attempts were concentrated on elaborating design criteria and on selecting material solutions, which together would allow standing severe working electric stresses, thus securing their reliable long term performance. Properties required for ceramic materials to be useful within high voltage outdoor insulator applications have been specified since long (IEC 60672). The situation regarding requirements for polymeric materials has been entirely different. Despite the long experience, an adequate standard has not existed until now. However, serious manufacturers have used own selection criteria of best materials, which caused that for vast majority of composite insulators available on the market the required quality can be assured. Some utilities have also elaborated own specifications defining material properties to be proven by insulator suppliers. This situation has become even more complicated by the fact that manufacturers and users of insulators have sometimes different opinions regarding the significance of specific material properties and their limits. As a result CIGRE working group WG D1.14 concentrated during recent years on defining the physical parameters important for the use of polymeric materials in outdoor insulation and on checking if relevant test methods are available today. Twelve properties have been identified [6], in alphabetical order including:

- Arc resistance
- Breakdown field strength
- Glass transition temperature
- Hydrophobicity
- Resistance to chemical and physical degradation
- Resistance to chemical attack
- Resistance to corona and ozone
- Resistance to flammability
- Resistance to weathering and UV
- Resistance to tracking and erosion
- Tear strength
- Volume resistivity

whereas standardized test methods and minimum requirements have been available for eight of them (●). Since 2004, the work of WG D1.14 has therefore focused on

developing new test methods and on setting minimum requirements for the remaining four properties (○), among which the resistance to corona and ozone was listed as being of great importance. Making known the material interaction with diverse electric discharges is also one of the main challenges that polymeric insulator manufacturers, utilities and researchers have long been encountering for.

The context above is the major motivation attributed to which the project was formulated. In this thesis, firstly, the work performed at Chalmers University of Technology within the activities of CIGRE WG D1.14 frame on the development of methodology for testing the resistance to AC corona and its by-product ozone of polymeric materials for high voltage outdoor insulation applications was described. The main goal of this part consists of two sequential steps – first on designing the necessary equipment as well as the test conditions; and then, samples of five types of commercially available polymeric materials were AC-corona treated and the consequent changes of dielectric, mechanical as well as chemical and structural properties were evaluated. Secondly, the investigations as regards dielectric properties as well as AC corona/ozone resistance performance of the model epoxy compositions differing in the proportions of micro- and nano-fillers were carried out. To this point the thesis will have finished elaborating the efforts made during the first half of the whole Ph.D. program, viz. the Licentiate program. Thereafter, as a significant step, the focus proceeded to put on the ageing effects of DC corona treatments on the performance changes of polymeric materials. The testing arrangement was modified for this purpose as well as the test conditions for DC corona were proposed, which was further evaluated by the experimental comparisons with the AC corona case in terms of corona discharge intensity characterized by the power released from as well as the total corona currents of the multi-needle corona electrode suggested by CIGRE WG D1.14. As well, two types of commercially available high temperature vulcanized (HTV) silicone rubber samples characterized by different resistivities and tensile strength were adopted to conduct the laboratory investigations as concerns comparing the effects induced by AC and DC corona/ozone ageing. The studied material properties included volume and surface resistivities/charging currents, dielectric response (DR), tensile strength and elongation at break, chemical formulation and structural variations, as well as hydrophobicity dynamics. The corresponding characterization experiments carried out were DR measurements in time and frequency domains, tensile test, Fourier transform infrared spectroscopy (FTIR) and X-ray photoelectron spectroscopy (XPS) analysis, as well as dynamic contact angle measurements. In addition to the two types of HTV silicone rubber samples, a batch of model nano-polydimethylsiloxane (PDMS) samples were also involved in the corona/ozone resistance evaluation procedure. The resistivities/charging currents as well as DR measurements were conducted for the AC/DC corona/ozone treated samples and the results were compared.

1.1 Thesis outline

The thesis is organized as follows:

Chapter 2 – **Literature review** first provides a review on the types and application history of polymeric materials for high voltage outdoor environments. And then, with a short introduction to the principle and the applications as regards the phenomenon of corona and its by-product ozone, a literature review upon the earlier field experiences as well as laboratory investigations regarding the corona discharges in polymeric insulators/materials is provided.

Chapter 3 – **Material testing and characterization techniques** in detail describes the development of methodology for the artificial 100 h corona/ozone ageing test, as well as the evaluation of the proposed test arrangement. In addition, the information on the techniques used for material characterizations is provided.

Chapter 4 – **AC corona ageing tests** focuses on reporting the results obtained from the AC corona ageing tests by adopting the testing approach described in **Chapter 3**. This chapter starts with elaborating the procedure proposed for the CIGRE round robin test. Thereafter, separately the evaluation of the resistance to corona/ozone of the five selected commercial grades polymeric materials, as well as the epoxy compositions filled with micro- and nano-fillers of various proportions were described.

Chapter 5 – **Material performance under AC and DC corona ageing tests** presents the divergences between the AC and DC corona ageing tests as regards the corona discharge intensity itself as well as the resulting effects on the two types of HTV silicone rubber samples by the characterization methods introduced in **Chapter 3**. Furthermore, the evaluation extended to a batch of nano-PDMS samples concerning the effects on dielectric properties was also reported.

The **Conclusions** drawn from this work are summarized in Chapter 6, and Chapter 7 provides suggestions on how the **Future Work** of the project should continue.

1.2 List of publications

The content of the thesis is mainly built on the investigations which have been summarized in the following publications:

- Stanislaw M. Gubanski, **Bin Ma**, Johan Andersson, Christine Leuci, “Evaluating resistance of materials for outdoor insulator housings to corona and ozone”, in Proceedings of INMR World Insulator Congress & Exhibition, paper E-3, Crete, Greece, 2009.
- **Bin Ma**, Johan Andersson, Stanislaw M. Gubanski, “Experimental comparisons of susceptibilities to long-term action of ac corona and ozone of non-ceramic outdoor insulation materials”, in Proceedings of Nordic Insulation Symposium (NORD-IS), pp. 221-224, Gothenburg, Sweden, 2009.
- **Bin Ma**, Stanislaw M. Gubanski, Andrej Krivda, Lars E. Schmidt, Rebecca Hollertz, “Dielectric properties and resistance to corona and ozone of epoxy compositions filled with micro- and nano-fillers”, in Proceedings of Annual Report Conference on Electrical Insulation and Dielectric Phenomena (CEIDP), pp. 7B-4, Virginia Beach, USA, 2009.
- **Bin Ma**, “Evaluating resistance to corona and ozone in polymeric materials for high voltage outdoor applications”, Licentiate thesis, Department of Materials and Manufacturing Technology, Chalmers University of Technology, Gothenburg, Sweden, 2009.
- **Bin Ma**, Johan Andersson, and Stanislaw M. Gubanski, "Evaluating resistance of polymeric materials for outdoor applications to corona and ozone", IEEE Transactions on Dielectrics and Electrical Insulation, vol. 17, pp. 555-565, 2010.
- **Bin Ma**, Stanislaw M. Gubanski, Henrik Hillborg, “AC and DC corona/ozone-induced ageing of HTV silicone rubber”, accepted for publication by IEEE Transactions on Dielectrics and Electrical Insulation.
- **Bin Ma**, Stanislaw M. Gubanski, Henrik Hillborg, “AC or DC corona ageing of HTV silicone rubber”, in Proceedings of Nordic Insulation Symposium (NORD-IS), pp. 37-40, Tampere, Finland, 2011.
- **Bin Ma**, Jiafu Wang, Henrik Hillborg, Stanislaw M. Gubanski, “Performance of HTV silicone rubber under artificial AC and DC corona/ozone test”, in Proceedings of International Symposium on High Voltage Engineering (ISH), paper E-036, Hannover, Germany, 2011.

1.3 Author's contribution

The major part of the experimental as well as analytical work described in this thesis was carried out by the author **Bin Ma** at the Division of High Voltage Engineering of the Department of Materials and Manufacturing Technology of Chalmers University of Technology, Gothenburg, Sweden.

However, in order to maintain the integrity as regards describing the evolvement of the project, the preliminary efforts regarding the electric field simulation, measurement of ozone concentration, as well as the power released from the multi-needle electrode made by Dr. Johan Andersson, et al. [7] before the author taking over the project are combined in Chapter 3.

In addition, for broadening the possibility of result elucidation, the structural and chemical analysis presented in Chapter 4 were performed by Dr. Christine Leuci at Bluestar Silicones, Saint Fons, France; while the testing of mechanical properties in this chapter was conducted by the manufacturers of the materials investigated. Also in this chapter, the model epoxy compositions were prepared and mechanically characterized at ABB Corporate Research, Dättwil, Switzerland by Dr. Andrej Krivda and his co-workers. The thermal and process properties of the investigated formulations were studied there as well.

Moreover, the FTIR experiments on the investigated samples described in Chapter 5 were conducted at ABB Corporate Research, Västerås, Sweden by Dr. Henrik Hillborg. The analyses on the obtained results were performed by the thesis author with the assistance by Henrik Hillborg. And, the XPS experiments as well as the tensile tests reported in this chapter were carried out at the author's department with the assistance by Urban Paul Einar Jelvestam associated with Henrik Persson respectively; the thesis author treated and analyzed all the obtained results.

Last but not least, the entire work was supervised by Prof. Stanislaw M. Gubanski.

2 Literature review

2.1 Polymeric HV outdoor insulation

2.1.1 Polymeric materials for HV outdoor environments

A typical modern polymeric suspension insulator consists of a fiberglass reinforced plastic (FRP) bonded rod onto which two metal end-fittings are attached. This is a mechanically supporting structure and its modulus to weight ratio is extremely high [8]. To protect the core from being subjected to environmental stresses, where moisture and pollution in conjunction with high electric field strengths exist, it is covered with a polymeric cover called housing. In addition to the protection from moisture and pollution, the housing material should also provide the extra creepage distance needed for securing the desired pollution performance, which can either be achieved through varying the shed diameters as well as their number. Most commonly used polymeric materials for the housings in outdoor environments are nowadays silicone rubber (SIR), ethylene-propylene-diene monomer (EPDM) based rubber, ethylene vinyl acetate (EVA) elastomeric materials and epoxies (EP). End-fittings are made of metal and the most common materials are cast, forged or machined aluminum and forged iron or steel [8].

A great variety of different polymeric materials have been tested for high voltage outdoor insulation applications over the past decades. Phenolic epoxies filled with quartz were used first. Cracks, tracking, erosion and insufficient UV-radiation resistance led to replacing the phenolic epoxy system by cycloaliphatic epoxies with aluminum trihydrate (ATH) filler. Often 40-60 % of the filler by weight (hereafter referred to as wt.%) is added [9] to fulfill the requirements regarding the tracking resistance. In normal environments the long-term performance of this material is acceptable, but in polluted environments the performance is far from being satisfactory. Variations of the ethylene-propylene based rubbers as EPR, EPDM and

Chapter 2. Literature review

ESP (mixture of ethylene-propylene and silicone polymers) exhibit similar problems as the EPs, though their tracking and UV-radiation resistance has been better. Nowadays their long-term performance is satisfactory in clean environments, but in polluted environments they have shown inferior long-term performance [10]. EVA elastomeric material has also been used, but less frequently. SIR, based on polydimethylsiloxane (PDMS), has become the dominant base polymeric materials for insulator housings.

There are three main types of silicone rubber used in high voltage insulation applications: High temperature vulcanized (HTV) silicone rubber, room temperature vulcanized (RTV) silicone rubber as well as liquid silicone rubber (LSR). The first type of SIR used in suspension insulators was RTV filled with quartz; around 1979 HTV rubber was introduced [10]. HTV rubber is cured at high temperature and pressure catalyzed by peroxide-induced free radicals or by hydrosilylation catalyzed by a noble metal i.e. platinum [11]. RTV rubber is cured at lower temperatures, i.e. around room temperature, by condensation reaction as a one-component system or by hydrosilylation as a two component system [11]. The one component system is cured by moisture diffusion from the surrounding air into the material and is rarely used for the production of insulators. LSR rubber is always a two-component system, and is vulcanized by hydrosilylation catalyzed by Pt [11]. It is cured at elevated temperatures. Fillers are added to the rubbers to control different properties of the product, such as mechanical stability and resistance to tracking, as well as to reduce the cost. Fumed silica is necessary for achieving good mechanical properties during processing, and ATH is added as a flame-retardant [12]. Adding ATH also has the positive effect of improving the dielectric strength and tracking resistance [12, 13]. Further information concerning micro- and nano-fillers in composites is reviewed in **section 2.1.2**.

The properties that make the use of polymeric materials in high voltage outdoor environments advantageous over traditional glass and porcelain are:

- High surface and bulk resistivity,
- Fracture toughness over a wide temperature range,
- Hydrophobicity (water repellence) and the ability of its recovery (mainly for SIR).

It is often desirable to decrease the leakage current in high voltage insulator applications, which can be influenced to a large extent by selecting adequate materials. The surface of polluted porcelain or glass insulators becomes completely wetted, allowing forming a conductive film during rain or in a fog. Some polymeric materials, for instance SIR, on the other hand, are well-known for exhibiting excellent water-repellent properties, namely they are strongly hydrophobic. Basically, it means that water will simply bead up on the material surface and run off instead of forming a

2.1. Polymeric HV outdoor insulation

continuous film. This is one of the reasons why SIR is favorable for application in heavily contaminated areas. Service experiences showed that SIR has in this respect a better performance than EPDM, porcelain and glass insulators in contaminated environments [2, 14-18], in severe marine sites [15, 18-21], and also during laboratory tests [22-24]; its hydrophobic property being considered as the main factor contributing to the better flashover performance [25-27].

The contamination performance of SIR is even better than EPDM due to the fact that, the initially hydrophobic surface properties of EPDM can be permanently lost when exposed to electrical discharges or pollution [28]. However, if the similar situation happens to SIR during exposure to electrical discharges (corona, dry band arcing) [28-30], or by rapid build-up of a continuous layer of pollution, i.e. salt or dust [31-34], after a subsequent period of rest, its hydrophobicity recovers. Migration of low molecular weight (LMW) polymer chains from the bulk to the surface of the material is considered to be the main mechanism behind the recovery [12, 24, 34].

Consequently, the superior characteristics of polymeric insulators over traditional glass and porcelain insulators consist of (i) better insulating properties (improved AC and lightning impulse (LI) strength, hydrophobic surface, less leakage currents), (ii) need for less maintenance (no cleaning required) thanks to the improved contamination resistance, and (iii) non-brittle construction providing improved resistance to vandalism, and lower risk for shipping or handling damages. In cases of faults that may lead to explosions, the adoption of polymeric insulators considerably lowers the risk of damages to people and property [27, 35]. Important is also low weight of polymeric insulators, about 90 % in weight reduction, which yields lower installation and transportation costs [36, 37]. Application of polymeric insulators enables therefore lighter tower designs for new lines as well as upgrade of transmission capacity of existing lines [27, 35, 38, 39]. Additionally, smaller size as well as lower weight of polymeric insulators decreases shipping costs significantly, compared to the counterparts made of porcelain and glass. This advantage can also be manifested during construction works, as different requirements refer to the size of cranes or other lifting devices [27]. However, even though the application of silicone rubber on HV outdoor insulators have been collecting long-term service experiences thanks to the superior performances, ageing phenomena induced by great variety of stresses in the operating environments are still of concern.

2.1.2 Polymeric micro- and nanocomposites

As polymers cannot perform satisfactory in numerous applications in pure form (unfilled) they are therefore compounded with diverse fillers, mainly in form of particles and fibers, for obtaining or strengthening the desired properties. If the dimension in any direction (diameter, thickness or width) of filler particle is within the

Chapter 2. Literature review

order of a few micrometers, the resulting composite material is called microcomposite. When the dimension of the filler particle is less than 100 nm, it is called nanocomposite. Traditionally, SIR as the base material with the addition of micro-fillers is used in the manufacturing of polymeric outdoor insulation.

Constituents of composite materials commonly have significantly different physical and chemical properties. For example, the major components of SIR material for high voltage outdoor insulators are uncross-linked PDMS, reinforcing silane-treated filler (10-20 wt.%) of amorphous silica. Moreover, typically ~50 wt.% of ATH is added as flame retardant. ATH decomposes to aluminum oxide and water when heated at above 200 °C. The liberation of water is endothermic and helps to cool down material surface, contributing to extinguishing of electric arcs and enhancing this way the resistance against tracking and erosion. Typical formulations also contain smaller proportions of silicone oil for process control, pigments, and agents used for vulcanization (cross-linking) reactions.

Micro-silica is classified as semi-reinforcing filler; the silane-treated micro-silica improves the physical properties of silicone compositions through molecular bonding with the silicone polymer. ATH fillers may exhibit a similar bonding by silinization at higher cost [40]. Instead of ATH or silica, calcium carbonate (CaCO_3) may also be adopted as a more economical filler. The use of CaCO_3 , however, reduces the tracking and erosion performances as well as the arc resistance of SIR as compared to ATH and increases the water absorption rate [41]. Additionally, CaCO_3 is more susceptible to acid attack [42]. Micro-fillers may incur both desirable and undesirable effects on the resistance to electrical ageing and on the ability to recover hydrophobicity in SIR. The desirable effects of fillers include improved thermal conductivity of the material, thereby improving heat dissipation and hence preventing the development of excessive hot spots; as well as reduced organic material exposure to heat from dry band arcing, thus decreasing the weight loss of the compound. One undesirable effect of the filler is that it acts as a “diffusion barrier” for the LMW fluid and slows down the recovery process. Moreover, the filler presence reduces the amount of silicone material available, thereby reducing the amount of LMW fluid for hydrophobicity recovery [2]. On the contrary, some results indicate that with increased filler content, the recovery may also be effective [43]. Thus, for a given formulation, including quantity, size and type of filler particles included in the formulation, becomes critical.

Recent years have been witnessing increasing attention on possible use of nanocomposite polymeric materials in electric power applications, since they may provide a number of new opportunities. A range of studies have been reported on comparing the performances of nano- and micro-particle-filled materials.

Investigations revealed that nanocomposites have satisfying resistant performance under the action of electrical discharges (partial discharges (PDs) and others). Lan, et al. [44] reported that sphere and layered nanocomposites could take the role of flame retardant with the flame suppression mechanism differing from that of conventional ATH filler. Afterwards, the nano-layered silicate (LS) associated with the preferable 5 wt.% nano-LSs was suggested for improving the integrated mechanical performances [45]. In addition, the nano-filled RTV, either nano-silica or nano-LS at 2 wt.% and 5 wt.% concentrations was revealed to have a superior corona ageing performance as compared with the virgin RTV material [46]. Besides, the significantly improved corona performance of SIR with the nano-silica filler loading was also reported by Venkatesulu, et al. [47]. It was observed that at 3 wt.% of nano-filler loading the surface roughness reduces by at least one order, crack width reduces by 7 times and the loss of hydrophobicity also reduces by at least 10 % as compared to the unfilled samples. As well, Kozako, et al. [48] proposed that the nano-filled (the nano-fillers used were Titania, two different particle sizes of silica, and LS) epoxy compositions were more resistant to PDs than that without fillers and with micro-fillers.

In the context of outdoor applications, the favorable properties of nanocomposites have also been foreseen in increased long-term stability and resistance to tracking and erosion [47, 49, 50]. Rätzeker, et al. [51] observed that the thermal conductivity rose in an approximately linear manner with the filler (nano-silica and nano-alumina) concentration and hence improved the resistance of HTV rubber to erosion. However, enhanced resistance to arcing with nano-silica is achieved only at high concentration of filler, approximately 40 wt.% [51], which did not agree with most of the available technical information suggesting that improvements in the nano-material properties are evident at low filler concentrations (1-10 wt.%). It was also presented by El-Hag, et al. [52] that 10 wt.% of nano-filled SIR (12 nm sized fumed silica) gave a performance that was similar to that obtained with 50 wt.% of micro-filled SIR (5 μm sized silica) as regards the erosion resistance. Additionally, the nano-silica filled RTV rubber was suggested better suited for contaminated environments than the micro-silica filled one by Meyer, et al. [53] due to the higher erosion resistance. Furthermore, Ramirez, et al. [54] presented that resistance to heat erosion equivalent to a SIR filled with 30 wt.% of micro-sized silica can be obtained with only 2.5 wt.% of fumed silica and surfactant; as well as the nano- and micro-filler (silica) mixture composites (NMMC) displayed significantly improved resistance to heat ablation than composites with only one or the other filler, especially when Triton™ X-100 was used for improving dispersion of the particles [55]. Also Tanaka, et al. [56] showed that the epoxy NMMC appeared to be superior over the single nanocomposite in terms of PD erosion resistance.

When it refers to the dielectric strength, Imai, et al. [57, 58] presented a higher dielectric strength in a NMMC made by dispersing nano-LS fillers and micro-silica fillers in epoxy resin. Contrary to this work, Fuse, et al. [59] stated that the dielectric strength of the investigated polyamide with LS nano-filler proportions ranging from 1 to 5 wt.% was almost independent of the nano-filler content for impulse, DC, and AC voltages. Another controversial point was suggested by Singha, et al. [60], who noted a difference in dielectric strength depending on the processing or mixing techniques used. The highest breakdown strength, with the inclusion of nano-fillers, was observed when the dispersion was carried out with mechanical mixing, followed by ultrasonic agitation. However, a higher dielectric strength was obtained for formulations with micro-fillers, rather than the formulations with nano-fillers [60]. Under such circumstances, it was therefore postulated [55, 61, 62] that more work is still needed to improve the dispersion of nano-fillers to enhance the bulk properties and to attain even better dielectric performances.

The possible reasons for the better performance of the nanocomposites were believed to be attributed to the better polymer holding capacity of the nano-filler [47]. The strong interfacial bonding between nano-particles and polymer matrix as well as small inter-filler spacing of the nano-dielectrics restricts material degradation [49, 51]. Also, it was proposed that stronger interfacial bonding should mitigate the pyrolysis of the polymer chains [51].

2.2 Corona and ozone

2.2.1 Corona discharges

The corona discharge is a weak luminous discharge that usually takes place in a strongly non-homogeneous electric field at or near atmospheric pressure. The discharge electrode, which has a small radius of curvature, like for example a sharp metal point, a plate edge or a wire, concentrates the field, while the passive electrode, which has much larger radius of curvature, e.g. a flat plate or a cylinder, is separated by a relatively large distance. The corona discharge is self-sustained, i.e., no external source of ionization is needed to maintain the current. The ionization region is constrained to a small volume close to the discharge electrode and in the remainder of the inter-electrode space, called the drift region, where the ions drift only in the electric field without additional ionization. The polarity of the discharge electrode influences the physical mechanism of corona.

The behavior of a corona discharge is usually described in form of a voltage-current curve, known as V-I characteristic. The field strength at which corona discharge is initiated has been studied extensively [63-65] and it depends on the ionization

potential of the gas, the mean free path of gas molecules, and the size and the surface condition of the corona electrode.

Peek [63] established a semi-empirical expression for the corona initiation field at a wire electrode in dry air,

$$E_i = 3 \times 10^6 \varepsilon (\delta + 0.03 \sqrt{\frac{\delta}{a}}) [V / m] \quad (2.1)$$

where the wire radius a is expressed in m, ε is the dimensionless surface roughness of the electrode ($\varepsilon=1$ for smooth surfaces and $\varepsilon<1$ for rough surfaces), and δ is the relative density of air ($\delta=T_0P/TP_0$), where T_0 and P_0 are reference temperature (293 K) and pressure (101,325 Pa) respectively. As the applied electric potential increases, the corona current increases and a stable discharge mode develops. For the stable corona, secondary electrons produced by photoionization (positive corona) or photoemission (negative corona) sustain the ionization process.

In reality, based on numerous observations of corona there are three primary causes for its development: geometric factors, spatial factors, and contamination. Geometric factors include sharp edges on conductors, connections and switchgear cabinet components [66]. Spatial factors include small air spaces between conductors, insulation board, etc. Furthermore contamination in the form of dust, water or other fluid drops and other particulates on conductors and insulators also produce corona. Therefore a well known effect is that corona gets intensified in humid or wet conditions.

- **Positive corona**

Figure 2.1 illustrates the positive-polarity DC corona process in a point-to-plane geometry. When a high positive voltage is applied to the small diameter electrode, e.g. a needle, and the larger diameter plate electrode is grounded, free electrons formed naturally in the inter-electrode space are accelerated towards the positive electrode. In the ionization region very close to the needle, inelastic collisions of electrons and neutral gas molecules produce electron-positive ion pairs, for example O_2^+ and N_2^+ dominate in dry air. The newly freed electrons are in turn accelerated by the electric field and produce further ionization, which is referred to as the electron avalanche. Secondary electrons sustaining the discharge are produced in the gas-phase by photoionization due to photons emitted during the de-excitation process in the positive corona plasma region. In this region electron-impact chemical reactions, e.g. generation of ozone, are significant [67]. In the positive corona, the corona plasma region coincides with the ionization region, which is not the case for negative corona.

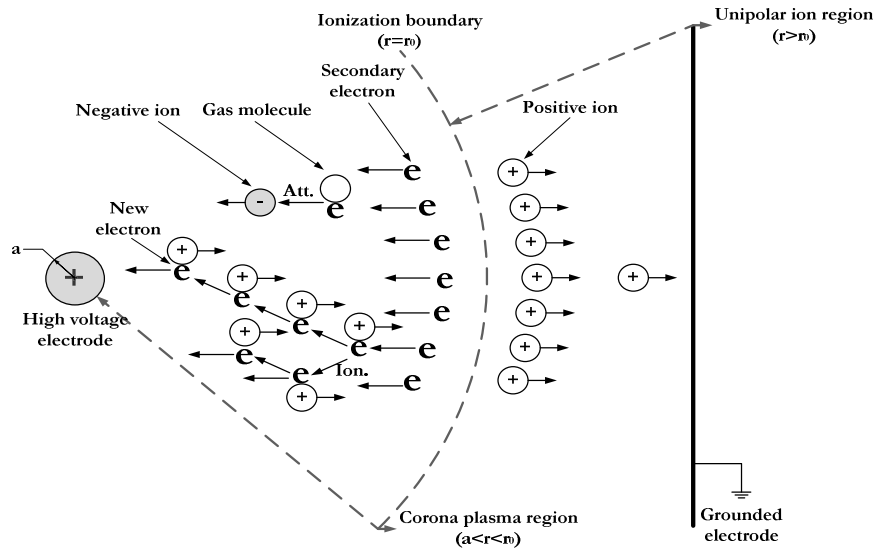


Figure 2.1: Sketch of a self-sustained positive DC corona discharge (not to scale).

Recombination between free electrons and positive ions may also occur during positive DC corona discharges but is usually negligible due to the small recombination coefficients [68] as well as the relatively low charge density. Therefore, ionization competes primarily with electron attachment to electronegative gas molecules (for instance O_2). In the vicinity of the high-voltage electrode, ionization dominates over attachment and new electrons are produced. All newly produced electrons attach to molecules to form negative ions due to the ionization rate equaling the attachment rate at the outer edge of the corona plasma a few needle diameters away. The electric field strength is insufficient to produce electrons beyond the corona ionization region. Positive ions drift into this volume toward the grounded electrode, responsible for the total current outside the active ionization region.

For the point-to-plane electrode geometry, when ionization by electron collision takes place in the high field region in the vicinity of the high voltage electrode, electrons produced are readily drawn into the anode due to their higher mobility, leaving the positive space charges behind. Consequently, the field strength close to the anode becomes reduce while the field further away is increased. The field reduction close to the anode due to the positive space charges may result in periodic extinction of the discharges. On the other hand, the high field region is in time moving further into the inter-electrode space, extending this way the region for ionization. The field strength at the tip of the space charge may be sufficiently high for the initiation of cathode-directed streamer, which subsequently may lead to a complete breakdown. A representative positive point-to-plane corona may typically pass through the following stages [69] as the corona current is increased usually by increasing the applied voltage: field intensified dark current (non-self-sustained), burst/pre-onset streamer corona (non-self-sustained), positive glow/pre-breakdown streamer corona (self-sustained), and eventually spark breakdown.

- **Negative corona**

Figure 2.2 illustrates the negative-polarity DC corona process in a point-to-plane geometry. When a high negative voltage is applied to the small radius point and the plate electrode is grounded, seed electrons produced in the natural ionization events initiate the electron avalanche process in the ionization region. However, the mechanisms for the generation of electrons and ions in the negative corona are different from those described for the positive corona [69-71]. In negative coronas, electrons are present outside the ionization region, and the most significant mechanism for the generation of secondary electrons is photoemission from the discharge electrode surface [72] since the work needed to remove photoelectrons from the electrode surface is considerably less than the ionization energy of oxygen and nitrogen molecules [73], although the short-wave photons emitted in the corona discharge are energetic enough to ionize the gaseous species. However, the positive ions with the mean kinetic energy in the order of 0.01-0.1 eV in the corona plasma are not energetic enough to knock out electrons from the electrode. Therefore, for negative corona discharges, the production of photoelectrons depends on the wavelength of photons as well as the work function of the discharge electrode material, indicating that the voltage-current characteristics of the negative corona may depend on electrode material as well as the condition of the surface.

Similar to the positive corona, in the ionization region, electron-impact ionization which results in the production of new electrons dominates over the attachment of electrons to ozone. With the reduction of the electric field beyond the ionization boundary, attachment prevails over ionization reflected by the gradual reduction of the number of electrons. Nevertheless, unlike in the positive corona just beyond the ionization boundary, electrons are of adequate number and energy to trigger electron-impact reactions. Therefore, the corona plasma region extends beyond the ionization region [74].

Space charges produced in negative corona result in the distortion of electric field distribution between electrodes. The electrons are repelled into the low field region. In the case of electronegative gases, they become attached to the gas molecules and tend to hold back the positive space charges, which remain in the space between the negative charges and the point electrode. As a result, in the vicinity of the point the field is dramatically enhanced whereas the ionization region is reduced. Therefore, to overcome this inhibiting action of the negative ions a higher voltage is needed for maintaining ionization. It is the reason for the negative breakdown voltage being higher than that of positive polarity in electrode system characterized by remarkable asymmetrical electric field distributions. Trichel [69] investigated in details the negative point-to-plane corona discharge. He observed during the discharge a current consisting of a train of very short pulses with a rather well defined repetition frequency, named Trichel pulses afterwards. In the air at atmospheric pressure the

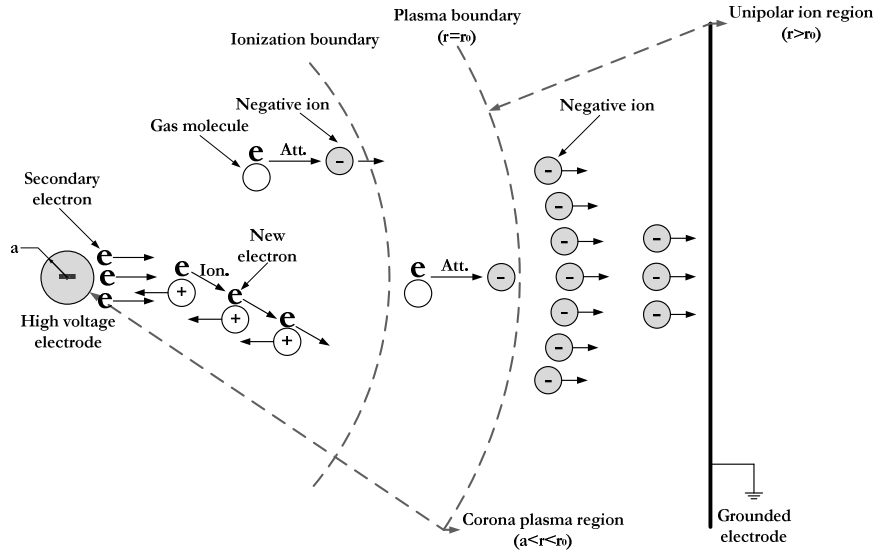


Figure 2.2: Sketch of a self-sustained negative DC corona discharge (not to scale). The plasma region is defined as the region in which electron-impact reactions are significant.

current pulses have a very fast rise time of approximately 1.5 ns and short duration with a relatively long period between individual pulses. It was also noticed that the waveform of regular Trichel pulses is almost independent of applied voltage and rather independent of cathode material and tip radius. On the other hand, the repetition frequency of the pulses extends from some kHz up to some MHz at atmospheric pressure, being roughly proportional to the magnitude of the average discharge current. If no sparking intervenes, a continuous glow is formed when Trichel pulses nearly merge in time [69]. A representative negative point-to-plane corona may typically pass through the following stages [69] as the corona current is increased: field intensified dark current (non-self-sustained), Trichel pulse corona (self-sustained), steady negative glow, negative streamers; or directly into spark breakdown.

- **Corona applications**

Corona is often considered as disadvantageous factor in power transmission applications – it causes losses and generates radio interferences in high voltage transmission lines and equipments. On the other hand, corona discharges in gasses have found many practical applications, for example in plasma reactors, cold plasma chemistry, electrophotography, electrostatic printing, electrostatic separation, air pollution control, etc. In many of these applications multipoint discharge electrodes of different shapes and configurations are utilized. The multi-needle corona discharge electrode was also selected in this project as an artificial ageing tool for the polymeric materials investigations.

Despite the numerous applications of multipoint-to-plate corona electrode geometry in flowing gases, the characteristics of such a discharge are not well described in literatures. Instead, most of the studies dealt with the corona characteristics from a single point-to-plate electrode geometry in stationary gases and only a few papers were devoted to the corona discharge in a flowing gas [75-79]. Among the papers published on the electrical discharges generated in gasses at normal pressure and in more complex electrode configuration one may list work of Lama and Gallo [80], who investigated a discharge between two points against a plate. The authors found that the frequency of Trichel pulses decreases as the points approach each other. Also Abdel-Salam, et al. [81] studied positive corona from two interacting needles, determining the corona current, corona onset voltage and pulse repetition rate, while Thanh [82] determined the current-voltage characteristics of a multiple-point electrode with needles arranged linearly or circularly. The distribution of the corona current at the grounded plate against a barbed (multipoint) discharge electrode was studied by McKinney, et al. [83]. They investigated interactions of two, seven (placed at a hexagonal mesh) and nine (placed at a square mesh) discharge points, and discovered that the space charges generated by the adjacent points did not overlap each other. The characteristics of the discharge between a set of 25 needles and a plate electrode were investigated by Jaworek and Krupa [84], but for stationary conditions only. Akishev, et al. [85] studied a DC multipoint glow corona discharge in a flowing air for the purpose of gas treatment at a pressure of up to about 200 kPa, flow velocity 70-200 m/s and voltage level up to 20 kV. The glow corona discharge was very stable in the flowing gas. The voltage level necessary to initiate discharges increased with the gas flow velocity and the rising pressure.

2.2.2 Ozone production in corona discharges

Ozone or trioxygen (O_3) is a naturally occurring molecule that is sometimes called “activated oxygen”, consisting of three oxygen atoms. It is an allotrope of oxygen that is much less stable than the diatomic O_2 . As one of the most powerful oxidants known, ozone is highly toxic to humans and animals, inflicts serious damage to plants, and produces deterioration in many materials [86]. The strong oxidation is due to the unstable gas molecule O_3 allowing it to readily decay into oxygen and a single highly reactive oxygen atom.

High in the atmosphere the ozone layer is created by the action of the harmful ultraviolet radiation from the sun on oxygen atoms. At ground level ozone is created by the effect of electric discharges on oxygen atoms. Ozone is also created naturally as a result of photochemical reactions due to the pollutants such as nitrogen oxides (NO_x) and sulphur oxides (SO_x) that exist in the atmosphere of cities and industrial areas. There are principally two methods of artificial ozone generation: ultra-violet radiation and silent corona discharge. First ozone generation system utilizing corona

discharges was built by Siemens already 100 years ago [87]. Nowadays silent corona discharge technology is utilized by industries and laboratories to generate a constant, controllable and reliable volume of ozone for odor control, disinfection, and scientific investigations [86, 88-90]. In these applications, ozone is almost always produced at high rates in dielectric barrier discharges in pure oxygen.

Ozone is generated during corona discharges in a two-step process – formation of oxygen free radicals and then reactions among them [91]. However, the generation of ozone in air is more complicated than that in pure oxygen, due to the presence of nitrogen and water vapor. Investigations [92-94] have considered the dependence of the ozone generation on various parameters such as discharge polarity, corona current level, electrode material, environmental temperature, etc. Also, it was observed experimentally that the ozone production rate in the negative corona is one order of magnitude higher than in the positive corona, which was revealed by the model simulation investigation [74] that this significant difference is due to the effect of discharge polarity on the number of energetic electrons in the corona plasma.

2.3 Corona discharges and polymeric insulators

Under the action of corona, surfaces of insulator housings are simultaneously subjected to a mixture of energetic and reactive species as well as radiations, e.g. electrons, ions, ozone, UV and high temperature. Diverse chemical reactions take place during the exposure. The most important ones include (i) an increase of the oxygen content at the surface by formation of silanol and hydroxyl groups [89, 95-98], (ii) oxidative cross-linking [99-101], and (iii) degradation of the polymer network structure resulting in the formation of low molecular mass compounds [102-105]. All these, by modifying material surface, yield changes of mechanical and electrical properties of the housing.

2.3.1 Field experiences

Corona discharge as an ageing factor to polymeric insulators has long been recognized. Generally, there exist two main sources of corona discharges on the surface of composite polymeric insulators in the field – poorly designed insulator hardware (including corona rings) or presence of water droplets on insulator housing surface. The former source acts locally and may promote ageing of insulator housing, even at dry conditions. However, proper hardware design of field grading devices allows avoiding it effectively [102, 106]. In contrary, unavoidable presence of water droplets on insulator surfaces acts as a discrete and distributed source of corona that

2.3. Corona discharges and polymeric insulators

yields ageing at different insulator parts [107-109]. Discoloration, erosion, and sheath/shed cutting were reported among the effects. Such damages can be attributed to the action of energetic ions and reactive gases from the discharge, ozone and nitrogen oxides, and possibly UV radiation [13].

Some field investigations were done to study the behavior of polymeric insulators and housing materials exposed to corona triggered by water droplets. For investigating water drop corona effects on full-scale 500 kV polymeric insulators, observations were made in a full-scale accelerated ageing chamber as well as in service, reported by Philips, et al. [107]. It was found that the electric field magnitudes on the sheaths of insulators investigated, both in the chamber and in a steel lattice tower, exceed the levels necessary for water drops corona. Besides, whitening of the surface material was observed and the whitening occurred correlated to the magnitude of the surface electric field. In addition, permanent loss of the water repellent property at highly stressed regions was found and the degree of loss was proportional to the magnitude of applied electric field [108]. It has been demonstrated however that surface erosion due to water drop corona can be avoided when insulator surfaces parallel to the electric field are not stressed more than 0.4-0.6 kV/mm. Reynders, et al. [109] identified corona and local arcing as the major ageing influences on silicone rubber surfaces. However it was proposed that the ageing induced by the arcing across dry bands was not as deleterious as corona ageing. In addition, experimental evidence on corona ageing and the stages in the ageing process in the field were presented.

Moreover, polymeric insulators can fail mechanically in service by rod fracture. One of the mechanical failure modes of the insulators is failure process called brittle fracture. Among the available so far three competing models of the brittle fracture process in polymeric insulators [110], the only model which can explain all aspects during such process is the one based on the development of nitric acid in-service due to corona discharges in the process of moisture, as reported by Kumosa, et al. [111]. For example, by performing FTIR analysis on the field failed polymeric insulators, it was revealed [112] that nitric acid generated in service due to water droplet corona activities (failures inside the fitting) and partial discharges at the rod/housing interfaces (failures outside the fitting) in the presence of moisture is the dominant cause of brittle fracture failures of polymeric insulators.

To figure out the mechanism of the corona damage phenomenon observed in the field, much work have concentrated on discussions regarding the behavior of water droplets on the surface of polymeric materials energized by high voltage stresses. The presence of water droplets deposited on hydrophobic polymeric surfaces distorts locally the distribution of electric field. The reason for this is twofold, the first one is the high relative permittivity of water and the second is the droplet deformations. The latter takes place independently of the voltage type, i.e. under AC and DC conditions. Field enhancement factors were experimentally and numerically determined as well as

current pulses were observed at around the peaks of applied AC voltage, while under DC voltage discharge activity was limited and occurred sporadically, as presented by Katada, et al. [113]. It was therefore suggested by Lopes, et al. [114] that PD could, for example, effectively be used for studying the insulation surface ageing. The dynamic behavior of water droplets on a hydrophobic surface of Teflon (PTFE) and SIR subjected to DC field was investigated in [115] by Higashiyama, et al. Corona discharges were found to occur at the tip of water droplets, which triggered the formation of larger water filaments. This behavior depended strongly on the polarity of the applied voltage. An extended research reported by Braunsberger, et al. [116] on epoxy resin systems concentrated on defining the onset conditions for water drop corona and revealed that the inception field strength was about 1 kV/mm for normal field stress and 0.5 kV/mm for tangential field stress, both valid for different drop sizes. Opposite to this, remarkable effects on the mode of corona discharges were found when varying volume and conductivity of water droplets, as observed by Yong, et al. [117]. In addition, Yong, et al. [118] presented that, when applying AC voltage, water droplets initially appeared to be charged negatively. Thereafter, with initiation of corona at their tips by increasing voltage level, the charge gradually changed to positive and this transition differed depending on material type, SIR and EVA. Anyhow, one of the most important conclusions drawn from a series of investigations by Moreno, et al. [119, 120] can be that even if assuming extremely severe weather conditions to be present during field operations, the degradation caused by water droplet corona, determined as the time to crack on a housing material surface, may require many years to develop.

2.3.2 Laboratory investigations

- **Corona ageing tests**

Due to the randomness of distribution and uncontrollability of discharge intensity of the water droplet corona, attempts to develop artificial tests employing continuous corona discharges from various electrode arrangements were carried out instead [96, 99, 104, 105, 121-125]. Many of these investigations concentrated on the impacts of long-term corona discharges on the hydrophobic characteristics of polymeric insulator surfaces and on elucidation of the ageing mechanisms involved [99, 120, 126-128].

Among the different test methods the procedure described in IEC 60343 standard “Recommended test methods for determining the relative resistance of insulating materials to breakdown by surface discharges” [129] can be used for testing the resistance to corona discharges, where a flat material specimen, located in a cylinder-plate electrode arrangement, is treated by discharges generated on its surface and the time until a breakdown is reported as lifetime behavior. The disadvantage of this

2.3. Corona discharges and polymeric insulators

procedure is that the discharges generated are a mixture of corona and capacitive coupled gliding discharges. Moreover, the treated area is not too large, which limits a possibility for performing any additional measurements of electric or mechanical properties of tested sample after the treatment.

A plane-parallel electrode arrangement was used for corona testing [6] as well. In such a case material specimen is placed between two horizontal glass plates (each 3 mm thick) and an air gap between the specimen and the upper plate is set at 2 mm. A voltage of approximately 20 kV_{rms} is applied between electrodes attached to the external surfaces of the glass plates. A voltage is adjusted for maintaining a current flow of 300 mA through the arrangement. The test duration is 100 h. It is required that the materials tested must not show any visible changes during and after the test. Color stability is also checked in comparison to the reference material.

Another corona ageing test, known as corona-cutting test, was introduced in [121]. A combination of corona and mechanical stress is used to accelerate the degradation of tested specimen, bent over a sized and grounded mandrel for introducing 30 % strain in the uppermost surface of the sample. A needle corona electrode is positioned 1 mm above the centre of the upper surface and energized at 12 kV_{rms}, resulting in a continuous corona discharge directly above the strained surface. The chamber in which the test is performed is sealed, accumulating at the same time a high concentration of ozone. The test is usually run until a mechanical failure of the sample happened. The minimum requirement of the test is that the sample should be able to survive 1000 h without cracking, splitting, cutting or flashover.

Other arrangements involving use of a single needle electrode have also been used for studying the effect of long-term exposure to corona [119, 120, 126, 130, 131]. Moreno, et al. conducted a series of such investigations and found that the degree of degradation caused by corona discharges could further be accelerated through increasing ambient relative humidity and applying additionally mechanical stress [119, 120]. Clear evidence of degradation was identified on surfaces of SIR and EPDM based materials by means of FTIR. The interaction between corona discharges and water generates acids [126, 131], which presence is in turn considered as one of the accelerating factors of the degradation process [127, 132, 133].

Since, similarly as in the standard arrangement, the treatment by means of a single needle electrode does not produce larger degraded areas, the obtained specimens are hardly suitable for other types of investigations. In contrary, a multi-needle corona test arrangement allowing for treating larger specimen areas was introduced by H. Hillborg [99] when investigating loss and recovery of hydrophobicity as well as degradation mechanism of polydimethylsiloxane (PDMS) after exposure to corona discharges. He showed [12, 89, 99, 103] that an oxidized surface layer is gradually formed on their surface in the process of treatment by corona discharges. Besides, the

Chapter 2. Literature review

surface oxidation was found to be faster in a more highly crosslinked polymer due to the higher susceptibility to oxidation of the C-C bonds in the crosslinks. XPS analyses revealed that typically observed oxidized surface layer was in a form of a brittle, micro-porous silica-like layer, with a remaining organic silicone content of at least 13-40 %. The thickness of the layer increased gradually with increasing corona exposure time, reaching approximately 100 nm after 3 hours of corona treatment. Thereafter a self-cracking of the layers occurred after a longer exposure. Therefore, the hydrophobic recovery behaved in two manners – occurring at a slow pace by diffusion of oligomers through the micro-porous but uncracked silica-like layer or at a much higher pace by transport of oligomers through the cracks. In addition, the hydrophobic recovery of specimens after exposure to corona obeyed Arrhenius dependence on temperature, with activation energies ranging from 0.31 to 0.62 eV. A homologous series of cyclic oligomeric dimethylsiloxanes (ODMS) with 4-10 repeating units (D₄-D₁₀) were identified as the migrating siloxanes responsible for the initial hydrophobic recovery after corona treatments.

Later on, Fateh-Alavi [128, 134-136] investigated in the same testing arrangement a possibility for improving the oxidation resistance in PDMS samples modified by different stabilizing agents, such as Irganox®, Tinuvin® 770 as well as Irganox® 565. The most efficient appeared to be Tinuvin® 770, addition of which allowed to increase the incubation exposure time for the formation of brittle silica-like layer by a factor of 9 with reference to the incubation exposure time of reference PDMS [135, 136].

Another modification of the multi-needle arrangement was recently applied by Du, et al. [137] for studying surface degradation of SIR at low pressures, whereas Yong, et al. [138, 139] used a system of comb-shaped and plate electrodes for the treatment. In the latter case corona was acting along the surface and the resulting weight loss, contact angle change were evaluated. In addition surface degradation was analyzed by means of FTIR as well as scanning electron microscopy (SEM).

In addition, applying another version of multi-needle electrode for corona treatments was presented by Venkatesulu, et al. [47] who investigated the corona performance of silicone rubber nanocomposites. Material characterization methods such as SEM, energy-dispersive X-ray analysis (EDX), hydrophobicity measurement, FTIR analysis, as well as optical profilometry was used to assess the relative performance of the samples with respect to corona ageing.

By means of SEM observations, FTIR analyses, EDX, as well as measurements of electric properties, especially surface resistance measurements, degradation mechanisms and property changes of materials exposed to corona can be studied. Surface erosion, seen in micrographs, and changes of color involving formation of hydrophilic hydroxyl and carbonyl groups was reported. The moisture absorbed by

2.3. Corona discharges and polymeric insulators

the hydrophilic OH groups was believed to play an important role in the decrease of the surface resistance [140]. Thermally stimulated current (TSC) characteristics of corona deteriorated HTV rubber were investigated in [141] and correlated with other parameters (hydrophobicity, SEM and FTIR). It was suggested that the TSC characteristics might be used as an effective index for assessing the corona deterioration of HTV silicone rubber.

- **Ozone ageing tests**

As one of the byproducts in the process of corona discharges in dry air, ozone contributes strongly to the ageing of polymeric materials. There exist a number of standards for testing the material resistance to ozone exposure [142-147], in which applied concentrations of ozone lie at the range of a few ppm (parts per million, mg/L).

Ozone attack to products made by utilizing polymers causes cracks to grow longer and deeper with time, the rate of crack growth depending on the load carried by the product and the concentration of ozone in the atmosphere. It has been found that without the inclusion of antioxidants, rubber cracking under stress can readily be detected within three to four hours when exposed to ozone levels as low as 0.03 ppm [148]. The resistance of SIR to ozone is, in general, high because the polymer matrix does not contain unsaturated functional groups. In spite of this, some degradation may be expected to take place. By carrying out an accelerated weathering and ozone exposure program involving a total of 38 rubber compounds, the fact that polymers vary greatly in their ozone resistance has been demonstrated [149]. It was proposed that, as an indication of performance in relation to service, a material passing a typical specification requiring no cracking after 7 days at 0.5 ppm and 20 % strain would be expected to give at least 5-year service without cracks under typical ambient conditions. Some SIR manufacturers claim [6] that silicone elastomers, including fluorosilicones, offer excellent resistance to ozone and only at its very high concentrations (much larger than 2 ppm) and long exposure periods (~30 days), changes of the mechanical properties of SIR can be observed.

Anyhow, since housings of polymeric insulators should withstand the chemical degradation associated with the action of corona discharges throughout their whole service lifetime, it is therefore necessary to test their resistance to ozone as well. However results obtained by means of the different procedures for separately testing the resistance to corona and to ozone cannot directly be compared. Therefore CIGRE WG D1.14 has discussed this issue and proposes that the resistance to ozone should simultaneously be evaluated within the new procedure for testing resistance to corona [6].

3 Material testing and characterization techniques

3.1 Corona ageing test development

3.1.1 General assumption

Following the recommendations mentioned in foregone section [6], the development of a methodology for testing material resistance to corona/ozone exposure presented in this work assumes that the treatments should be performed in a ventilated chamber in order to control the treatment atmosphere in association with the use of electrode arrangement proposed by H. Hillborg [12, 99]. It was additionally requested that the tests on elastomeric materials should include mechanical pre-stressing of the samples during the treatment and the surface area exposed needs to be sufficiently large to allow evaluating the effect of treatment on the mechanical and electrical properties as well as on chemical and structural integrity. Details on this work are elucidated below.

3.1.2 Components

A photograph of the test setup for corona treatment and its electric circuit are both illustrated in Figure 3.1. The circuit components include a variable AC voltage source (0-220 V, 50 Hz), an isolation transformer (220/220 V, 3 kVA, 50/60 Hz), a step-up high voltage testing transformer (220/60000 V, 600 VA), a water resistor R_1 (current limiter, 400 k Ω), a coaxial resistive shunt R_2 (9.96 Ω), a resistive voltage divider (R_3 : 100 M Ω , R_4 : 4.65 k Ω), and an oscilloscope (Tektronix DPO 7054). As a second method used for measuring the released power from the multi-needle electrode during AC corona treatments, a measuring capacitor (4.7 μ F) associated with a computer equipped with a data acquisition card (DAQ NI-6132) was adopted to complement the shunt resistor in combination with the oscilloscope. The details of the method are introduced in *section 3.1.3*. During the DC corona treatment, a single

phase half cycle diode rectifier (D in Figure 3.1 (b)) is connected to the output of the step-up transformer. For filtering purposes, a 45 nF smooth capacitor bank (C in Figure 3.1 (b)) is also included in the rectifier circuit. For comparing the influences of the 100 h long AC and DC corona treatments, voltages of ± 28 kV DC, the peak values of the applied sinusoidal 20 kV AC voltage, were utilized.

- **Corona electrode**

A schematic view of the proposed corona electrode arrangement is demonstrated in Figure 3.2 (a). The electrode arrangement consists of an upper corona electrode and a metallic grounded plane electrode on which the sample to be treated is mounted. The upper corona electrode is built of a circular metallic disc with 31 sewing needles made of stainless steel sticking out from it. The electrode was designed to achieve a nearly homogeneous electric field distribution in the vicinity of the treated surface. According to Figure 3.2 (b), the electrode diameter is 87 mm. The length of the seven innermost needles protrudes 12 mm, the twelve in the intermediate circle 11 mm and the twelve outermost 9 mm. The tips of the needles have radius of 48 ± 1.6 μm and the needle electrode is supported by plastic holders with adjustable height. The distance between the tips of the innermost needle and the surface of treated sample is kept at 40 mm. It is also of great significance that brand new needles are used in each test round in order to guarantee similar treatment conditions.

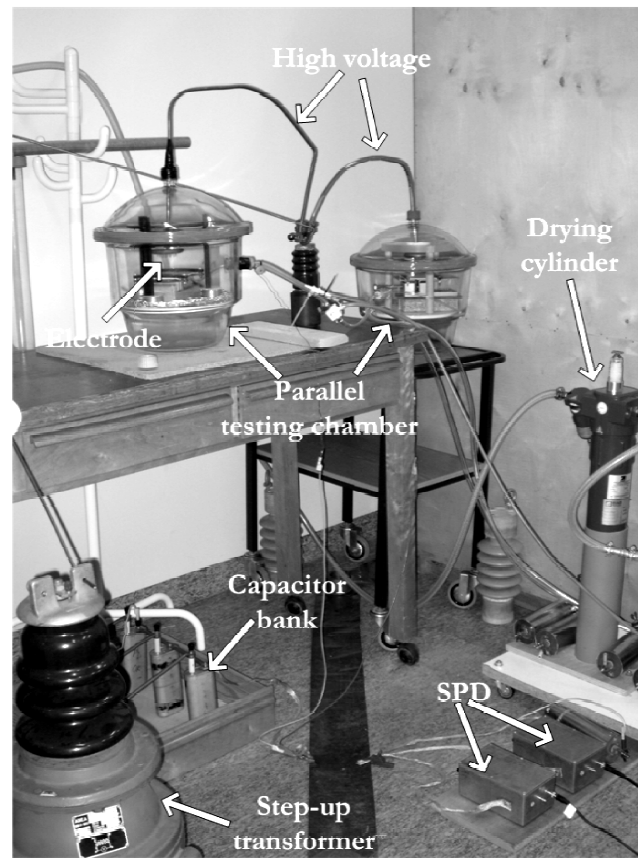
- **Sample Holder**

Each tested elastomeric specimen should be subjected to mechanical stretching, i.e. to be elongated by approximately 3 %, whereas the specimens of rigid material (i.e. epoxy) remain un-stretched during the treatments. The stretching is done in a sample holder that acts simultaneously as the bottom part of the electrode arrangement, as shown schematically in Figure 3.2 (c). A sample (e.g. $120 \times 100 \times 2$ mm³) to be treated is placed in the holder and fixed firmly by clamping bars at both ends. It is then stretched by ~ 3 % of its total length. Thereafter the holder is placed in the corona chamber and the corona electrode is adjusted above it.

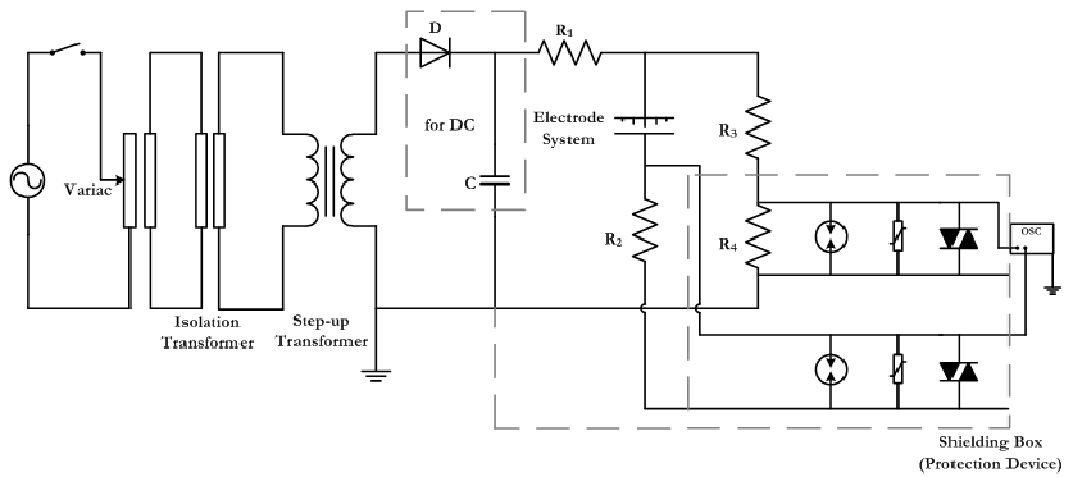
- **Test Chamber**

The chamber (a glass desiccator) has a volume of 20×10^{-3} m³ and allows control of the atmosphere inside. Voltage supply as well as air inflow and outflow pipes are connected to the interior via bushings. The chamber is continuously ventilated during the treatment for controlling humidity and ozone levels as well as for the removal of gaseous decomposition byproducts. The air flow supply consists of an air cylinder (alternatively air compressor with humidity filter) equipped with a pressure regulator and a flow meter. A continuous rate of dry air flow at 5 L/min is set. The temperature inside the desiccator is kept at 20 ± 2 °C and the humidity of the air is less than 20 ppm.

3.1. Corona ageing test development



(a)



(b)

Figure 3.1: Picture of the test setup for the corona treatments (a) and its electric circuit (b).

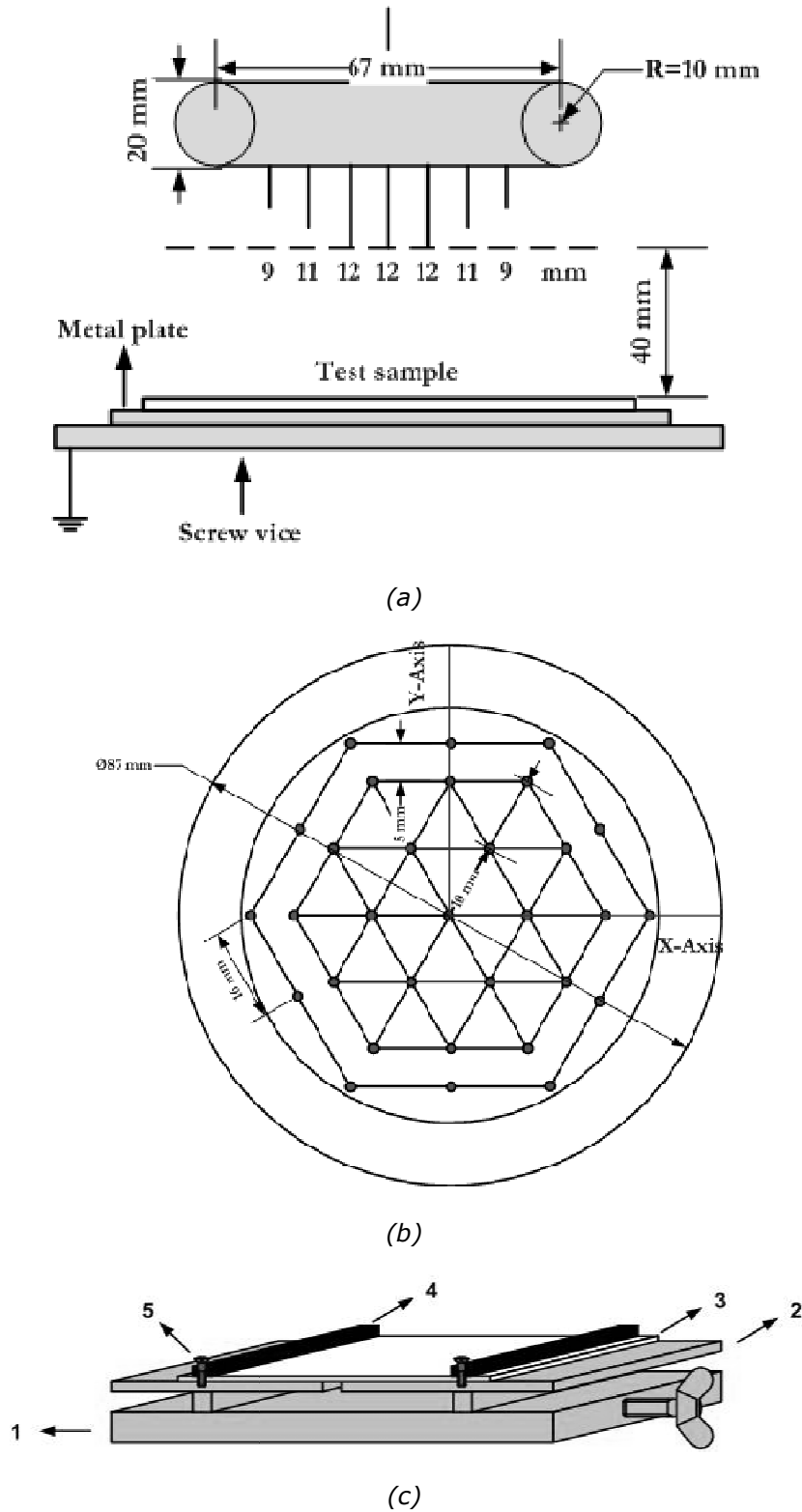


Figure 3.2: Side view (a), positioning of needles (b) in the corona electrode arrangement, and sample holder ((c), bottom electrode) employed to elongate the tested samples; 1 – screw vice; 2 – supporting brass plate (grounded electrode); 3 – treated specimen; 4 – clamping bars; 5 – fitting screws.

3.1.3 Evaluation of corona test arrangement

- **Electric field simulation**

Simulations of the electric field distribution were performed to determine an optimum distance between the innermost needle tips of the corona electrode to the corona/ozone treated samples. The requirement is that the lateral field distribution in the vicinity of the sample should remain homogeneous. A 3D model of corona electrode was built up, as illustrated in Figure 3.3. The static finite element method (FEM) solutions of electric field strength at different distances from the needle tips were obtained [7]. The model was solved with a simulated needle tip radius of 40 μm with an applied voltage of AC 20 kV_{rms}. The simulated field distributions are presented in Figure 3.4, where the field strengths along the X- and Y-axes, as defined in Figure 3.2 (b) are plotted. The distributions are shown for 6 different distances, ranging from 1 mm to 40 mm. The results indicate that the electric field becomes increasingly homogenous with increasing distance from the needle tips. At 40 mm distance the difference between the maximum and minimum field strength is 1 % only, which can be compared with 20 % at 5 mm distance. As a result of the performed simulations, the distance for sample treatments is set at 40 mm.

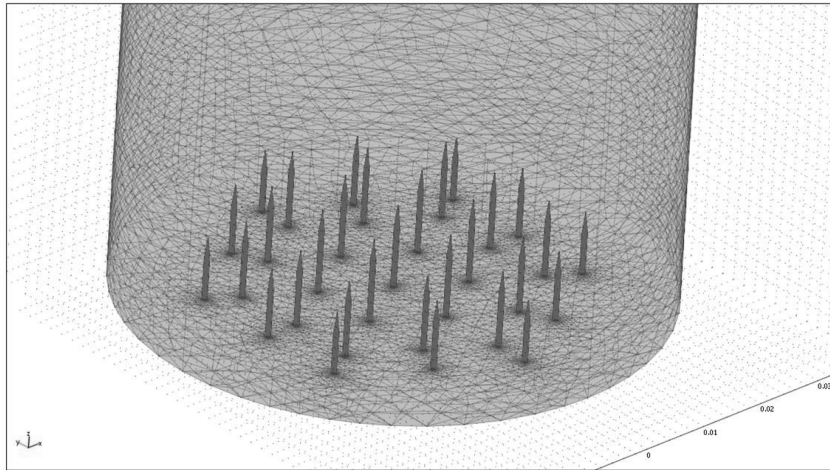
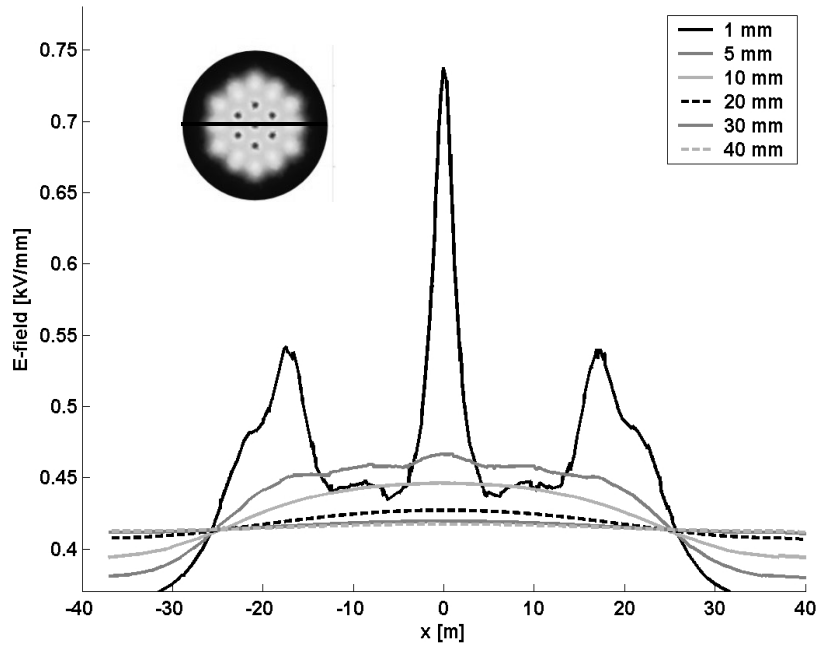


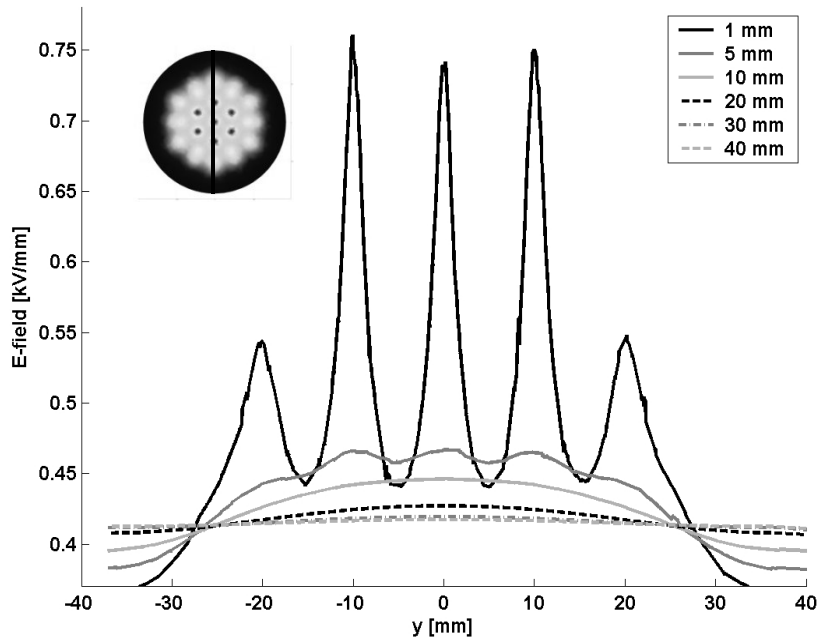
Figure 3.3: 3D model of the corona electrode for FEM simulations.

- **Released power measurement**

For evaluating the amount of power released during the corona treatments, a measurement technique based on the method reported in [88] was adopted. It was implemented by connecting a shunt capacitor in series with the corona electrode associated with a resistive voltage divider in parallel. Simultaneous sampling of the two signals was achieved with a commercially available data acquisition card (NI-6132) [7]. The power W released during a 50 Hz cycle was calculated according to (3.1).



(a)



(b)

Figure 3.4: Plots of the electric field distributions along the X- (a) and Y-axes (b) at different distances between the innermost needle tip of the corona electrode and the surface of treated samples.

3.1. Corona ageing test development

$$W = \int_T v(t) \cdot i(t) dt \quad (3.1)$$
$$i(t) = \frac{dq}{dt} = C \frac{dv_{cap}}{dt}$$

where $v(t)$ is the applied power frequency voltage, $i(t)$ is the current of the corona discharges, q is the released charge, C the shunt capacitance and v_{cap} the voltage drop across the shunt capacitor. The voltage across the series capacitor is proportional to the released charge. It is then possible to calculate the total power released in a 50 Hz cycle of the voltage and thereafter convert it into power as in the Equation 3.2.

$$W = \int_T v(t) \cdot C dv_{cap} \quad (3.2)$$
$$P = \frac{W}{T}$$

The correlation between the magnitude of applied AC voltage and the released power is illustrated in Figure 3.5 for a 3 mm thick polymeric sample at three different distances from the innermost needle tip to the sample surface. The influence of the electrode distance was not significant when changing it from 40 mm to 38 mm. However when the distance was reduced to 30 mm, a large increase could be noticed. The continuously released power larger than 1 W from the corona source is assumed to be sufficient for obtaining desired deterioration of the material surface during the corona/ozone exposure. At AC 20 kV_{rms} and with 40 mm distance to the sample, the corona power was found to be ~1.5 W, which fulfilled the requirement on the released power level and was comparable with the earlier results as described in [99].

To verify the accuracy of the released power measurements with a computer-DAQ based system [7], the measurements were repeated with a tan δ bridge (HAEFELY TAN 470) as well as with a commercially available oscilloscope (Tektronix DPO 7054). By assuming all the measured losses originated from the discharges at voltages above corona inception level, both the techniques provided comparable results – ~1.4 W at 20 kV_{rms} from the bridge measurements compared to ~1.5 W achieved by means of both the computer-DAQ based system and the oscilloscope.

- **Ozone concentration measurement**

For determining the ozone concentration level present in the test chamber, Kitagawa gas detector was applied [150]. This technique is a cost effective method, where a chemical substance in the tube changes its color according to the concentration of ozone in the gas mixture. A new tube must be used for each sampling. The required sampling time is ~2 min. Figure 3.6 shows the dependence of ozone concentration on the AC corona power dissipated at two different air flow rates of 5 L/min and 10 L/min respectively with the presence of specimens placed at different distances

from the needle tips. The higher flow rate of 10 L/min yielded a decreased concentration of ozone by 10 ppm. It is also worth pointing out that the ozone concentration was slightly higher, at the same level of dissipated power, when the

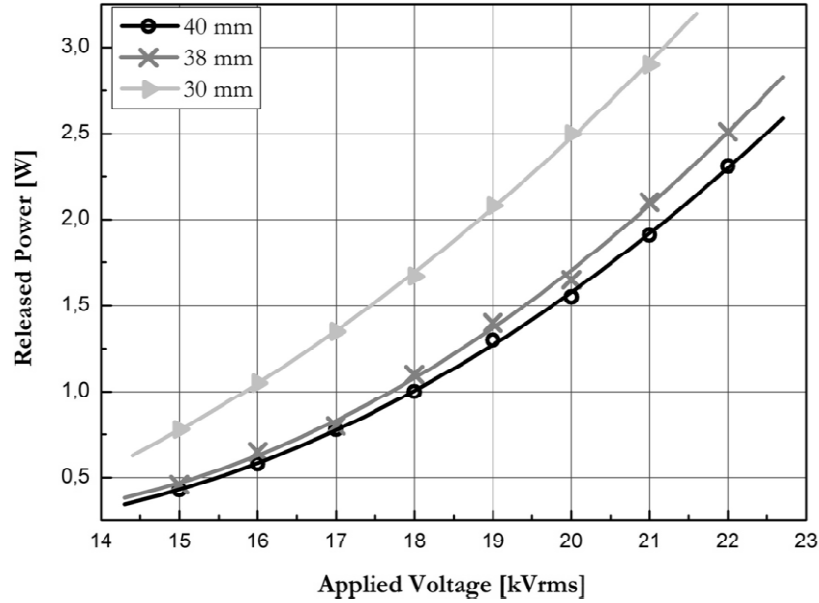


Figure 3.5: Correlations between the dissipated power and the AC voltage applied to the corona electrode at different distances between the innermost needle tip of the corona electrode and the surface of treated samples.

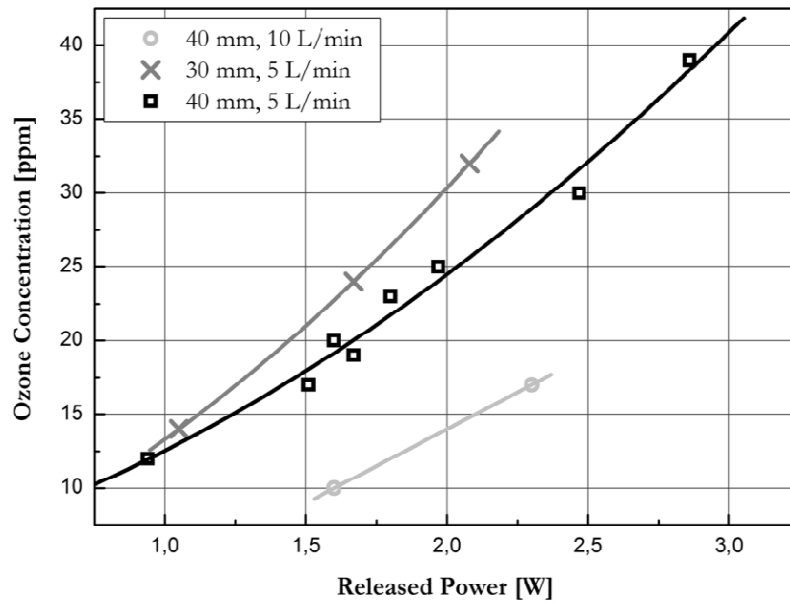


Figure 3.6: Ozone concentration measured at different dissipated AC corona power levels, sample distances and air flow rates.



Figure 3.7: View of corona discharge activity over a treated surface.

samples were closer to the corona electrode (30 mm compared to 40 mm). For the case where no test sample was placed on the grounded brass plate, the ozone concentration showed a tendency to increase compared to the situation when a polymeric sample was present, forming a dielectric barrier on the grounded electrode. On top of these, one of the most significant observations was that the ozone concentration measured during corona treatments was dependent on material dielectric parameters as well as processing procedure for both AC and DC corona/ozone exposures, which is presented and elucidated in detail in the following chapters.

- **Corona discharge characterization**

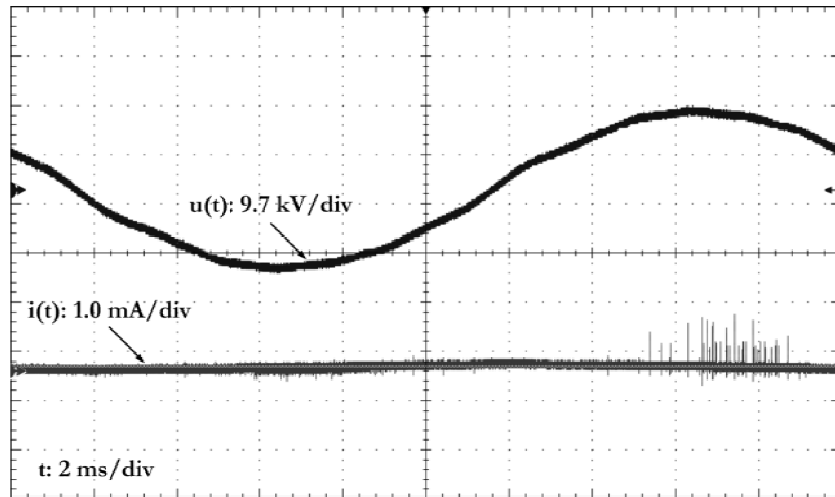
Experimental observations confirmed that the corona discharges generated by the designed arrangement were able to affect the whole treated surface. A picture illustrating the corona behavior is shown in Figure 3.7. It has been revealed that, generally, the frequency band of air corona discharges is in the range of 150 kHz to 5 MHz, though the magnitude decreased dramatically beyond 1 MHz [151]. The bandwidth was hence set at 20 MHz as well as the sampling rate 100 MS/s of the Tektronix DPO 7054 oscilloscope which was employed to trace the development of corona current by means of a resistive shunt connected in series with the corona electrode. This investigation was performed with the presence of an HTV rubber specimen on the sample holder.

The captured waveforms of the applied voltage and corona current are illustrated in Figure 3.8 and Figure 3.10 for AC and DC corona respectively. For AC voltage, first of all, it was observed that the corresponding corona inception voltages for positive and negative voltage semi-cycles are at approximately the same level of about 10 kV (see Figure 3.8 (a)). The corona pulses in the positive semi-cycles are less frequent and of higher magnitude whereas a much higher repetition rate characterizes the pulses during the negative semi-cycles. In addition, information about the average magnitude of power released from the corona discharges as well as the released charge per cycle can also be obtained by the programmable oscilloscope. This is illustrated in Figure 3.9. It can be seen from Figure 3.9 (a) that the contribution to the released power from the negative semi-cycle is a bit higher than that from positive one, taking up to 53 % of the total. This is due to the fact that although the current magnitude is much lower, the repetition rate of the corona pulses occurring in the negative semi-cycles is much higher than of those occurring in the positive semi-cycles. The typical magnitude of the charges released during a complete sinusoidal voltage cycle is illustrated in Figure 3.9 (b). For DC corona, see Figure 3.10, if comparing the single pulses between positive and negative corona currents at the treatment level (± 28 kV), the magnitudes of the positive corona current pulses are higher than those of negative ones, and the duration time of positive corona pulses is longer as well. However, again, the repetition rate for the negative pulses is much higher than that of the positive pulses. As a consequence, the total current as well as the power released from the multi-needle electrode, is higher for the negative corona than for the positive one, as illustrated in Figure 3.11. At the corona treatment voltages, the powers released from the electrode are ~ 1.6 W, ~ 0.7 W and ~ 1 W for AC, positive DC and negative DC corona discharges respectively. This somewhat surprising result can be explained by the fact that the DC corona discharge activity in the test arrangement is impeded by electrostatic charging of the treated polymeric surface, which in turn modifies the electric field distribution in the discharge region. What is worth further pointing out is that the corona discharge intensities characterized either by the total corona current or the released corona power during AC or DC corona exposures are dependent on the dielectric parameter of the materials treated, which is reported in **Chapter 5**.

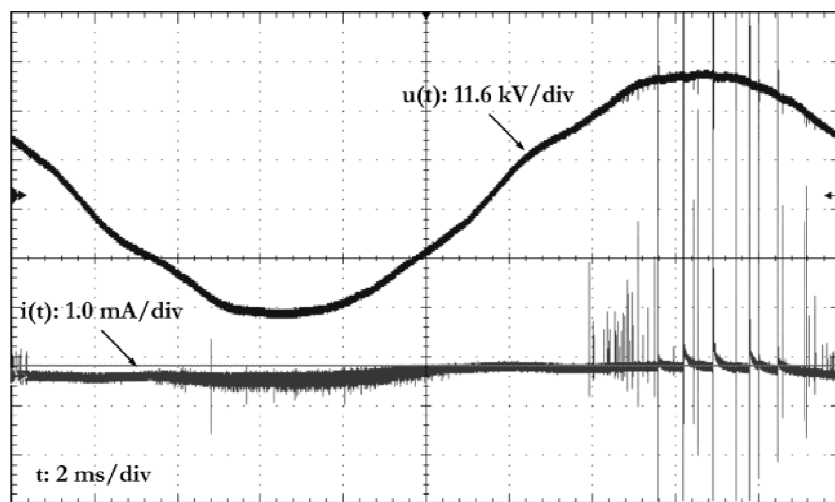
For investigating whether or not the corona discharge intensity can remain stable during the treatment period (100 h), as the intensity of the discharge may change during the process if the needles in the corona electrode erode, the erosion of the needles was monitored through the measurements of corona current and released power, as shown in Figure 3.12. As the discharge intensity during AC corona was found higher than that during DC case, AC corona treatment was therefore selected for this investigation. When using one set of the needles in 3 rounds of 100 h lasting tests, a clear difference with respect to the corona discharge intensity could be noticed between the new and eroded needles (Figure 3.12 (a)). Up to the voltage of 17 kV the current curves almost overlap, above the level of which, the difference becomes larger

3.1. Corona ageing test development

($\sim 45 \mu\text{A}$ at AC $20 \text{ kV}_{\text{rms}}$), giving rise to a difference in the released power (Figure 3.12 (b)) of $\sim 10 \%$ more for the eroded needles than for the new ones. It is therefore recommended that a new set of needles should be used for each of the 100 h lasting treatments.

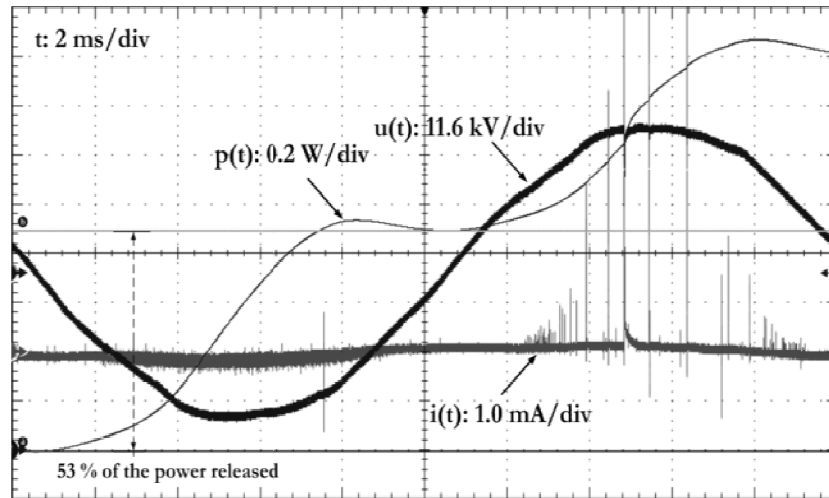


(a)

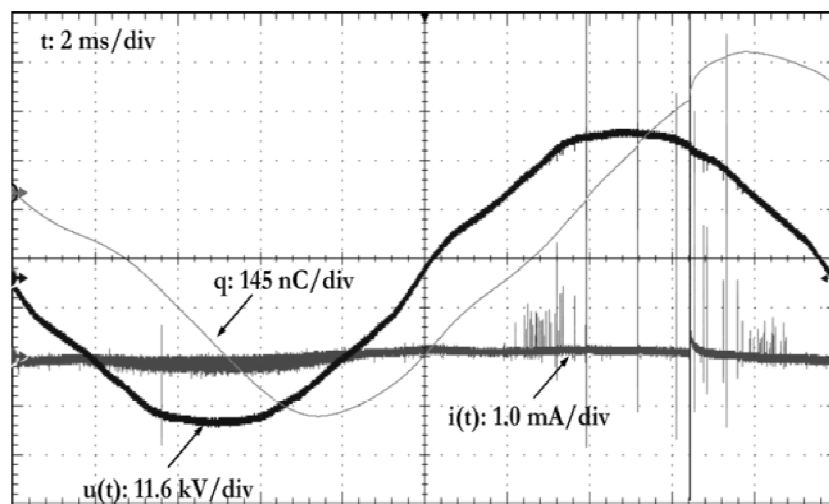


(b)

Figure 3.8: Oscillograms of the corona currents from the multi-needle electrode at the inception level of AC $10 \text{ kV}_{\text{rms}}$ (a) and at the treatment level of $20 \text{ kV}_{\text{rms}}$ (b) in the test chamber with air ventilation at the flow rate of 5 L/min .

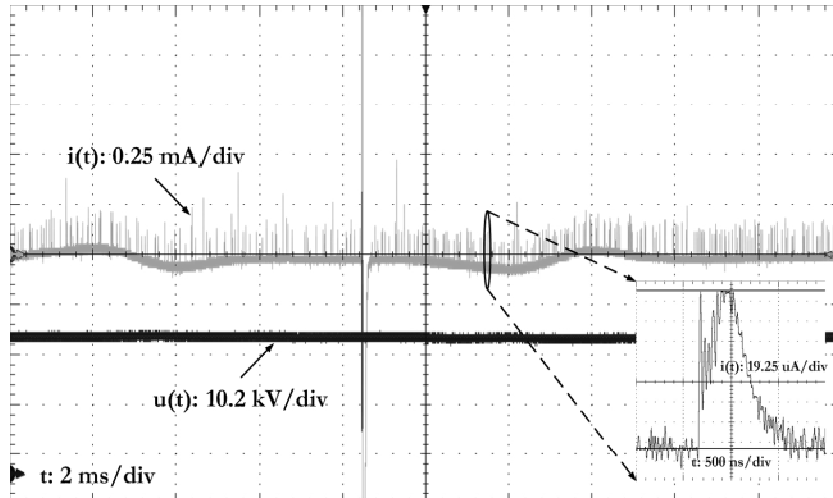


(a)

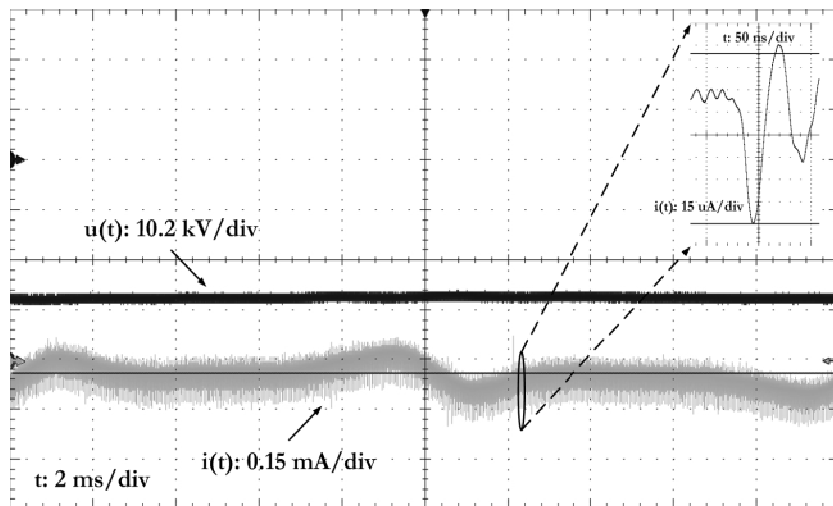


(b)

Figure 3.9: Oscillograms of power (a) and charge (b) released from the multi-needle electrode at AC 20 kV_{rms} in the test chamber with air ventilation at the flow rate of 5 L/min.

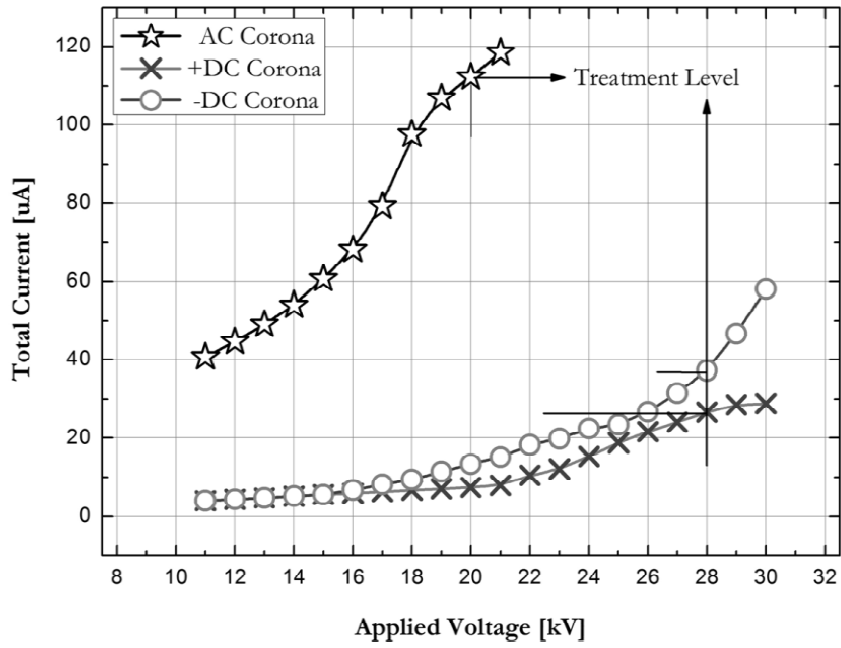


(a)

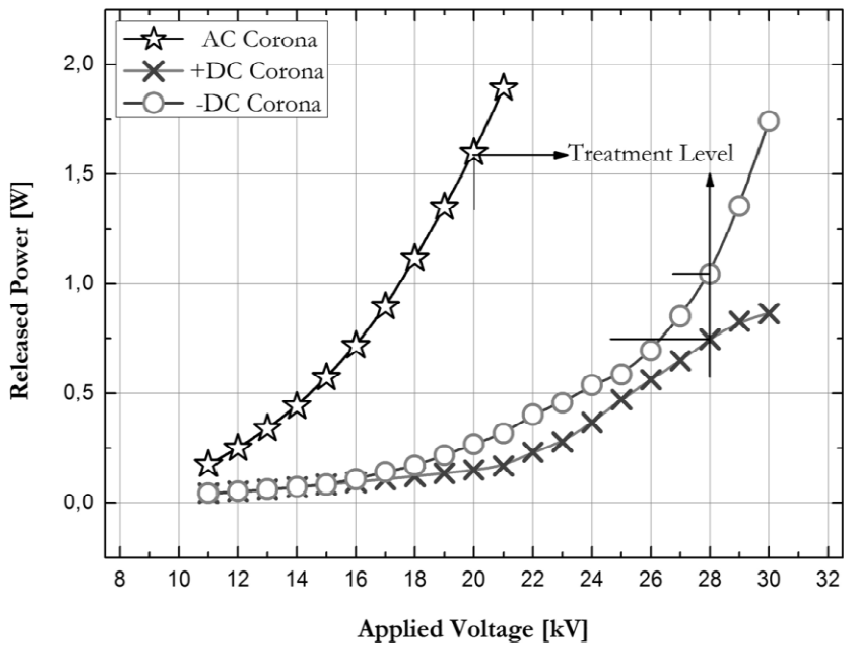


(b)

Figure 3.10: Oscillograms of the corona currents from the multi-needle electrode at the treatment levels of ± 28 kV for DC voltages: positive DC corona (a) and negative DC corona (b), in the test chamber with air ventilation at the flow rate of 5 L/min.



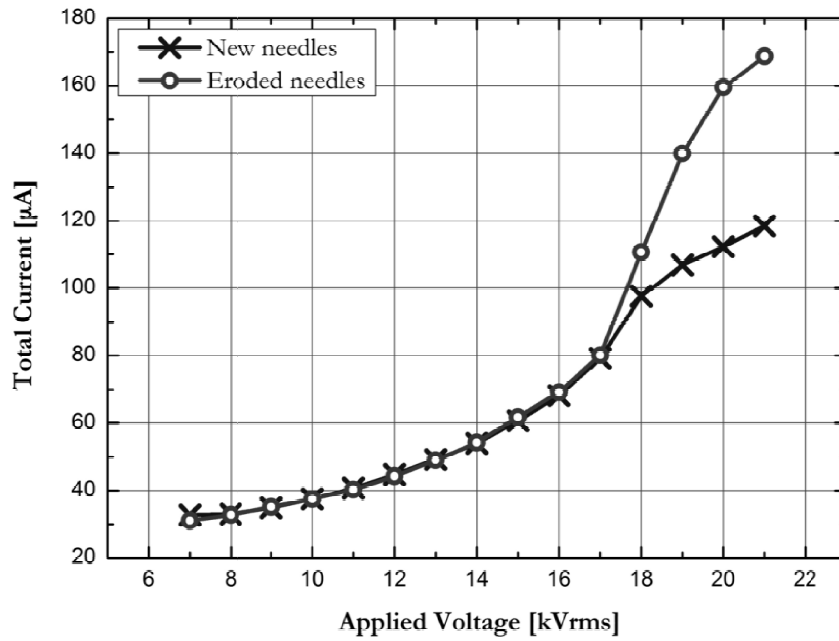
(a)



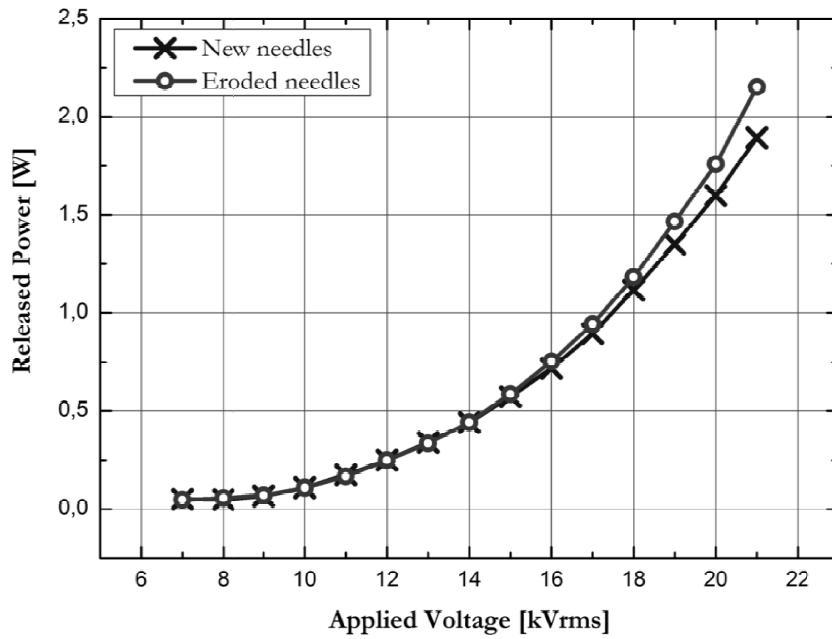
(b)

Figure 3.11: Comparisons of currents (a) and released power (b) from the multi-needle electrode, initiated by AC and DC corona discharges.

3.1. Corona ageing test development



(a)



(b)

Figure 3.12: Comparisons of the corona current (a) and released power (b) from the multi-needle electrode before and after 3 rounds of 100 h lasting treatments.

3.2 Material characterization techniques

3.2.1 Volume and surface resistivities/charging currents

Resistivity is one of the fundamental dielectric properties of polymeric materials and it can be used as an indicator of changes due to ageing. Resistivity is usually measured by applying a known voltage to a material sample, measuring the resulting current and calculating the sample resistance using Ohm's law. It is however important to point out that, due to the instantaneous influence of conduction and polarization processes in the investigated material, the resulting current is often varying with time. It is therefore recommended to perform the measurement long enough for reaching the state when polarization effect ceases and the remaining current is mainly due to conduction process [152, 153]. Following the measurement of the sample resistance, the physical dimensions of the sample such as its diameter and thickness are considered whereby the resistivity is then calculated. Besides, resistivity measurements are relatively susceptible due to the parameters dependency on external and internal factors [154]; the former include temperature, humidity, surface contamination, electrification time of the applied voltage, the latter consists of structural impurities and additives. Furthermore resistivity may also vary with the applied voltage.

In this work the measurements were carried out by means of Keithley 6517A electrometer equipped with a test fixture Keithley 8009, with a measuring range from 1 fA to 20 mA. The Keithley 8009 resistivity test fixture has a concentric ring electrode configuration to measure surface and volume resistivity. The concentric electrodes are made of stainless steel and enclosed in a shielded box to minimize stray electrostatic pick-up and measurement errors. Volume resistivity is measured across the sample thickness; see Figure 3.13 (a). Surface resistivity is measured along the surface of the test sample between electrodes, as shown in Figure 3.13 (b). The test fixture used enables easy change between surface and volume resistivity configurations by means of an integrated toggle switch. The Auto V-source of Keithley 6517A was used to achieve optimum accuracy for resistivity measurements. With the Auto V-Source selected, the electrometer was automatically set for either 40 V or 400 V. For the range of 2 T Ω through 200 T Ω , 400 V test voltage was set, which was thereby used to perform the resistivity measurements presented in this work. The adequate range for volume resistivity is 10^{13} to 10^{18} Ω cm and that for surface resistivity is 10^{13} to 10^{17} Ω .

It is important to state that comparisons of the measured resistivity data can only be done if all the samples compared are subjected to the same measurement conditions which include the applied voltage, the electrification time and environmental

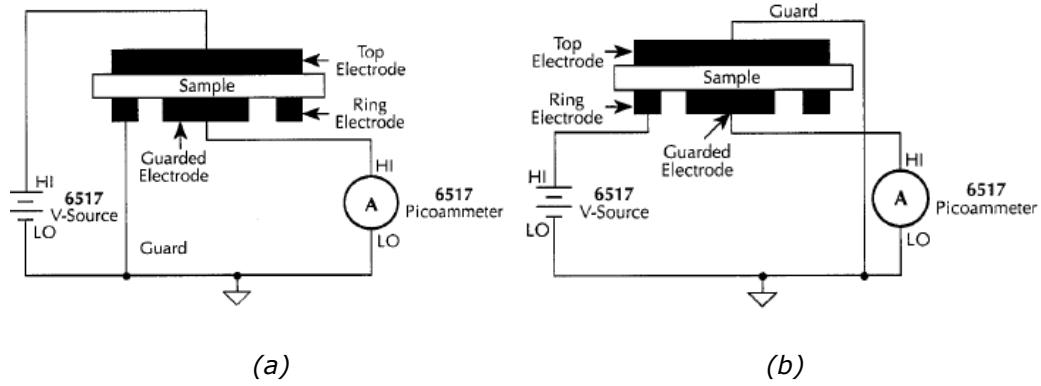


Figure 3.13: Electrode arrangements during resistivity measurements: volume resistivity test connection (a), surface resistivity test connection (b).

conditions. Having a constant applied voltage in all measurements ensures no-voltage dependency of the measured resistivity. A longer electrification time ensures that polarization processes in the material are completed so that stationary values of resistivity of the sample are reached. Maintaining the same environmental conditions, for instance temperature and humidity, is important for the integrity of results as humidity might have an influence on especially surface resistivity. Other factors to consider include contact between electrodes and the sample as well as keeping the electrodes free of dirt and other contaminants. The test samples must also be handled in such a manner as not to contaminate them before and during measurements as contaminants may influence the testing results. The other way around on top of these, the volume and surface charging currents allowing for the combination of conduction currents as well as polarization processes were monitored during each long lasting measurement to find out the difference as concerns the ageing influences induced by AC/DC corona exposures.

3.2.2 Frequency domain dielectric response

This technique refers to the slow polarization processes in an insulation material studied by measuring both the magnitude and phase of the current due to a sinusoidal excitation. Since single frequency component is considered at a time, the resulting current can be expressed as:

$$\begin{aligned}
 I^*(\omega) &= j\omega C_0 \left\{ \epsilon_\infty + \chi'(\omega) - j \left[\chi''(\omega) + \frac{\sigma_0}{\epsilon_0 \omega} \right] \right\} U^*(\omega) \\
 &= j\omega [C'(\omega) - jC''(\omega)] U^*(\omega) \\
 &= j\omega C^*(\omega) U^*(\omega)
 \end{aligned} \tag{3.3}$$

where $U^*(\omega)$ is the applied voltage; $\chi'(\omega)$ and $\chi''(\omega)$ are the real and the imaginary components of the complex susceptibility $\chi^*(\omega)$ accounting for all kinds of polarization processes within a dielectric, while $C'(\omega)$ and $C''(\omega)$ the real and the imaginary components of the complex capacitance $C^*(\omega)$. This equation allows the calculation of the complex permittivity by measuring magnitude and phase of the response current when C_0 (geometrical capacitance, determined by the dimensions of the measuring electrode as well as the thickness of the investigated samples) is known. The significance of the term $\sigma_0/\epsilon_0\omega$ in Equation 3.3 is that the DC conductivity contributes to the measured apparent dielectric losses. Therefore, it is not easy to distinguish between conduction and polarization losses in the insulation this way. Nevertheless, at low frequencies, the conduction loss is often dominating. During these conditions, $C''(\omega)$ or $\epsilon''(\omega)$ has a slope of -1 in the log-log scale and neither $C'(\omega)$ nor $\epsilon'(\omega)$ depends on the applied frequency. With additional low frequency relaxation mechanisms present, e.g. hopping, the distinguishability is lower. Another possible way of separating the two types of losses is by calculating the dielectric relaxation losses $\chi''(\omega)$ using the Kramers-Kronig transformation of $\chi'(\omega)$ [155]. For calculating $\chi'(\omega)$ it is necessary to subtract the ϵ_∞ from $\epsilon'(\omega)$. The accuracy of this technique depends on both the size of the measured frequency window and the resolution of the extrapolations of the measured data at the lowest frequency measured [155].

If the geometrical capacitance is known, the frequency dependent dissipation factor $\tan \delta(\omega)$ can be expressed as:

$$\tan \delta(\omega) = \frac{\epsilon''(\omega)}{\epsilon'(\omega)} \quad (3.4)$$

However, for this case information on important dielectric parameters ($\chi^*(\omega)$, σ and ϵ_∞) cannot be obtained since the dissipation factor is a ratio of the real and imaginary components of the complex permittivity. The practical significance of $\tan \delta(\omega)$ is that it presents the ratio of the energy dissipated per radian in the dielectric to the energy stored at the peak of the polarization [155].

Frequency domain dielectric response measurements were used in this work for identifying changes of the dielectric losses and relative permittivity of the polymeric specimens resulting from the corona ageing. The relative permittivity values were derived from the measured values of the capacitance and geometry of the measuring electrodes used for the resistivity measurements. The instrumentation used in this investigation is IDA 200 which allows performing measurements within the frequency range of 10^{-4} Hz to 1 kHz under a sinusoidal voltage excitation at 141 V_{rms} (200 V_{peak}).

3.2.3 Temperature dependency of dielectric response

The dielectric response in frequency domain is not only a function of frequency but also a function of temperature. However, for most materials, the spectral shape of the response does not change with temperature, at least over a temperature range during which the structure of the material does not alter significantly. This allows for normalizing the frequency dependent spectra for different temperatures by shifting the corresponding spectra until these coincide into a single curve, which is called a master curve. The master curve contains more information than a single temperature measurement since it covers a wider range of the frequency span [155]. The shift between any two frequencies (ω_1 and ω_2), in logarithmic scale, corresponding to the same magnitude of the spectral function at two temperatures T_1 and T_2 , can be expressed as:

$$shift = \log(\omega_1) - \log(\omega_2) = \frac{E_a}{k} \left(\frac{1}{T_2} - \frac{1}{T_1} \right) \quad (3.5)$$

where E_a is the activation energy and k is the Boltzmann's constant.

The master curve technique in frequency domain is applicable for both real and imaginary components of the frequency dependent complex susceptibility since both parameters contain similar information. Before using data from complex capacitance measurements to form a master curve, it is necessary to subtract the contribution of ϵ_∞ (dielectric permittivity at high frequencies) as well as $\sigma_0/\epsilon_0\omega$ (DC losses) from the complex permittivity [155]. However, in **Chapter 4**, master curves for the model epoxy formulations were formed directly by using the permittivity data obtained due to including the contribution from DC losses by the DR measurement, as elucidated in the previous section. In addition, relaxation processes of different formulations were characterized by different activation energy calculated by means of Equation 3.5.

3.2.4 Scanning electron microscopy

SEM images investigate surfaces by scanning with a high-energy beam of electrons in a raster scan pattern. The electrons interact with the atoms that make up the sample producing signals containing information about the surface topography, composition as well as other properties, such as electrical conductivity. The modification of surface topography in the polymeric materials investigated caused by the artificial corona exposure has been evaluated by means of SEM in this work.

The SEM examinations presented in **Chapter 4** were carried out with a Hitachi TM 1000 scanning electron microscope (chemical contrast method); test samples were

coated with a thin layer (5 nm) of Au/Pd prior to the analysis in order to avoid charging of the samples surfaces, which otherwise would reduce the quality of the images.

3.2.5 Infrared spectroscopy

IR-spectroscopy is a frequently used technology to characterize the chemical structure of a polymer near-surface region. This method allows for rapid sampling, it is sensitive and the cost of analysis is relatively low. On the other hand the limitation of the technique is mainly the possibility for performing quantitative analysis, which has been considered as its main drawback [156]. There are many approaches to apply IR-spectroscopy. A commonly used infrared (IR) spectroscopy by the attenuated total reflection (ATR) technique [12, 89, 157, 158], called the attenuated total reflection Fourier transform infrared spectroscopy (ATR-FTIR) was used for characterization of the polymer surfaces investigated in this thesis. The ATR technique enables identification of specific molecules and groups located in the surface layer, typically 1 to 10 μm deep [12]. Vibration modes of molecular bonds are analyzed in the range from 4000 cm^{-1} down to 400 cm^{-1} . A crystal with a high refractive index is placed in contact with the specimen surface and acts as a waveguide. The penetration length into the surface is in the same range as the wavelength of the radiation, though is also dependent on the inclination angle of the incident radiation beam and the refractive index of the crystal.

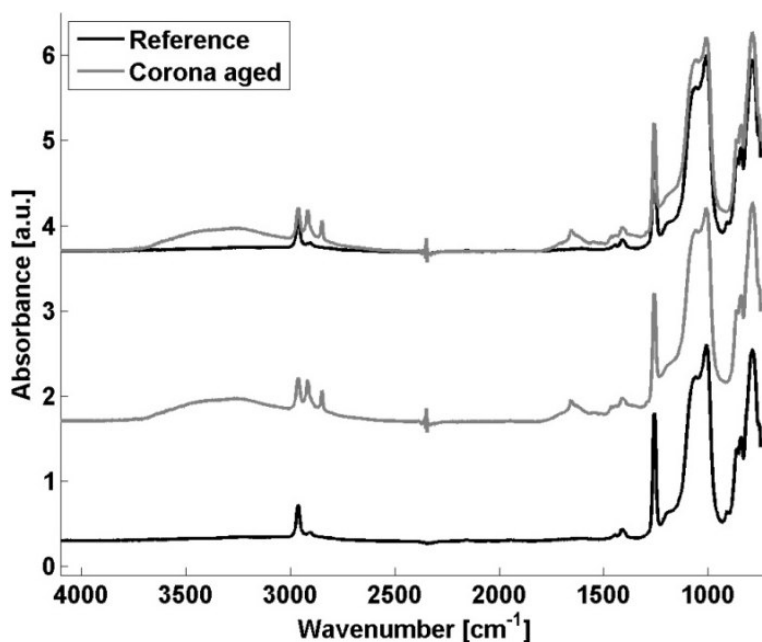


Figure 3.14: IR spectra of non-ATH-filled silicone rubber before and after 100 h long corona-ozone treatment.

A typical example of IR-spectrum of SIR is plotted in Figure 3.14 where the important chemical structural modifications due to corona ageing can be observed. A broad absorbance peak around 3300 cm^{-1} appears as a consequence of an increased amount of hydroxyl groups [18]. While oxidative crosslinking broadens the Si-O-Si peak at $\sim 1000\text{-}1200\text{ cm}^{-1}$, which can be clearly seen in the figure made by overlapping the two IR spectra before and after the 100 h lasting corona treatment. Additional information concerning the infrared spectroscopy of AC and DC corona aged polymeric material samples are presented in the following two chapters. In **Chapter 4** the FTIR analyses presented were carried out on a Bruker Tensor 27 spectrometer equipped with an attenuated total reflection (ATR) IR analysis device (Specac Silver Gate-ZnSe crystal); whereas in **Chapter 5**, the spectrometer used was a Perkin Elmer 2000X equipped with a 'Golden Gate' single reflection attenuated total reflection unit with a diamond crystal (angle of incidence 40°).

3.2.6 X-ray photoelectron spectroscopy

XPS or Electron Spectroscopy for Chemical Analysis (ESCA) is a surface sensitive analysis technique operated in ultra high vacuum ($\sim 10^{-9}$ mbar), and the penetration depth is typically several nm. If a photon from the X-ray source has enough energy to ionize an electron bounded in an atom, the electron is released and its energy is measured by a detector. Only electrons near the surface region are detectable with this method since the probability for an emitted electron to reach the detector is limited by the mean free path within the material. Electrons from regions deeper than ~ 10 nm can therefore not be registered by XPS. The resolution of XPS is in the order of 0.5 eV [159]. In addition to the information on the presence of different element on the sample surface, it is also possible, by performing high resolution scans, to further evaluate the composition of the surface. An example of high resolution scan on Si 2p of HTV rubber filled with silica is presented in Figure 3.15. Due to the surface oxidation by corona discharges, the dominant peak at 102.1 eV representing the organic form of PDMS splits and the second peak at ~ 103.5 eV the inorganic silica phase grows, as illustrated in Figure 3.15 (b) [12, 18, 99].

XPS analysis was employed in this study to investigate the modification of the chemical surface structure of the polymeric material samples, before and after the corona treatments. The XPS spectra were obtained by a PHI 5500 ESCA System utilizing Mg $K\alpha$ radiation ($h\nu=1253.6$ eV). The X-ray gun was operated at 14 kV and 400 W. Survey spectra were recorded at 93.9 eV pass energy and the high resolution spectra of the Si 2p peak was obtained at 23.5 eV pass energy. The binding energies were referenced to the C 1s binding energy of the hydrocarbon of the PDMS (285 ± 0.1 eV) [160]. The curve fitting of the Si 2p peak was performed with a non-linear least-square curve fitting program using a combination of Gaussian and Lorentzian functions.

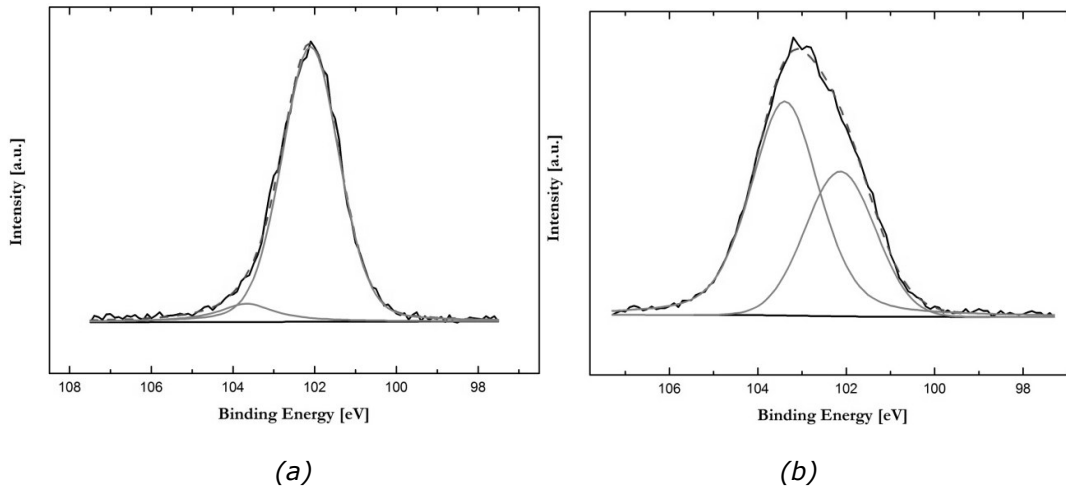


Figure 3.15: High resolution scan on Si 2p binding orbital performed on a virgin HTV rubber sample (a) and an HTV rubber sample exposed to corona discharges (b).

3.2.7 Tensile tests

To evaluate the influences of corona/ozone exposures on the mechanical integrity of the polymeric samples investigated, tensile tests were performed according to the method standardized in ISO 527 and ASTM D638. Specimens were punched out in dumbbell shapes and clamped in a jaw-like apparatus where each end is clamped in one jaw [161]. The tensile strength (in MPa) and the elongation at break (in %) were evaluated in a universal 100 kN test machine with a 500 N load cell at a tension speed of 500 mm/min. The strain at the tensile tests was measured with a Lloyd long distance extensometer.

3.2.8 Dynamic contact angles

Contact angle measurement is a method to characterize surface wettability and is probably the most used technique in studies of loss and recovery of hydrophobicity in SIR. The hydrophobicity of a solid surface is determined by its free surface energy [12, 28]. It is often defined on the basis of the static contact angle between the surface and a water droplet. A surface can be considered as hydrophilic if the contact

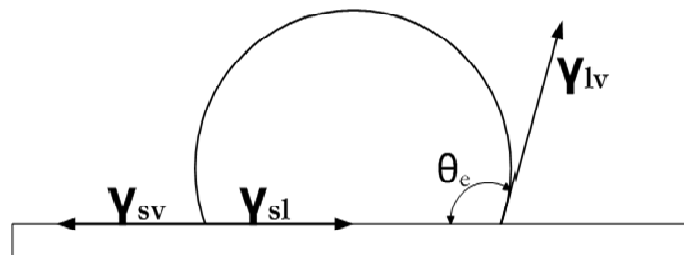


Figure 3.16: Illustration of the interfacial surface tensions and the equilibrium contact angle in Yong's equation.

3.2. Material characterization techniques

angle is $< 90^\circ$ or hydrophobic if the angle is $> 90^\circ$. The fundamental relation is as described by the Young equation:

$$\gamma_{sv} - \gamma_{sl} = \gamma_{lv} \cos \theta_e \quad (3.6)$$

where γ_{sv} , γ_{sl} and γ_{lv} are the interfacial tensions between solid/vapor, solid/liquid and liquid/vapor phases respectively, and θ_e is the equilibrium contact angle (defined in Figure 3.16).

The most commonly used method for contact angle measurements is the sessile drop technique. A droplet of purified liquid is placed on a surface using a syringe. The resulting angle between the droplet and surface is measured, generally using a goniometer or a charge coupled device (CCD) camera fitted onto a microscope. The angle formed by adding liquid to the droplet, causing it to advance over the surface is named the advancing contact angle (θ_a). The angle formed by removing liquid from the droplet, causing it to recede over the surface, is named the receding contact angle (θ_r) (Figure 3.17). The difference between the advancing and the receding contact angle is referred to as the hydrophobicity hysteresis and it is dependent on the surface roughness and the surface heterogeneity [162]. The contact angle and the hysteresis are also dependent on the contact time between the droplet and the surface. The contact angle recorded for SIR shows a decrease with increasing contact time of the water droplet [159]. Segmental motions of the polymer and water diffusion into the rubber may cause these time dependent effects [159]. The advancing contact angle tends to reflect the hydrophobic (lower surface energy) regions whereas the receding contact angle reflects the hydrophilic (higher surface energy) regions.

The sessile drop technique was also employed in this work to trace the dynamics of hydrophobicity recovery of AC/DC corona/ozone treated HTV rubber samples. The details of the investigations are presented in **Chapter 5**.

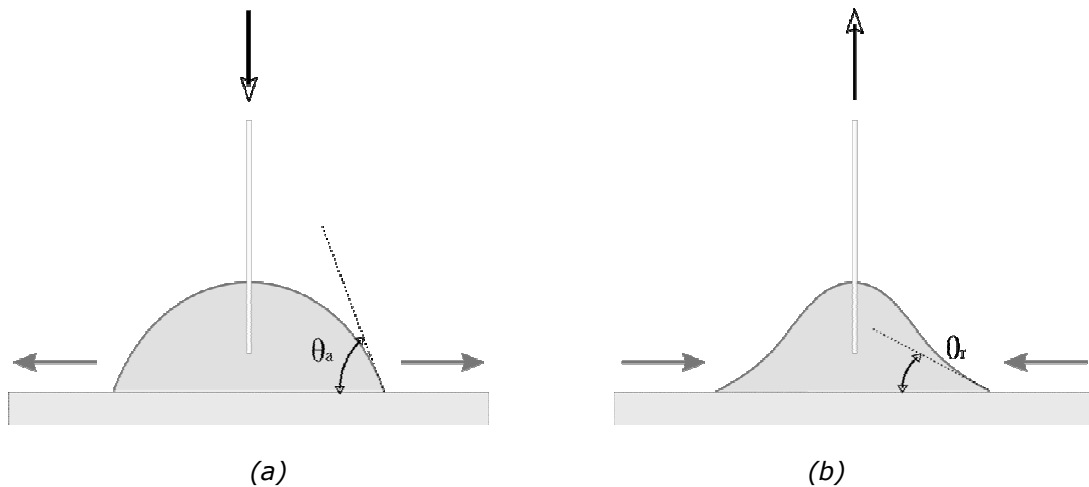


Figure 3.17: Sessile drop technique for contact angle measurements. Measurements of advancing contact angle θ_a (a), receding contact angle θ_r (b).

3.3 Concluding remarks

This chapter mainly discusses the designing of the test arrangement and the defining of test conditions; both the adopted corona and the test parameters have been carefully analyzed. A forced ventilation of the chamber with dry air flowing at 5 L/min was set for maintaining a controlled concentration of humidity, ozone, and gaseous byproducts inside the chamber. By performing static electric field simulation using the finite element method (FEM), the distance between the tip of innermost needle and the surface of the specimen to be treated was set at 40 mm to ensure a homogeneous electric field in the vicinity of the sample during the corona treatments. Duration of the test was 100 h and the voltage applied to the corona electrode was 20 kV_{rms} for AC corona treatment as well as ± 28 kV for DC corona treatments, which are the peak values of the applied sinusoidal AC voltage. The voltage level was determined based on measurements of released AC power of ~ 1.5 W from the multi-needle corona electrode. The AC/DC corona discharge intensities were characterized by measuring the corona currents as well as the power released from the multi-needle electrode; the DC corona discharge intensity was found to be weaker than that in the AC case. Elastomeric specimens were mechanically stretched by 3 % during the corona exposure. Also the erosion of the electrode needles was monitored through observations of the corona current and the released power. It has therefore been recommended that for securing repeatability of test results, a new set of needles should be used for each of the 100 h lasting treatment. Kitagawa ozone detection system was employed to monitor the ozone concentration during the process of corona treatments.

To evaluate the ageing effects induced by AC/DC corona/ozone treatments, material characterization methodologies as well as techniques either for tracing the material property changes from a macroscopic point of view (volume/surface resistivities/charging currents and dielectric response measurements, tensile tests, hydrophobicity measurement), or for analyzing the surface oxidation as well as the physical and chemical structure variations of the materials investigated from a microscopic point of view (SEM, FTIR, XPS) were introduced in this chapter also.

4 AC corona ageing tests

4.1 Testing procedure

4.1.1 Procedure for the samples involved in RRT

The testing procedure presented in this section has been proposed for evaluating the resistance to AC corona/ozone treatment of five commercial grade polymeric material specimens within the organized by CIGRE WG D1.14 Round Robin Test (RRT). Four samples of each material are necessary for fulfillment of the whole testing program. The program starts with preparation of the samples for evaluation of electrical and mechanical properties as well as for performing chemical and structural analyses of the changes caused by corona/ozone treatments. The samples to be treated are consequently labeled A, B and C and the direction of mechanical stretching must be clearly marked. Sample A is used for evaluating the mechanical strength, sample B for the electrical measurements and sample C for the structural and chemical analyses. To describe the condition of a specimen the following terms are used: ‘initial’ refers to the state before the exposure while ‘treated’ refers to the state after 100 h lasting exposure to corona discharges. The recommended time sequence for the whole procedure is illustrated in Figure 4.1 and the overall process for the electrical measurements is summarized in the flow chart diagram shown in Figure 4.2.

For each material batch to be tested, the procedure is preceded by the conditioning of specimens in room environment. The initial specimens are cleaned with isopropanol or another suitable solvent and then left in air until drying out (3 h at least). The cleaned specimen designated for mechanical testing (the sample labeled A) is thereafter directly mounted in the chamber for corona treatment, whereas the specimen for structural and chemical analysis (the sample labeled C) is wrapped with aluminum foil waiting for the corona treatment. The specimen for electrical measurements (the sample labeled B) is cut to fit the test fixture (Keithley 8009) for

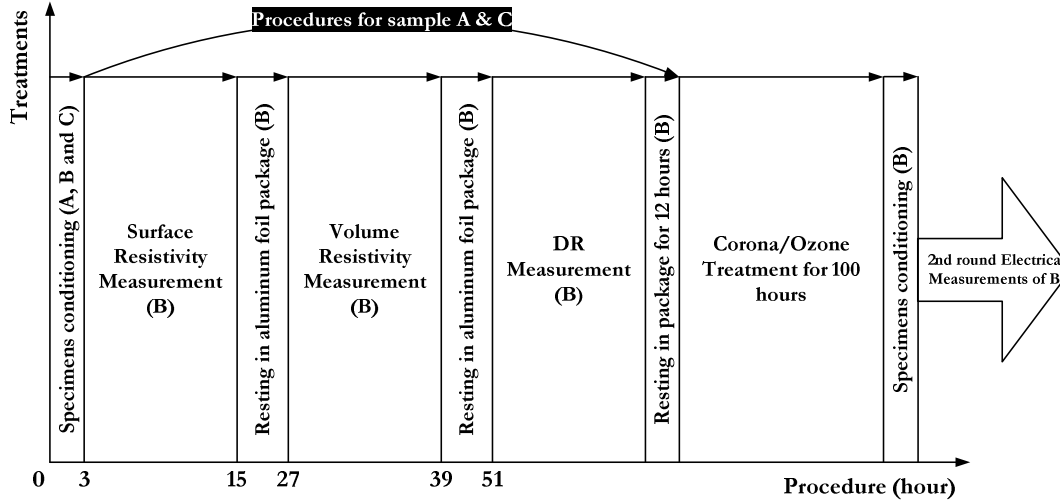


Figure 4.1: Recommended time sequence for the overall procedure.

resistivity/charging currents measurements. The resistivity/charging current measurements are performed twice, i.e. before and after the corona treatment.

This treatment procedure can be summarized as:

- The testing (1st treatment) starts with specimen A, which afterwards is used for the mechanical characterization.
- Electrical measurements are performed prior and after 2nd corona treatment on specimen B.
- 3rd treatment is applied to specimen C, which afterwards together with the fourth specimen acting as initial reference is used for chemical analyses.

4.1.2 Procedure for the model nano-epoxy samples

A batch of epoxy based compositions filled with micro- and nano-fillers of silica at different proportions has also been tested. For investigating the influences of micro-/nano-filler compositions on the corona/ozone resistance, two sequences of the corona/ozone treatments, lasting 100 h each, were conducted. Measurements of surface and volume charging currents as well as of dielectric response in frequency domain were carried out on both the reference samples and the treated samples after each of the two rounds of the corona treatment.

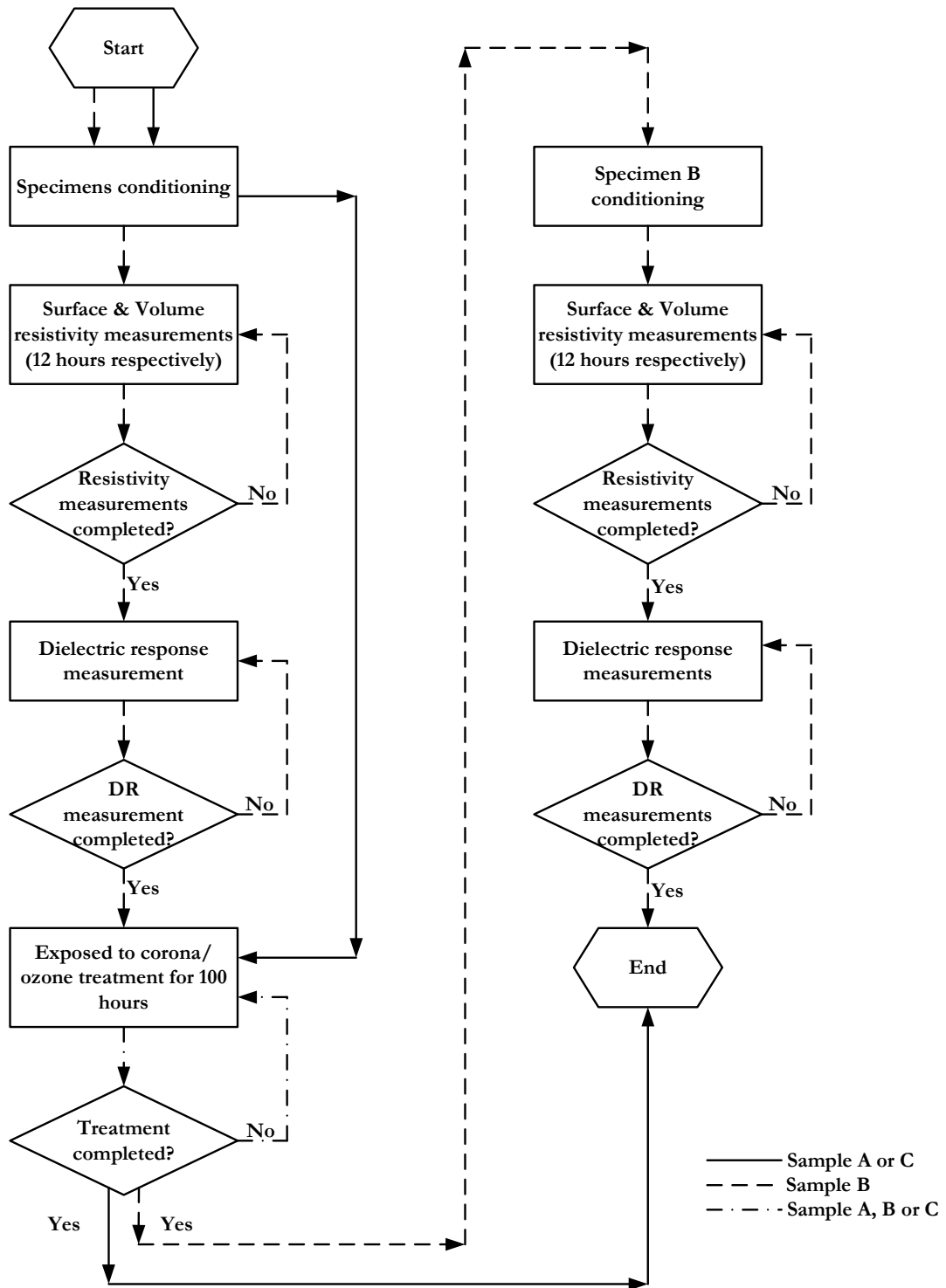


Figure 4.2: Flow chart of the testing procedure.

4.2 CIGRE Round Robin Test

4.2.1 Material description

Commercial grades of five different materials designated for applications in high voltage outdoor conditions were used for checking the proposed test procedure. These included samples of epoxy resin (HCEP CFB 500 – from Huntsman), two rubbers based on silicone resins (LSR HV 1551/55P – from Dow Corning and HTV PS 310 – from Wacker), EVA elastomer (from Tyco Electronics), as well as EPDM elastomer (from Sediver). Samples of each of these materials were evaluated according to the above described procedure.

4.2.2 Ozone concentration

The average ozone concentrations during the treatments of the five types of polymeric material specimens have been measured at airflow of 5 L/min at constant temperature of 20 ± 3 °C and the results are presented in Figure 4.3. Clear differences in the ozone concentrations were found, depending on the material type. One possible reason for this effect is that corona intensity during the treatment, and therefore the rate of ozone generation, became modified by the electric charges accumulated on the sample surfaces.

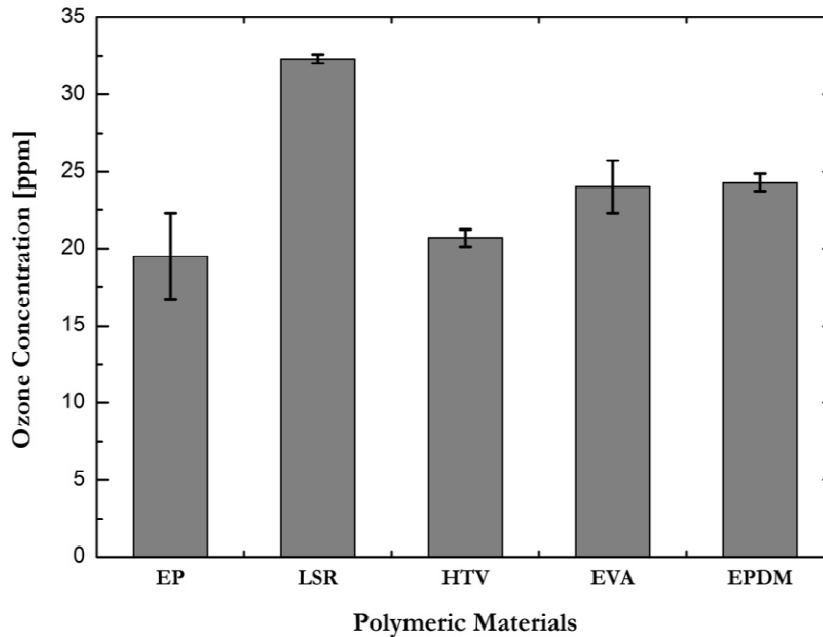


Figure 4.3: Ozone concentration measured during the AC corona treatments of the investigated samples.

4.2.3 Dielectric properties

Figure 4.4 and Figure 4.5 demonstrate the behavior of volume and surface charging currents for the polymeric materials investigated, which both increased after the treatments with exception for the volume charging current of the LSR sample.

The results summarized in Table 4.1 show that the treatment by corona/ozone has obviously influenced the levels of both surface and volume resistivities of practically all the tested specimens, though more severe effects could be observed in surface resistivity. The arrows in the columns ‘effect of treatment’ indicate the varying trends in logarithmic scale as compared with the initial reference values. For surface resistivity the respective decrease varied between one and four orders of magnitude. It decreased most for the EPDM sample, though the reduction was also strong for the EP and SIR materials (both the LSR and HTV rubbers). Only the EVA sample did not exhibit much effect.

Table 4.1: Values of surface and volume resistivities for the tested materials calculated for the time of measurement equal to 3.6×10^4 s.

Batches	Surface resistivity ($\Omega/\text{sq.}$)		Effect of treatment (decades)	Volume resistivity ($\Omega \text{ m}$)		Effect of treatment (decades)
	Initial	Treated		Initial	Treated	
EP	2.14×10^{17}	3.02×10^{15}	↓ 1.91	3.91×10^{16}	3.85×10^{15}	↓ 1.01
LSR	5.72×10^{16}	1.32×10^{15}	↓ 1.44	1.47×10^{14}	2.20×10^{14}	↑ 0.07
HTV	1.52×10^{17}	1.46×10^{14}	↓ 3.01	3.90×10^{13}	1.80×10^{13}	↓ 0.21
EVA	4.16×10^{16}	2.88×10^{16}	↓ 0.13	3.08×10^{13}	2.26×10^{13}	↓ 0.08
EPDM	2.55×10^{17}	8.37×10^{13}	↓ 3.42	1.72×10^{14}	1.28×10^{14}	↓ 0.04

Less pronounced changes (reductions) were found in volume resistivity of all the materials except for the LSR sample, for which a slight increase was noticed instead. A ‘recovery’ of volume resistivity of the treated LSR sample had also been noticed after a rest for a couple of weeks in laboratory environment. It is important to stress that, despite the fact that the 100 h long treatment influenced the surface and the volume resistivity values of the treated materials, the changes incurred still remains considerably low as compared to the levels that could be considered as dangerous for their performance in outdoor environments.

As illustrated by Figure 4.6 and Figure 4.7 the results of DR measurements did not exhibit high sensitivity to the corona-ozone treatment. Though the dependences of

Chapter 4. AC corona ageing tests

dielectric permittivity upon frequencies do not follow similar regularities for the different materials tested, some weak variations were observed in the respective spectra. These however were more likely to be a result of geometrical effects in the test fixture during sample fixing rather than a real effect of the treatment. An appearance of an anomalous behavior of the real part of permittivity of LSR and HTV elastomers, in form of a peak in the low frequency range, should also be noticed. This behavior was also observed earlier [163] and requires further elucidation. It is probably associated with measurement conditions used in the test.

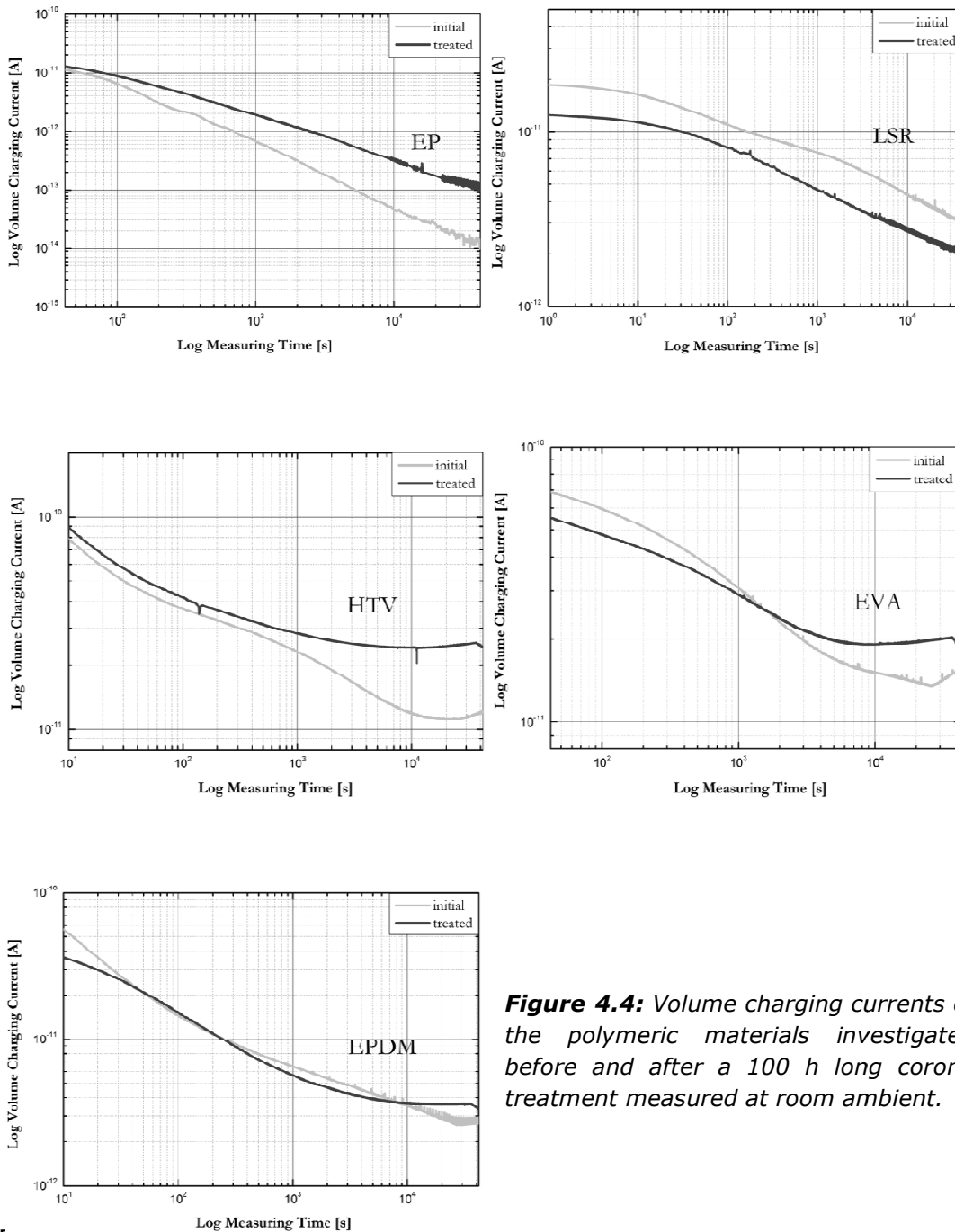


Figure 4.4: Volume charging currents of the polymeric materials investigated before and after a 100 h long corona treatment measured at room ambient.

4.2. CIGRE round robin test

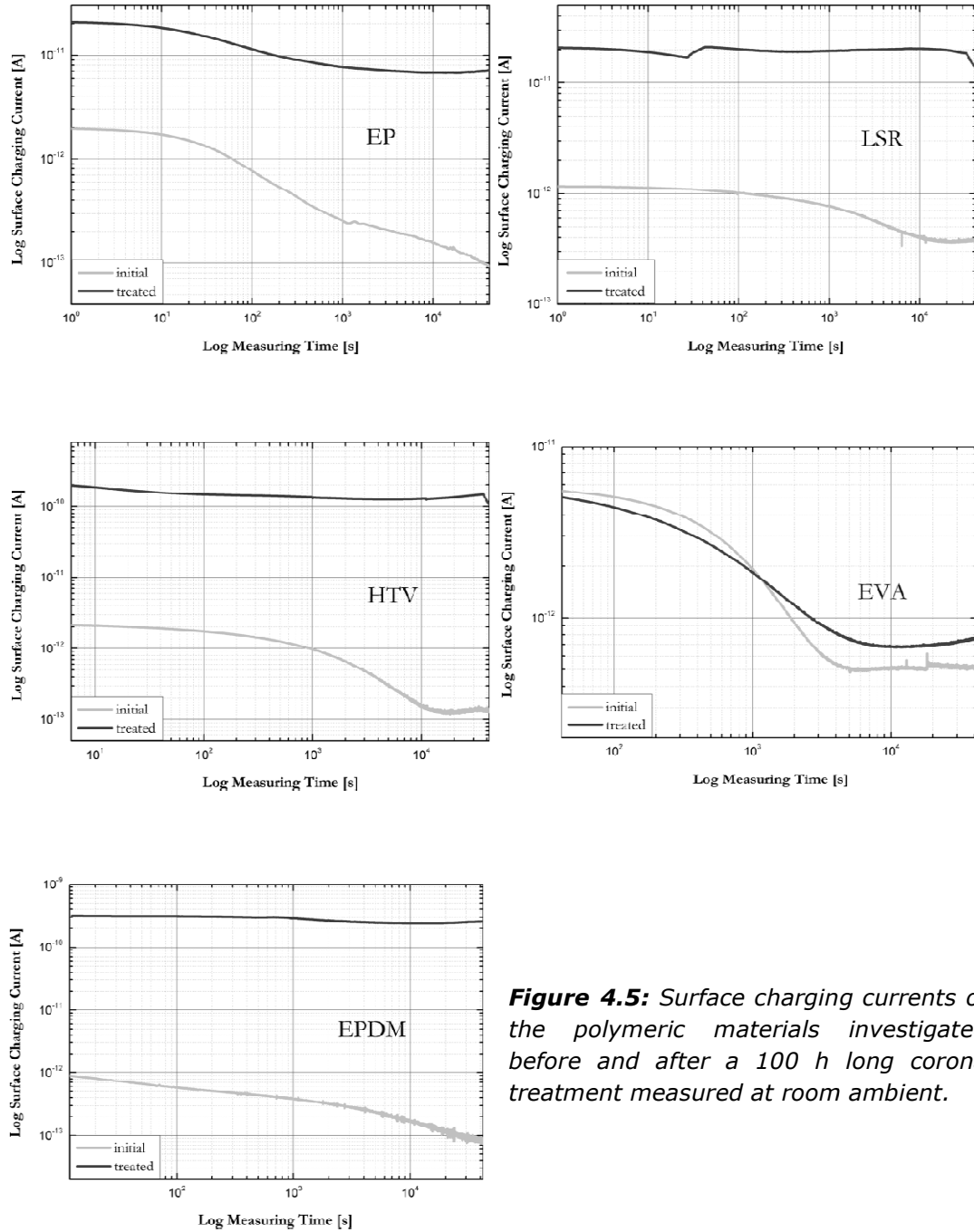


Figure 4.5: Surface charging currents of the polymeric materials investigated before and after a 100 h long corona treatment measured at room ambient.

Chapter 4. AC corona ageing tests

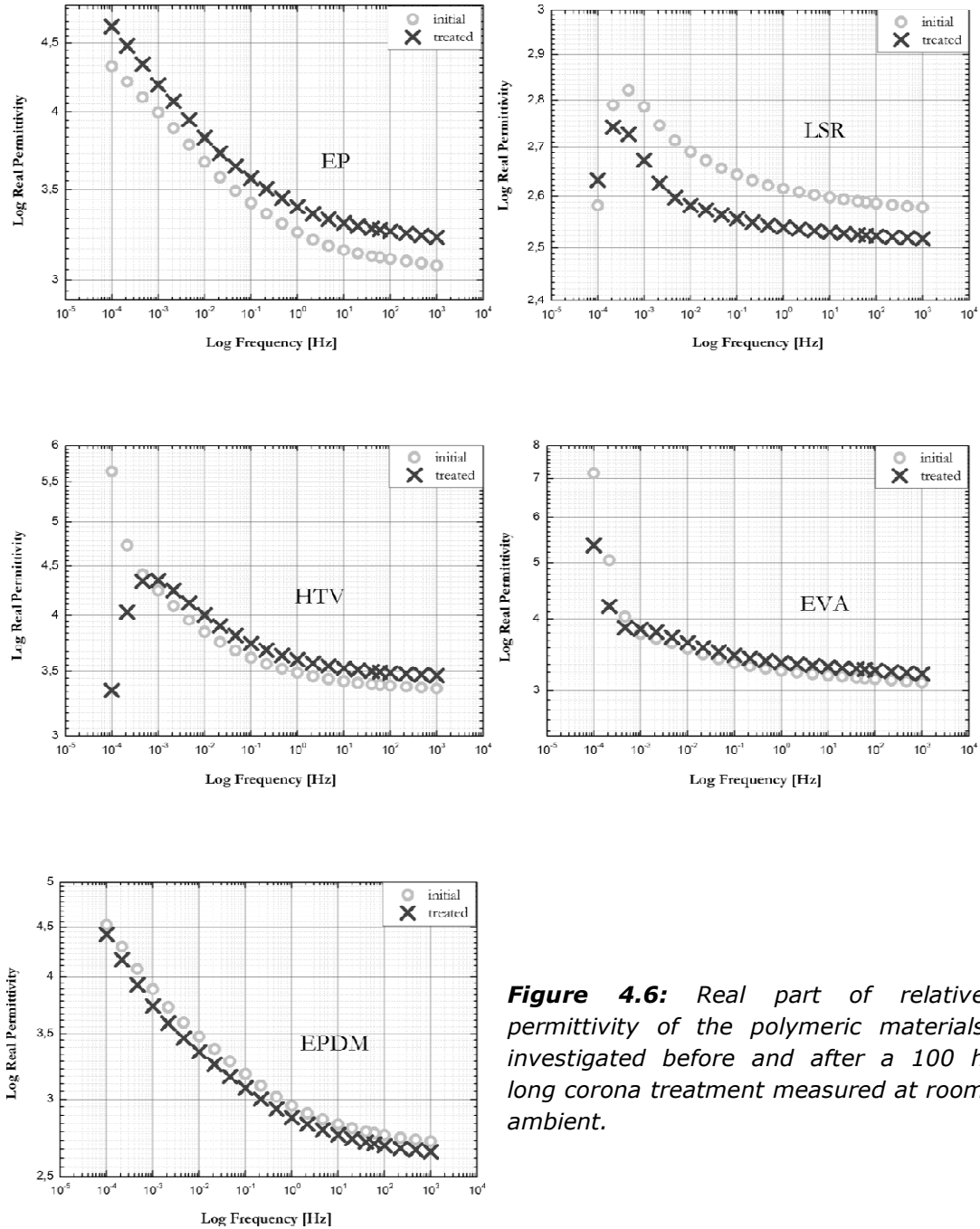


Figure 4.6: Real part of relative permittivity of the polymeric materials investigated before and after a 100 h long corona treatment measured at room ambient.

4.2. CIGRE round robin test

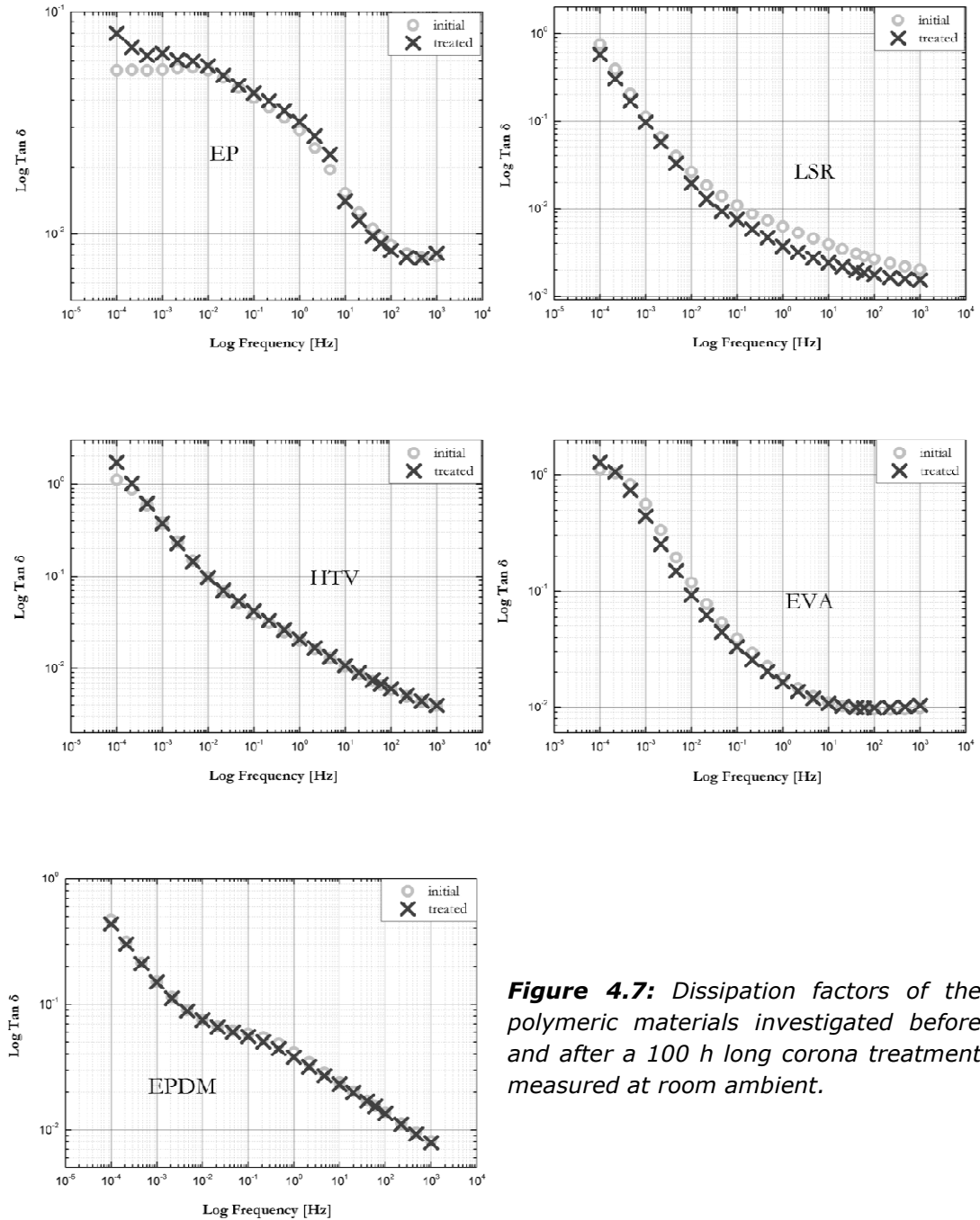


Figure 4.7: Dissipation factors of the polymeric materials investigated before and after a 100 h long corona treatment measured at room ambient.

4.2.4 Mechanical properties

It is plausible to assume that for applications in outdoor insulation, polymeric housing materials should retain their mechanical integrity. Damages in form of cracking, splitting or cutting are not acceptable. Therefore one of the main purposes of the testing relied on assessing the influence of the corona/ozone exposure on the mechanical properties of the materials. The mechanical properties were evaluated separately by the manufacturers of the tested material samples. As explained in the previous section, one of the treated samples was used for evaluating this influence on changes in tensile strength and elongation at break. For obtaining statistically significant results, specimens for the mechanical testing were cut out, as illustrated in Figure 4.8 (a). This way a fair number of samples could be obtained. An example of tensile strength results obtained on specimens cut of a treated EVA sample is illustrated in Figure 4.8 (b). A reduction of the strength among specimens cut of the central part of the treated sample can be noticed compared to the specimens located at the sample edges (practically not treated areas).

All of the tested elastomeric materials, i.e. SIR, EPDM and EVA, showed some reduction of the tensile strength (3-25 %) as well as elongation at break. It is believed that, the changes were however not of the type that might endanger mechanical integrity of insulators made with these materials. Absolute limits for the decay of the mechanical properties are still to be set and agreed upon internationally.

4.2.5 Physical and chemical characteristics

The surfaces of the tested materials were also characterized in order to check if the corona and ozone treatment yields any structural and chemical modifications: Physical and chemical analyses of the surface layers of each material before and after the treatment were carried out by means of optical observations and SEM. Additionally FTIR analysis was performed in the case of SIR samples.

Table 4.2 provides a summary of the visible modifications of color, aspects, and superficial structures that can be observed on the different materials after the 100 h long treatment.

In the case of LSR sample, SEM (see Figure 4.9) shows that corona treatment leads to the formation of micro-cracks. These cracks are mainly located in the centre of the zone that has directly been exposed to corona discharges. The formation of such surface cracks confirms previously published results [7]. These small cracks ($<2 \mu\text{m}$) are the result of a superficial oxidation of the upper silicone layer by ozone (thickness 10-12 nm) [120, 164, 165].

The superficial oxidation was confirmed by FTIR analysis, as illustrated in Figure 4.10. The following typical chemical bonds can be identified in the spectrum before corona treatment: C-H bonds in CH₃ groups at 2960 cm⁻¹, Si-CH₃ bonds at 1260 cm⁻¹ as well as Si-O-Si bonds at 1054 cm⁻¹. After the treatment, OH groups at 3700-3200 cm⁻¹ (silanols, Si-OH) are visible. In addition, the ratio of Si-CH₃/Si-O-Si decreases from 0.57 to 0.3 (optical density ratio) after the corona treatment [96]. According to this report, C=O bonds could also appear at 1740 cm⁻¹ after corona exposure, but no such groups were detected in this work. The increase in detected amount of Si-O-Si bonds is due to the formation of silica at the surface, which is the result of the condensation of Si-OH groups that are formed by the oxidation process of the Si-CH₃ groups [12]. Despite the surface modifications observed, the capability for hydrophobic recovery remains very efficient; within a few hours of rest the LSR sample surface can recover to its original level of hydrophobicity [96]. This is the result of diffusion of the low molecular weight (LMW) silicone derivatives that are present within the material or formed by the corona treatment [89, 103, 104, 166].

In contrast to the LSR, no cracks were observed after the treatment in the case of HTV silicone rubber material; only some small holes (craters) were visible by SEM, as shown in Figure 4.11. The FTIR spectra shown in Figure 4.12 yielded the same conclusion as for the case of LSR material, although the ratio of Si-CH₃/Si-O-Si decreased to a less extent and water bonds appeared, as well. In addition the OH groups that correspond to ATH vibration decreased too, which can be explained by the fact that the oxidized surface layer prevented the ATH vibration for the AC corona/ozone treated HTV elastomer sample case.

Figure 4.13 shows that the EVA material did not exhibit any visible modifications of the superficial physical-chemical structures after the treatments. There are no cracks, similarly as in the case of HTV rubber. The absence of surface modification is perhaps due to the high hardness level (high filler load) of those materials (HTV – 74 ShA and EVA – 95 ShA). This conclusion is however not in line with findings of Yong et al [138], who reported formation of cracks on EVA after corona discharge exposure. The difference might be due to the fact that EVA studied in [138] contained a lower amount of ATH filler. Also in case of EP no visible surface modification could be noticed, as illustrated in Figure 4.14.

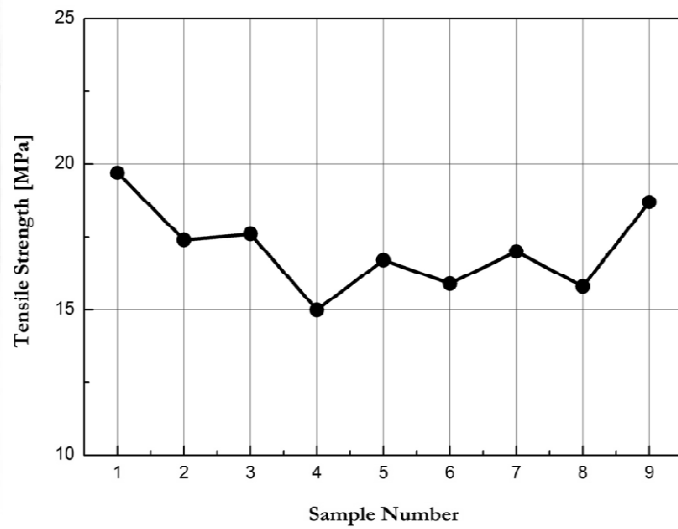
The last studied material was EPDM rubber. It appeared that corona treatment yielded also some surface modifications in form of micro-cracks, as shown in Figure 4.15. The width of the cracks was less than 1 μm. It is supposed that also in this case the effect was the result of a superficial oxidation.

Table 4.2: Optical and SEM observations after corona treatments.

	Optical observations	SEM
LSR	Irisation which disappears with time	Visible cracks (<2 μm)
HTV	Brightness of treated zone	Some visible holes (<2 μm)
EVA	No modification	No modification
EP	No modification	No modification
EPDM	Change of color & brightness	Visible cracks (<1 μm)

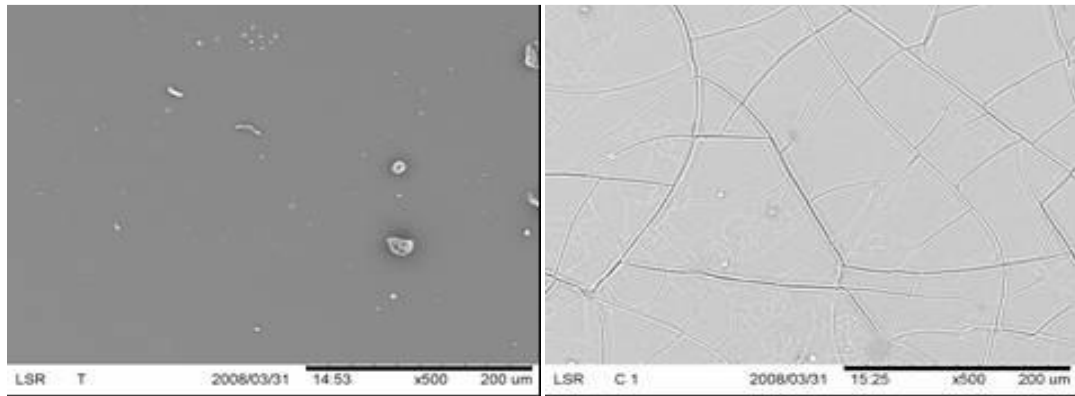


(a)



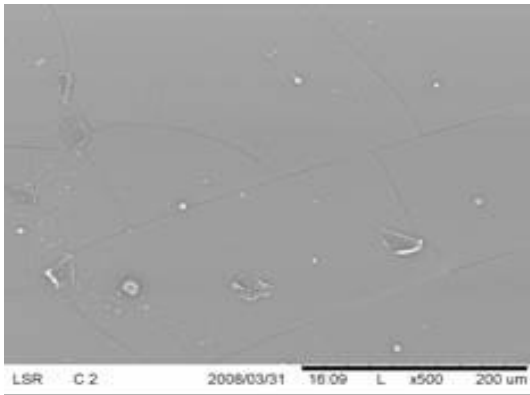
(b)

Figure 4.8: Preparation of specimens for evaluation of mechanical properties (a) and tensile strength distribution among specimens cut from a corona/ozone treated EVA sample (b).



(a)

(b)



(c)

Figure 4.9: SEM images of the LSR sample surface before and after corona treatment (untreated sample (a), central part (b) and periphery (c) of sample after corona exposure).

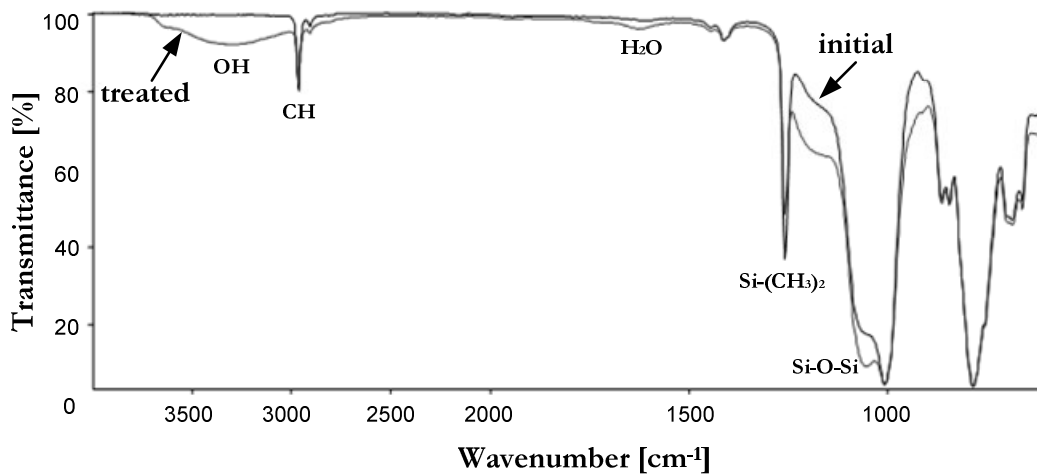


Figure 4.10: FTIR spectra of the LSR sample before and after corona treatment.

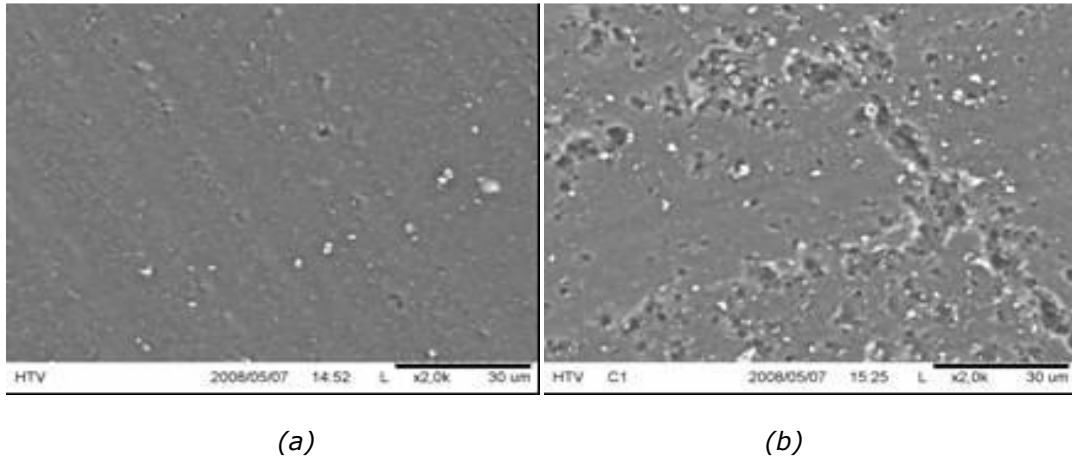


Figure 4.11: SEM images of the HTV silicone rubber sample surface before and after corona treatment (untreated sample (a) and corona exposed material (b)).

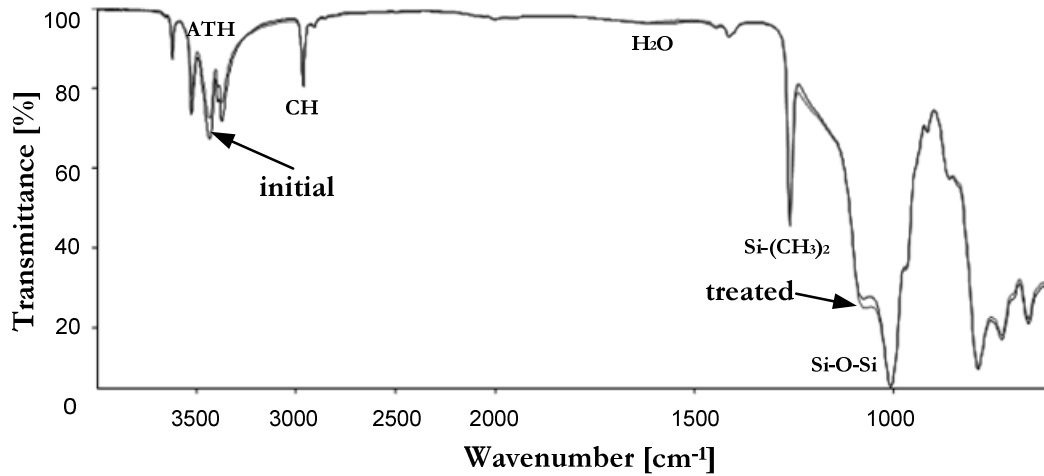
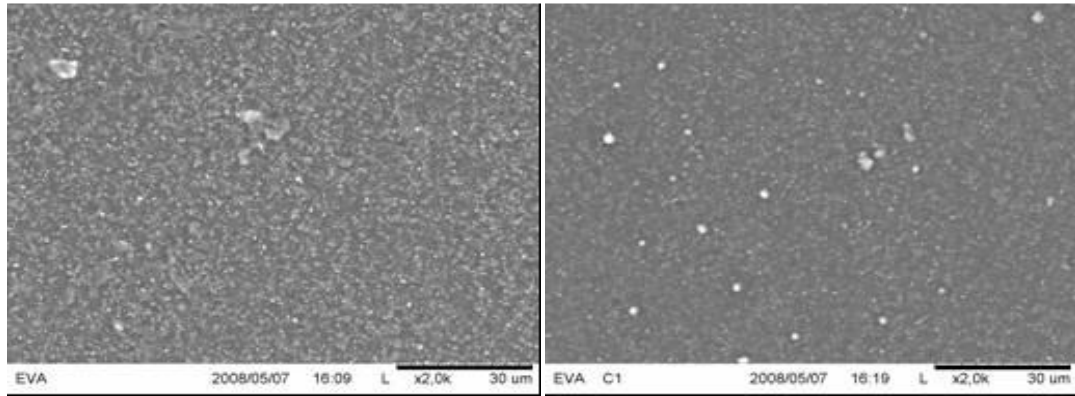


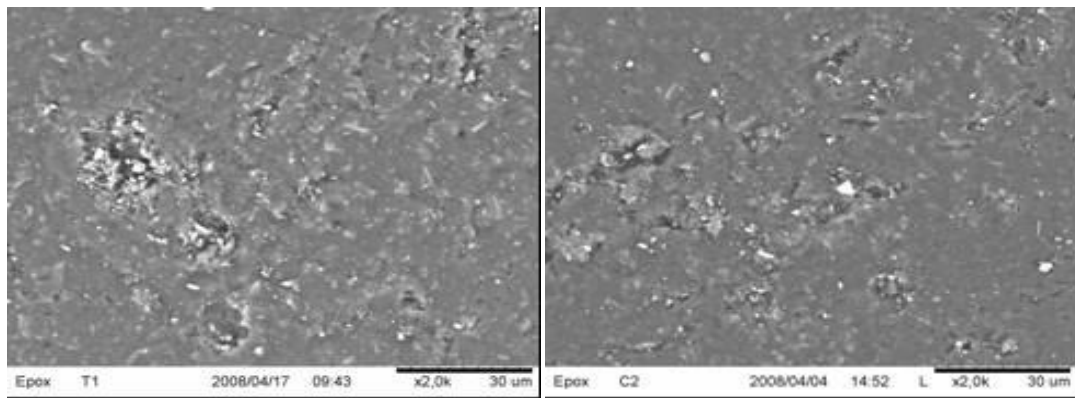
Figure 4.12: FTIR spectrum of the HTV elastomer before and after corona treatment.



(a)

(b)

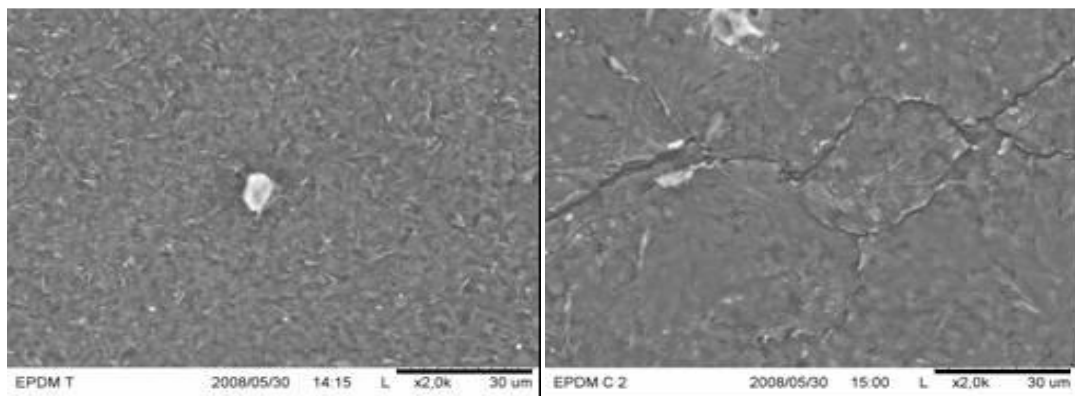
Figure 4.13: SEM images of the EVA sample surface before and after corona treatment (untreated sample (a), corona exposed sample (b)).



(a)

(b)

Figure 4.14: SEM images of the EP sample surface before and after corona treatment (untreated sample (a), corona exposed sample (b)).



(a)

(b)

Figure 4.15: SEM images of the EPDM sample surface before and after corona treatment (untreated sample (a), corona exposed sample (b)).

4.3 Tests upon epoxy micro- and nano-composites

4.3.1 Preparation and characterization of specimens

Details on compositions of the tested samples are provided in Table 4.3.

Table 4.3: Description of the model epoxy compositions.

Epoxy Nanocomposites	Denotation
5 wt.% nano	P1
60 wt.% micro & 5 wt.% nano	P2
62.5 wt.% micro & 2.5 wt.% nano	P3
65 wt.% micro	P4
65 wt.% micro & 5 wt.% nano	P5

Plates of epoxy composites were prepared according to the following procedure. The components were preheated to 65 °C and mixed for one hour at 65 °C. The mixture was degassed, cast into a mould held at 90 °C and degassed again. The cast samples were cured at 90 °C for 2 h and post-cured at 140 °C for 24 h. The oven was turned off and the samples were left inside for slow cooling.

Details regarding the mechanical characterization as well as the thermal and process properties of the investigated epoxy formulations were reported in [167]. When comparing the mechanical properties of micro-filled epoxy (P4) to those of epoxies where 5 wt.% of micro-filler is either substituted with nano-filler (P2) or 5 wt.% of nano-filler is added additionally (P5), a slight increase in Young's modulus, tensile strength and elongation at break is found. At the same time the toughness of the systems decreased with the addition of nano-fillers, indicating a poor particle-matrix interaction of the nano-filler particles, similarly as shown in a study of Sanctuary et al. [168].

4.3.2 Dielectric properties

Figure 4.16 and Figure 4.17 demonstrate behavior of the volume and surface charging currents for the epoxy compositions investigated. As regards the volume charging currents it appears obvious that practically none of the compositions reaches a

4.3. Tests upon epoxy micro- and nano-composites

steady-state condition in new samples, despite the long charging time. This indicates the domination of low frequency dispersion in the charging process. After the treatment, only composition P1 shows a tendency for saturation of the current. However, the varying trend of the volume charging currents for each filler proportions did not follow similar regularity after each of the two sequences of corona-ozone exposure. Comparing with one another the combinations of P1, P2 as well as P5, it can be observed clearly from Figure 4.16 that the increased content of micro-sized fillers in the epoxy compositions, which have the same proportion of nano-fillers, gave rise to the volume charging current after each of the two rounds of corona treatment, as compared with the initial bulk currents. When comparing compositions P4 and P5, both having 65 wt.% of micro-fillers, an addition of 5 wt.% of nano-filler caused an increase of bulk charging currents after each corona-ozone treatment as well.

As seen in Figure 4.17, the changes observed in the surface charging current were much stronger responsive to the treatment. After the first sequence of corona-ozone exposure, the surface charging currents for all the compositions investigated were much higher, compared with the initial states. For the compositions P1, P2 and P3, the surface charging currents measured after the second round of the exposure were lower than after the first round. For composition P5 there was only tiny difference between the two surface charging currents after the first and the second sequence of 100 h corona exposure. Opposite to this, the level of surface charging current for the composition P4, containing only micro-filler, increased further after the second round of the treatment. These results indicate that presence of the nano-filler has a significant role in retarding further degradation on the surface of the epoxy compositions.

The results of charging current measurements are summarized in Table 4.4. For comparison, the data represent current values read after 3.6×10^4 s. As already shown, more severe effects are found in surface charging current values. The arrows in the columns “effect of treatment” indicate the varying trends of surface and volume charging currents after the treatment in comparison with the initial referenced ones. For surface charging currents the respective increase varied between one and three orders of magnitude. After the first sequence of corona exposure, surface charging current increased most for composition P2, followed by compositions P3, P5, P1 and finally P4. Also for composition P2, the surface charging current recovered most after the second treatment, i.e. by nearly one order of magnitude. At the same time, surface charging current for composition P4 increased further after the second treatment by 0.9 orders of magnitude. Less pronounced changes were found in volume charging currents for all the compositions, except for P1, for which the volume charging current decreased by 1.23 orders after the first treatment. It is however important to stress that, despite the fact that the two rounds of 100 h long corona treatments

influenced both the surface and volume charging currents of the tested epoxies, the changes incurred lie still away from the level that could be considered as dangerous for their performance in for example outdoor environments.

Figure 4.18 and Figure 4.19 illustrate the results of DR measurements, which did not exhibit high sensitivity to the corona-ozone treatment, although some weak variations, as for example those seen for composition P1, were characteristic. The measured DR data at three different temperatures allowed obtaining master curves and activation energy for each of the investigated materials, as illustrated in Figure 4.20 and Table 4.5. The latter were obtained by shifts of the responses along the frequency axis, following the procedure described in **Section 3.2.3**.

Table 4.4: Values of surface and volume charging currents for the tested materials read for the time of measurement equal to 3.6×10^4 s.

Batches	Surface charging current (A)			Effect of treatment (decades)		Volume charging current (A)			Effect of treatment (decades)	
	Initial	Treated (100 h)	Treated (200 h)	1 st round	2 nd round	Initial	Treated (100 h)	Treated (200 h)	1 st round	2 nd round
P1	3.66 $\times 10^{-12}$	5.42 $\times 10^{-11}$	4.94 $\times 10^{-11}$	↑ 1.19	↑ 1.13	1.44 $\times 10^{-12}$	9.14 $\times 10^{-14}$	2.92 $\times 10^{-13}$	↓ 1.23	↓ 0.85
P2	3.04 $\times 10^{-14}$	2.25 $\times 10^{-10}$	2.29 $\times 10^{-11}$	↑ 3.92	↑ 2.93	9.93 $\times 10^{-13}$	2.23 $\times 10^{-13}$	5.52 $\times 10^{-13}$	↓ 0.77	↓ 0.44
P3	1.72 $\times 10^{-14}$	1.64 $\times 10^{-11}$	8.59 $\times 10^{-12}$	↑ 2.99	↑ 2.69	8.41 $\times 10^{-13}$	7.02 $\times 10^{-13}$	8.10 $\times 10^{-13}$	↓ 0.14	↓ 0.03
P4	1.31 $\times 10^{-13}$	1.68 $\times 10^{-12}$	1.02 $\times 10^{-11}$	↑ 1.04	↑ 1.97	8.43 $\times 10^{-13}$	9.30 $\times 10^{-13}$	1.10 $\times 10^{-12}$	↑ 0.09	↑ 0.27
P5	1.41 $\times 10^{-13}$	2.39 $\times 10^{-11}$	2.68 $\times 10^{-11}$	↑ 2.10	↑ 2.13	9.79 $\times 10^{-13}$	1.51 $\times 10^{-12}$	1.62 $\times 10^{-12}$	↑ 0.17	↑ 0.18

Note, the current values for compositions P2 and P3 are for the time of measurement equal to 1×10^4 s and 5×10^3 s respectively due to the measurement range of the electrometer. The corresponding values for the treated samples were therefore selected at the same timings.

The values of activation energies for all the compositions listed in Table 4.5 indicate that increasing nano-filler content yields an incremental tendency in the activation energy value and this effect is being reduced by adding micro-fillers. The lowest activation energy was found for composition P4, not containing any nano-filler. It is also worth pointing to the high frequency part of the master curve for composition P1, which clearly indicates appearance of another relaxation process characterized by different activation energy.

4.3. Tests upon epoxy micro- and nano-composites

Table 4.5: Calculated activation energy of dielectric response for the epoxy compositions investigated.

Compositions	P1	P2	P3	P4	P5
E_a (eV)	0.48	0.40	0.39	0.22	0.25

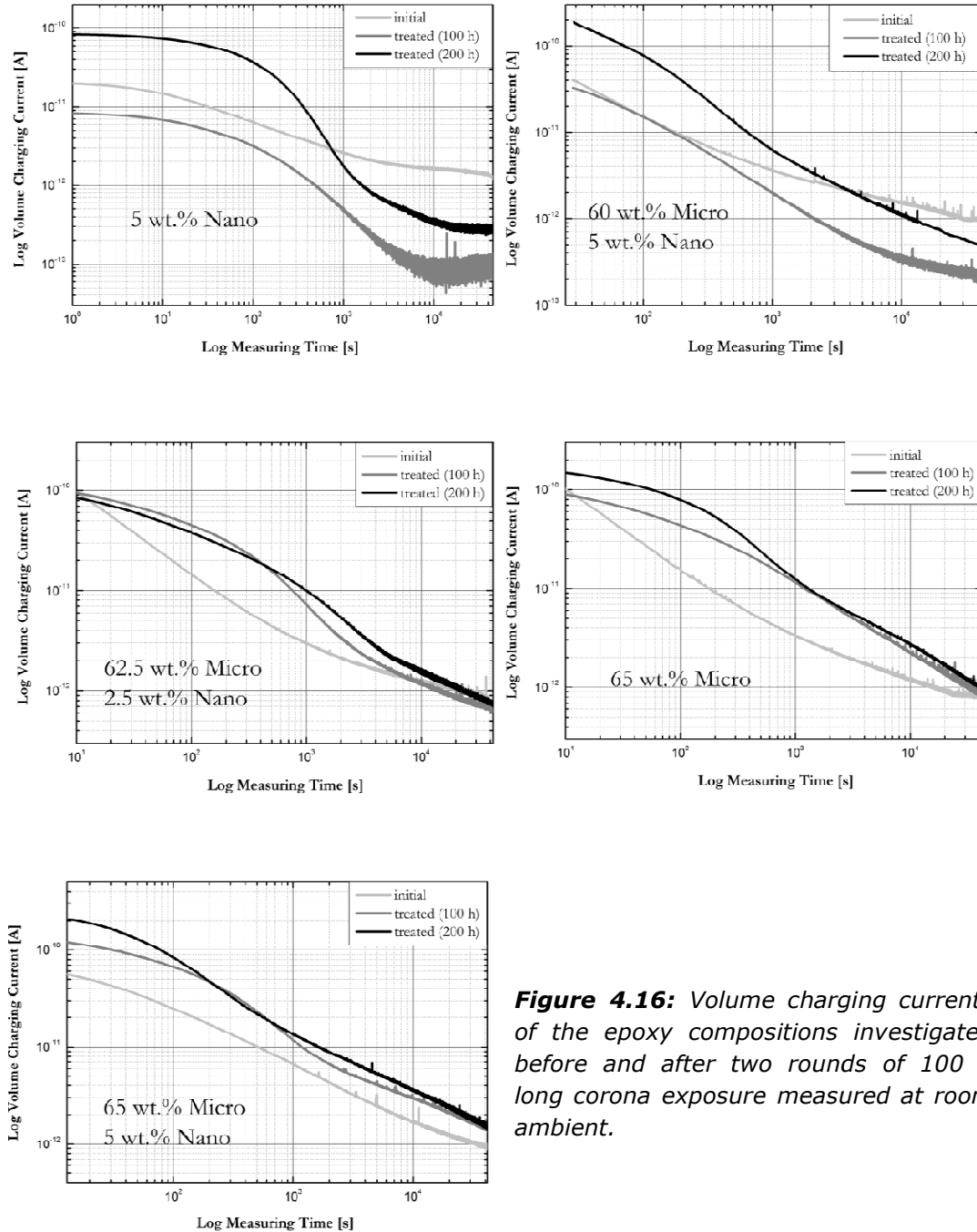


Figure 4.16: Volume charging currents of the epoxy compositions investigated before and after two rounds of 100 h long corona exposure measured at room ambient.

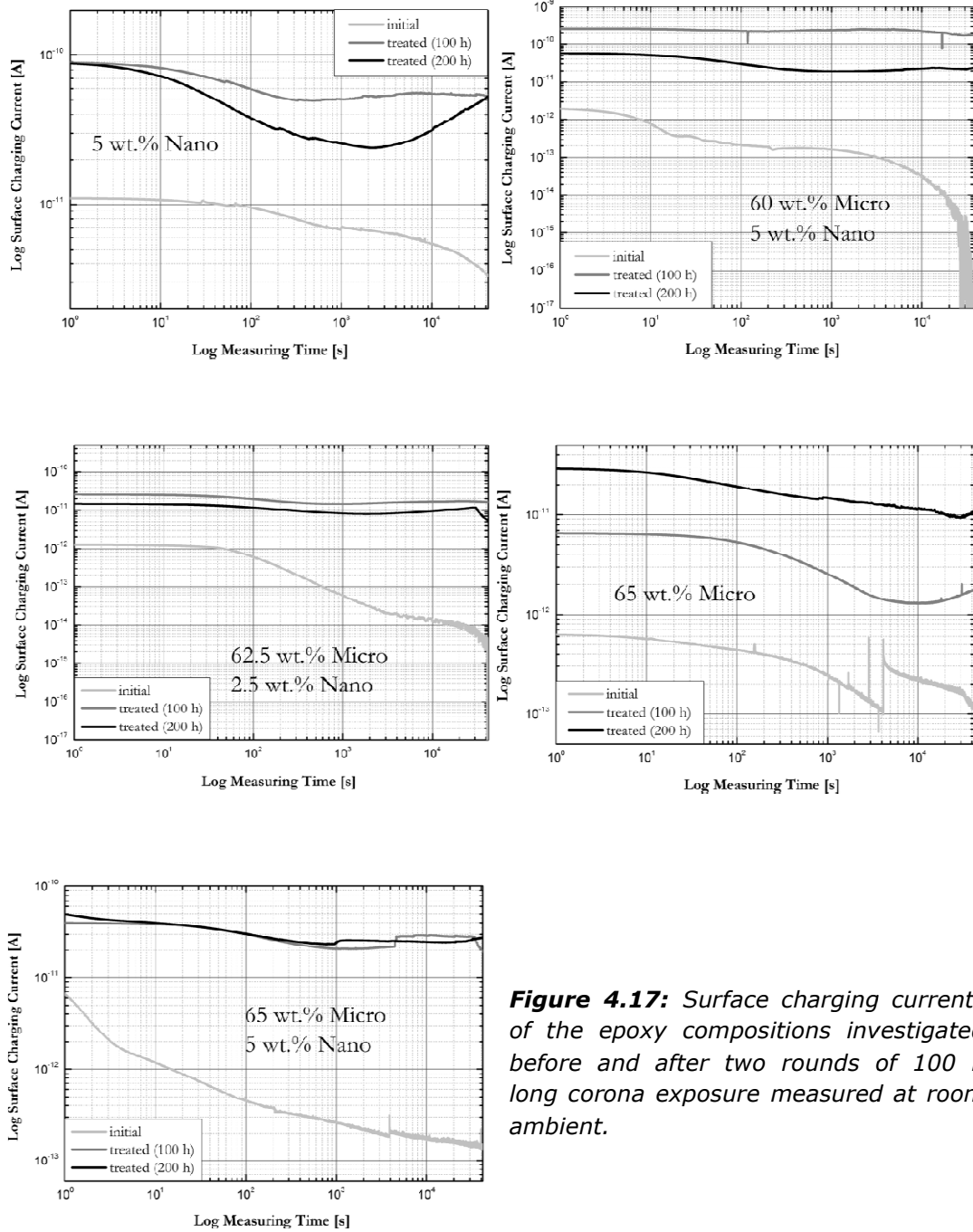


Figure 4.17: Surface charging currents of the epoxy compositions investigated before and after two rounds of 100 h long corona exposure measured at room ambient.

4.3. Tests upon epoxy micro- and nano-composites

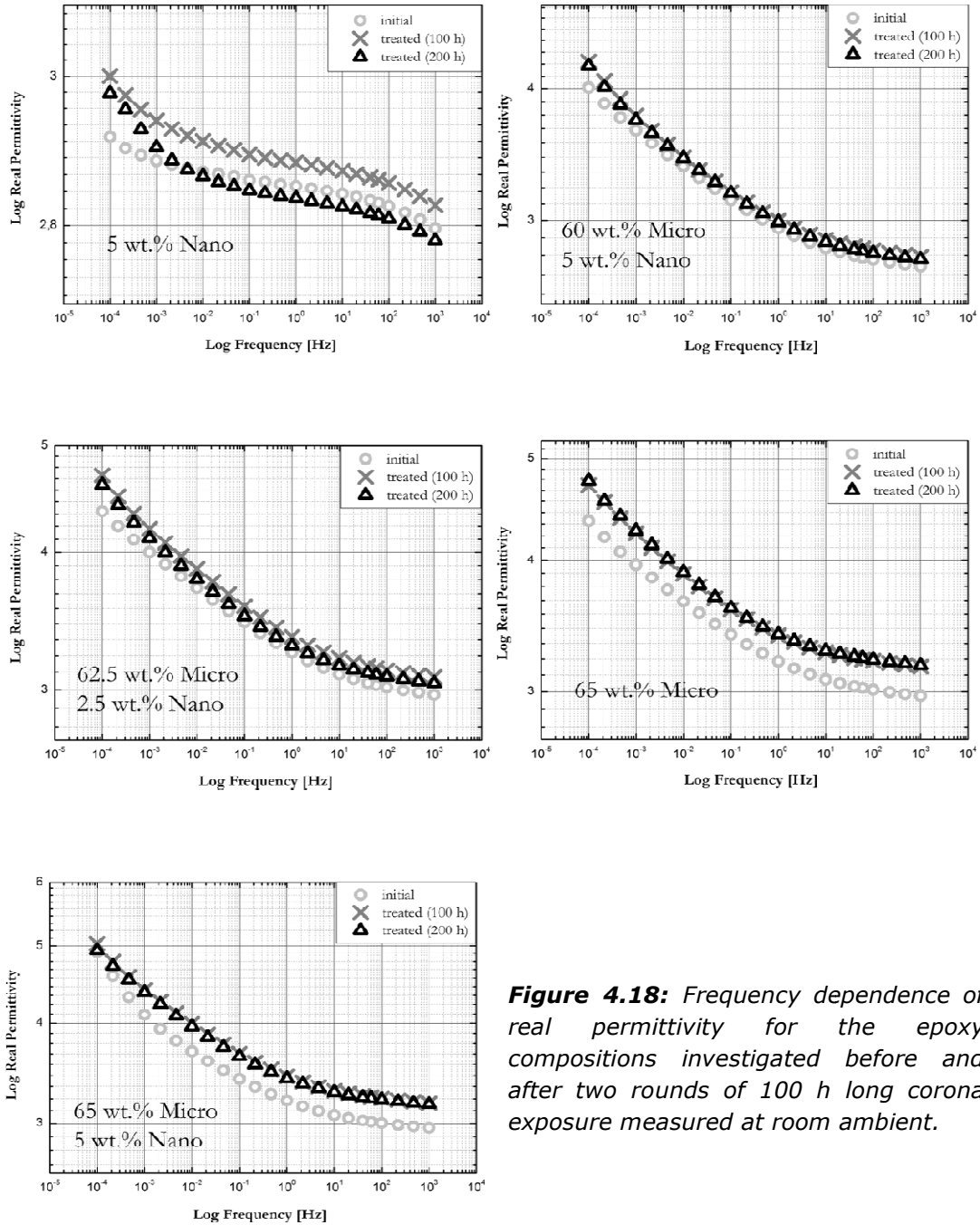


Figure 4.18: Frequency dependence of real permittivity for the epoxy compositions investigated before and after two rounds of 100 h long corona exposure measured at room ambient.

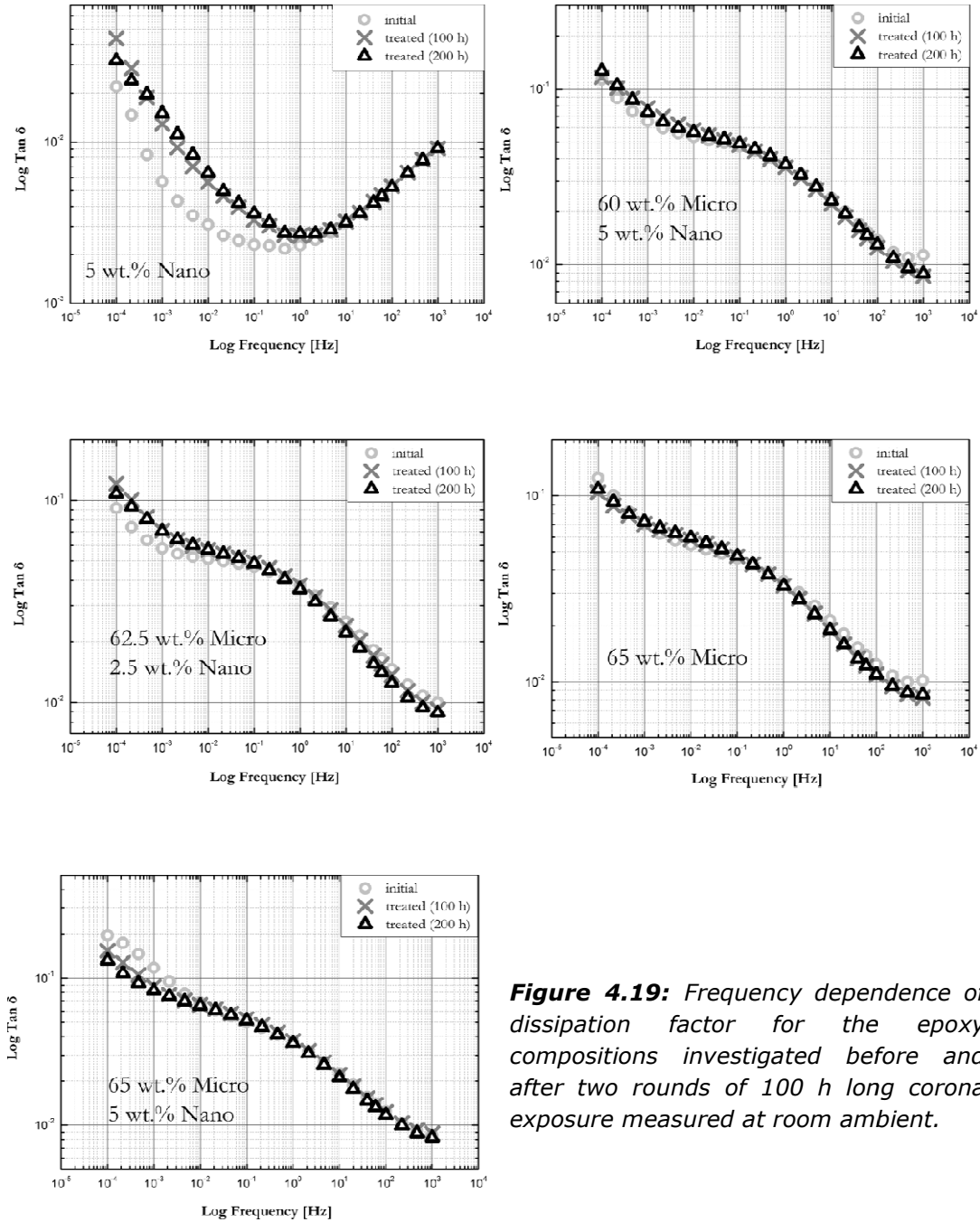


Figure 4.19: Frequency dependence of dissipation factor for the epoxy compositions investigated before and after two rounds of 100 h long corona exposure measured at room ambient.

4.3. Tests upon epoxy micro- and nano-composites

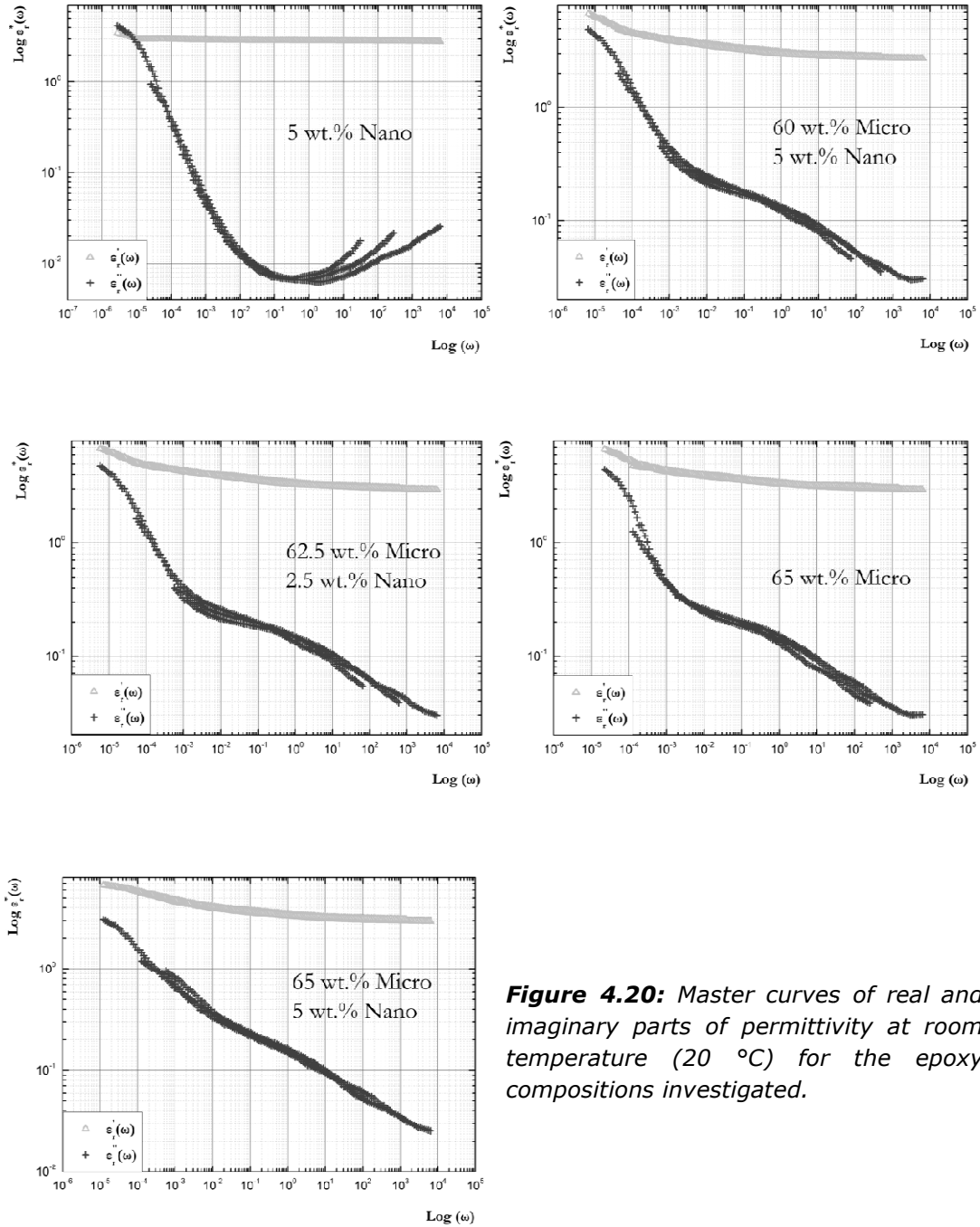


Figure 4.20: Master curves of real and imaginary parts of permittivity at room temperature (20 °C) for the epoxy compositions investigated.

4.4 Concluding remarks

This chapter describes investigations of the changes in material properties (dielectric, mechanical, as well as chemical structure) imposed by the AC corona/ozone treatment of five commercially used polymeric materials (EP, LSR, HTV, EVA and EPDM) by adopting the testing methodology as well as procedure proposed to the CIGRE WG D1.14. In addition, the elaborated methodology was used for evaluating the properties of epoxy compositions filled with micro- and nano-fillers at different proportions.

The 100 h long corona/ozone treatment yielded significant changes of surface resistivity on nearly all the materials tested. The treatment also had an influence on the mechanical properties, including breakdown strength and elongation at break. The observed changes could mainly be attributed to oxidation reactions taking place on material surfaces, as revealed by the performed physical-chemical analyses. On the other hand, the effects of the treatment on volume resistivity, dielectric permittivity and dissipation factor (dielectric losses), all being properties of the material bulk, did not exhibit high sensitivity to the treatment.

Since presence of corona and ozone in the vicinity of high voltage outdoor insulators especially influences material's mechanical integrity, resulting in surface cracking and reduction of mechanical strength, the performance of insulation systems may be strongly influenced by them, especially when the materials remain under continuous tension. On the other hand, as regards the dielectric parameters, the influence of corona/ozone does not seem to be too critical, despite the relatively strong variations imposed on the surface resistivity.

The study of epoxy nanocomposites focused on evaluation of the changes in their electrical parameters imposed by the corona/ozone treatment. Similarly as for the commercial materials, the 100 h long corona/ozone exposure had obvious effects on the surface properties for all the compositions investigated and the contents of the micro- and nano-fillers played a significant role in the observed changes. A clear effect of the nano-filler addition on activation energy of the polarization phenomena could be seen. Increase of the nano-filler content yielded an incremental tendency in the activation energy value, while the effect was reduced by adding micro-fillers.

5 Material performance under AC and DC corona ageing tests

5.1 Specimens and testing procedure

Two types of HTV silicone rubber samples were used in this work. The first type was HTV silicone rubber, Elastosil R401/60 from Wacker Silicones ($\rho = 1.14 \text{ g cm}^{-3}$), based on polydimethylsiloxane (PDMS) and reinforcing silica filler. It was crosslinked with 0.7 wt.% dicumylperoxide (dispersed in 0.7 wt. silicone oil). Samples of this material were further divided into two test batches; the first batch consisted of samples crosslinked at 165 °C/100 bar (10 MPa) for 15 min and then postcured at 170 °C/4 h in a hot oven. The second batch was crosslinked at 165 °C/100 bar (10 MPa) for 15 min but not postcured, meaning that the samples still contained some residuals from the crosslinking process. This way of selecting materials for the studies aimed at figuring out if the crosslinking by-products could play any role in the corona damage mechanism. The second type of HTV rubber, Powersil 310 from Wacker Silicones ($\rho = 1.52 \text{ g cm}^{-3}$), is formulated as an outdoor insulation material with excellent tracking and erosion properties. The material is based on PDMS filled with silanized aluminatrichydrate (ATH) and reinforcing silica filler. The Powersil 310 samples used in this work were cured for 15 min at 165 °C followed by a post-curing at 150 °C for 4 h in a hot air oven. The dimensions of all the rubber samples put into the treatment vessel were $\sim 100 \times 100 \times 2 \text{ mm}^3$, while the corona discharge activity affected its central circular part of approximately 90 mm in diameter.

Before the treatment, all the prepared samples were cleaned with isopropanol and then left in air until drying out for at least 3 hours. Three samples of each material were treated one after another, by AC and DC (positive and negative polarities) coronas for 100 h, to fulfill the whole testing program. Measurements of dielectric parameters (volume and surface resistivities and DR) were conducted prior and after the corona treatments for each of them. Thereafter, the treated samples were cut into

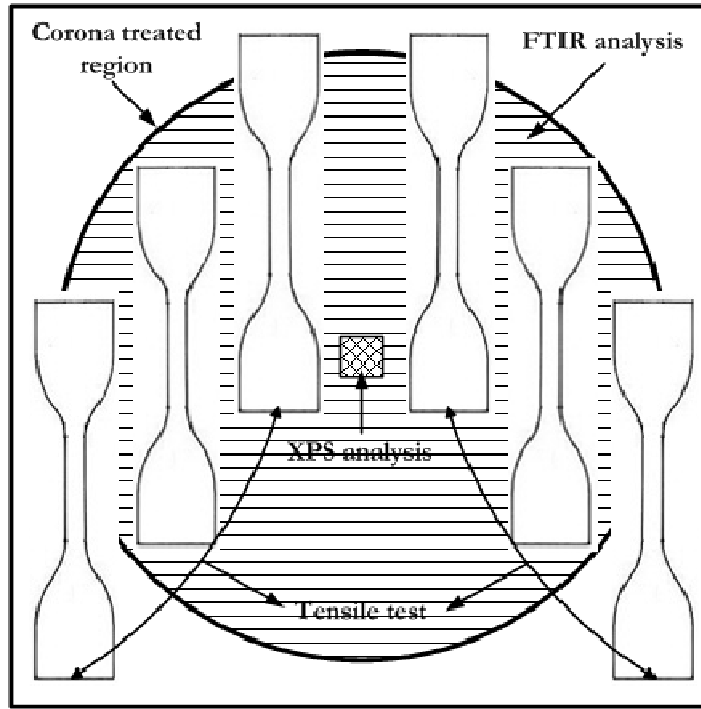


Figure 5.1: Sketch illustrating the way samples for mechanical tensile testing and for chemical analyses were cut from corona-treated specimens (diameter of the treated region was equal to ~90 mm).

smaller pieces, as demonstrated by Figure 5.1, to satisfy different purposes, i.e., the very central square (with the dimensions of 5 mm × 5 mm) was used for XPS analysis; the left part was punched into 6 dumbbell-shaped samples for performing tensile tests (tensile strength and elongation at break); meanwhile, the remaining part within the corona-treated region was used for FTIR investigation. Additionally, virgin reference samples were characterized according to the same procedure.

5.2 AC and DC corona/ozone treatments

5.2.1 Corona discharge intensities

Corona discharge intensities for different corona types, i.e. AC or DC, were characterized by measurements of the released power from the multi-needle electrode, while with the investigated sample was mounted underneath, on the grounded sample holder. At the selected treatment levels (AC 20 kVrms as well as DC 28 kV), the discharge intensities were observed to be dependent on the type of material under test. For the Elastosil samples in case of either AC or DC corona exposures, see Figure 5.2, the released power for the postcured samples was relatively higher than for the uncured samples. However, the power released under negative DC corona was

higher than that of positive polarity; for the postcured samples, the value measured at negative polarity was even close to that from AC corona (~ 1.8 W), up to ~ 1.6 W at the treatment level. For the unpostcured Elastosil samples, the power released from the electrode was approximately 1.5 W, 0.9 W and 1.1 W for AC, positive DC and negative DC discharges, respectively. These are close to the power levels measured for the Powersil samples at the treatment voltages, which are ~ 1.6 W, ~ 0.7 W and ~ 1 W for AC, positive DC and negative DC corona discharges respectively.

5.2.2 Ozone concentration

The results of ozone concentration measurements during the treatments are illustrated in Figure 5.3. The overall concentration of ozone during the DC corona treatments were observed to be significantly lower than that of the AC case, which is a consequence of the experimentally verified, lower DC corona discharge intensity. Since ozone is generated during corona discharges in a two-step process – formation of oxygen free radicals and then reactions among them [91], weaker corona discharge intensity indicates smaller amount of energetic electrons which are necessary for generating oxygen free radicals and then ozone. Besides, as also shown in *Chapter 3*, for a specific polymeric specimen, the ozone concentration during AC corona treatments is proportional to the power released from the corona source. This correlation is however no longer valid when compared with DC corona cases. As revealed in the previous section for the postcured Elastosil samples, the corona power measured during the AC discharge was comparable with that for negative DC corona, while at the same time the measured for these two cases ozone concentrations were remarkably different. This may indicate that the generation mechanism of ozone during AC corona exposure differs from that during DC corona. On the other hand, ozone concentration was also found, under identical corona exposures, to depend on the type of material investigated. For instance, the ozone concentration monitored during the treatment of Powersil samples by negative DC corona was higher as compared to the unpostcured Elastosil samples; although the respective corona power measured (~ 1 W and ~ 1.1 W) were very similar. It is therefore postulated that the behavior of accumulated charges on the surface of polymeric materials, which is closely related to the material's dielectric parameters, e.g. resistivity, may be responsible for this effect. However, its nature still remains to be explained.

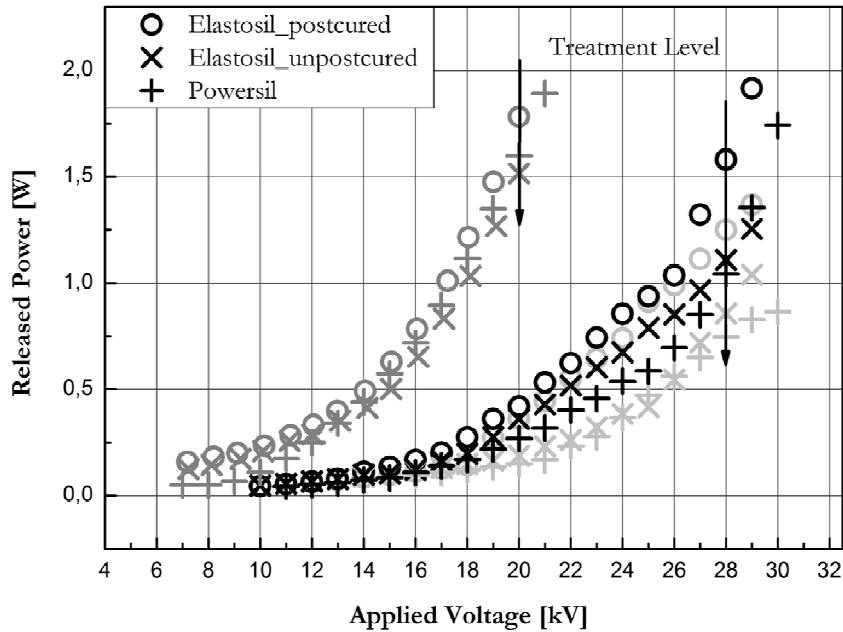


Figure 5.2: Comparisons of released power from the multi-needle electrode, initiated by AC and DC corona discharges, as measured for the HTV rubber samples investigated. (light gray – +DC corona, gray – AC corona, black – -DC corona).

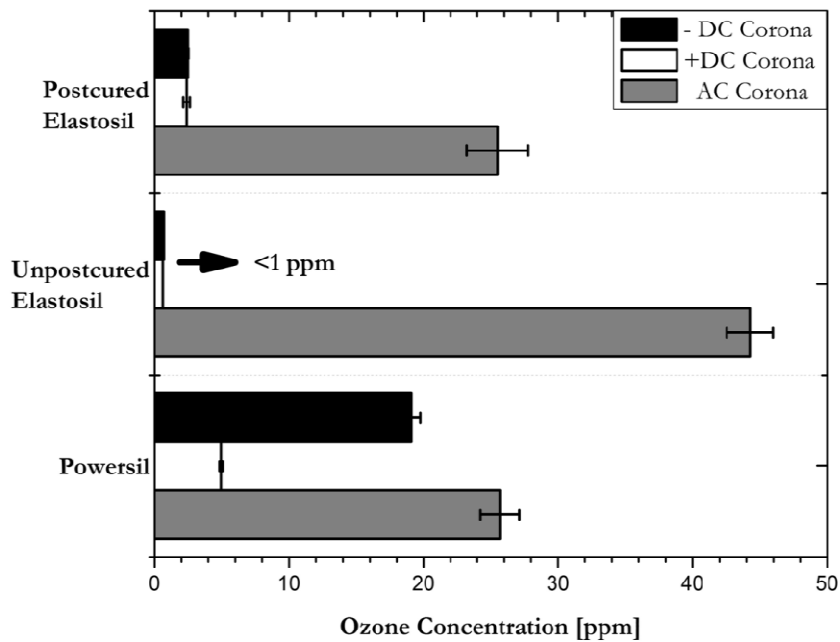


Figure 5.3: Ozone concentration measured during the AC and DC treatments of the investigated samples.

5.3 Effects upon HTV silicone rubber properties

5.3.1 Dielectric properties

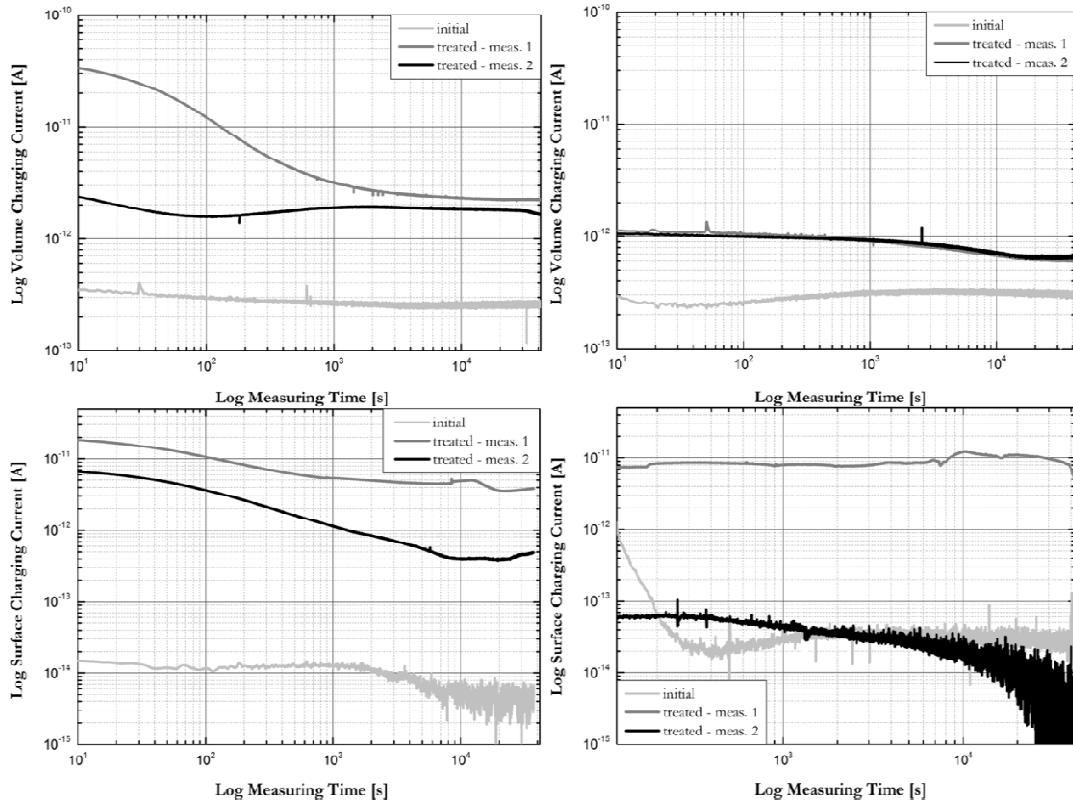
To investigate the dynamic behavior of the electric conduction after corona treatments the measurements of the charging currents were carried out twice. The first measurement was therefore performed immediately after the treatment and the second one was done two weeks later. The observations are summarized in Figure 5.4 for the postcured Elastosil material. For the first round of measurements, both volume and surface charging currents increased after AC or DC corona treatments. The changes observed on the surface were however stronger responsive to the treatment than in the volume. At the same time, the effects of AC corona treatments were more pronounced than the DC ones, for both the volume and the surface charging currents. However, after two weeks of resting, the surface charging currents for the DC corona treated samples recovered to the initial state while for the AC corona treated sample the degree of recovery was not that strong. Meanwhile, the volume charging currents remained unchanged after the resting. One possible explanation of the surface current recovery behavior is that the resting allowed low molecular weight (LWM) silicone derivatives diffusing to the surface and shielding the hydrophilic OH groups generated during the corona treatments. On the other hand, for the AC corona treated sample, since much more severe surface oxidation was recognized (presented in following sections) diffusion of LMW silicone derivatives to the material surface could not equally efficiently influence the surface dielectric properties, as it did on the DC corona treated surfaces.

The results are summarized in Table 5.1 and show that the treatments by all types of corona have obviously influenced the levels of both volume and surface resistivities. The arrows in the columns “Effect of treatment” indicate the trends in logarithmic scale as compared with initial reference values. First of all, when comparing the postcured with unpostcured Elastosil samples, for each specific type of corona exposure as regards either volume or surface resistivity, the postcured Elastosil samples exhibited more susceptibility to the corona treatments that also agrees with the measurement results on corona power. Apparently, for each specific type of corona treatment those most severe effects were imposed on surface resistivity. In addition, for surface and volume resistivities, more pronounced influences were imposed by AC corona due to the higher discharge intensity. One exception is that the influence of negative DC corona on the volume resistivity reached a comparable level to the AC case for postcured Elastosil, i.e. a reduction by 0.94 decade. Such a

degree of reduction is in line with the measured similar levels of corona power released under negative DC and AC coronas.

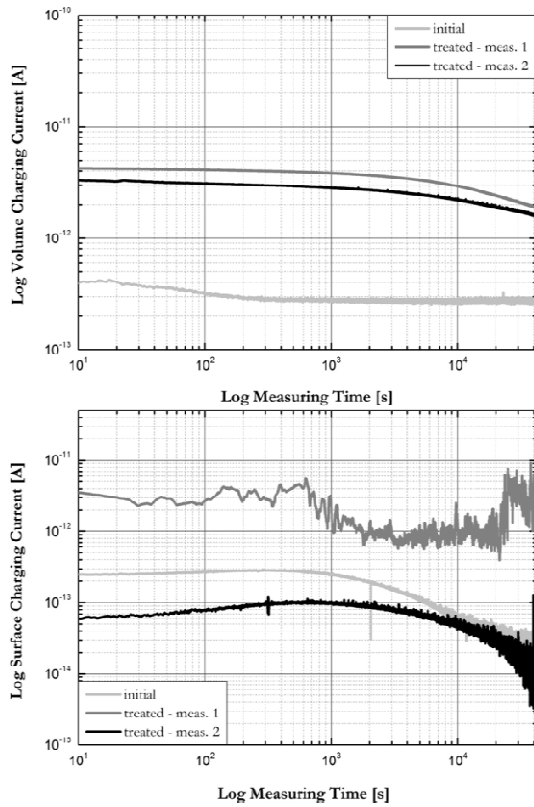
Furthermore, as illustrated by Figure 5.5, the results of DR measurements for the Powersil samples did not exhibit high sensitivity to all types of corona-ozone exposures. The spectra in the low frequency region indicate the low frequency dispersion mechanism, with a possible tendency for turning to a DC behavior at frequencies below 10^{-4} Hz. Though some weak variations could be found in the respective spectra, these however were more likely to be a result of geometrical effects in the test fixture rather than a real effect of the treatments. However, for the postcured Elastosil samples (see Figure 5.6), the spectra in the low frequency region (below 10^{-2} Hz for the initial state and after the AC corona treatment as well as below 10^{-1} Hz for the samples treated by DC corona) a typical DC conduction behavior can be seen, while no significant variations can be found in the real part of permittivity. The imaginary permittivity however showed obvious trend to increase after the corona treatments; most significantly in the sample treated by AC corona, followed by the one treated by negative DC corona and finally the one treated by positive DC corona – the same ranking sequence as regards the corona power monitored from the multi-needle electrode. By using the data derived from the first volume charging current measurement (see Figure 5.4) for Elastosil the calculated by means of Equation 3.3 DC losses have a satisfactory fitting with the imaginary part of permittivity in low frequency region (DC region), as shown in Figure 5.6 (b). If compared with the Powersil samples, a superior performance of suppressing the increase of conductive losses after corona ageing due to the existence of ATH fillers can be seen.

5.3. Effects upon HTV silicone rubber properties



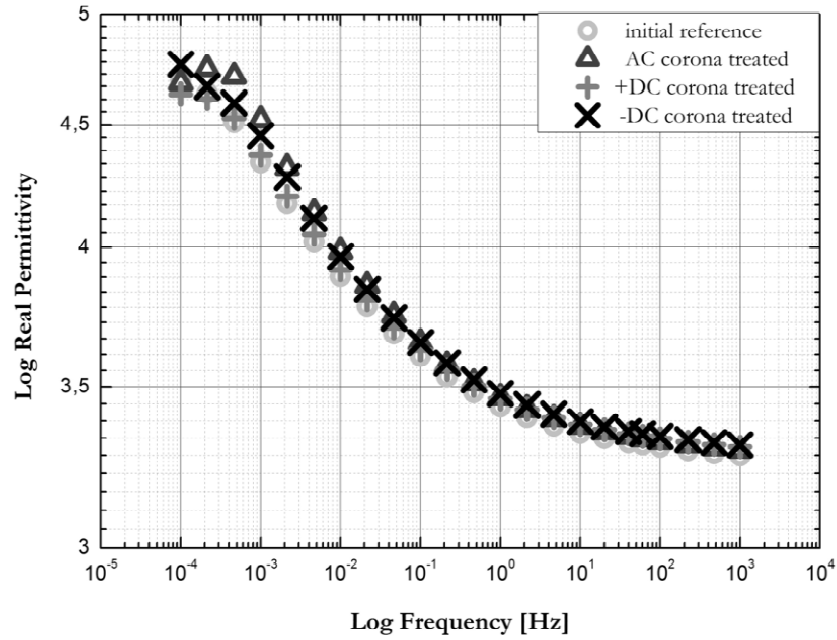
(a)

(b)

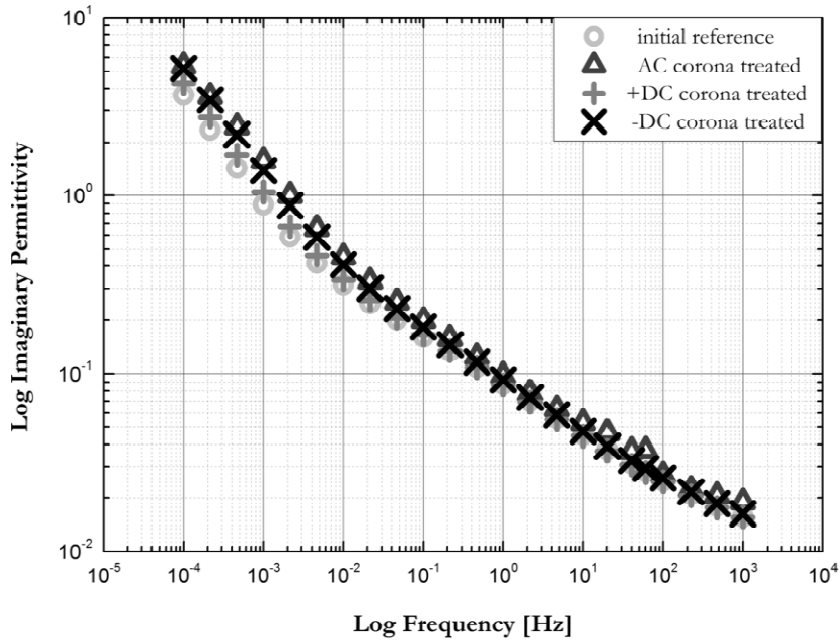


(c)

Figure 5.4: Volume and surface charging currents for the postcured Elastosil samples treated by AC corona (a), positive DC corona (b) and negative DC corona (c). Measurements performed directly after an end of corona exposure ('treated - meas. 1') as well as two weeks after end of exposure ('treated - meas. 2').



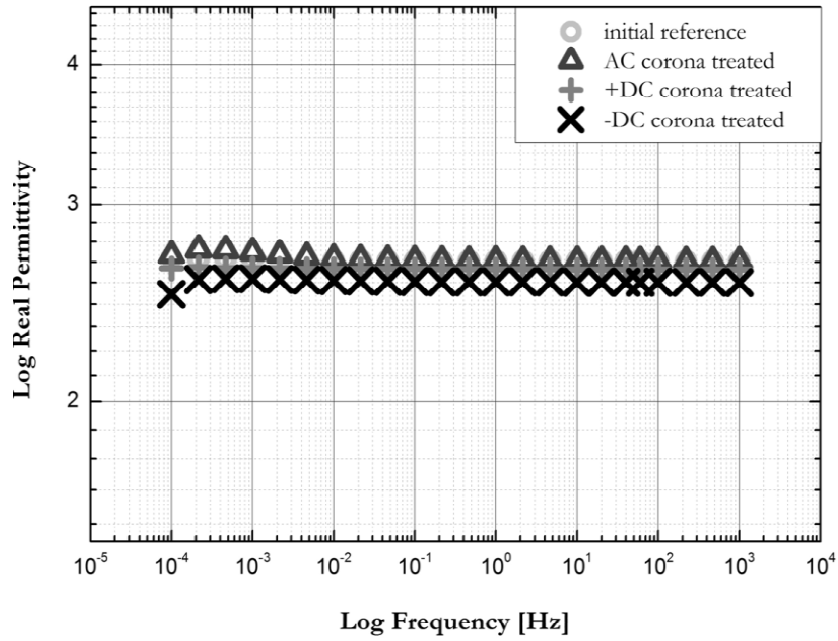
(a)



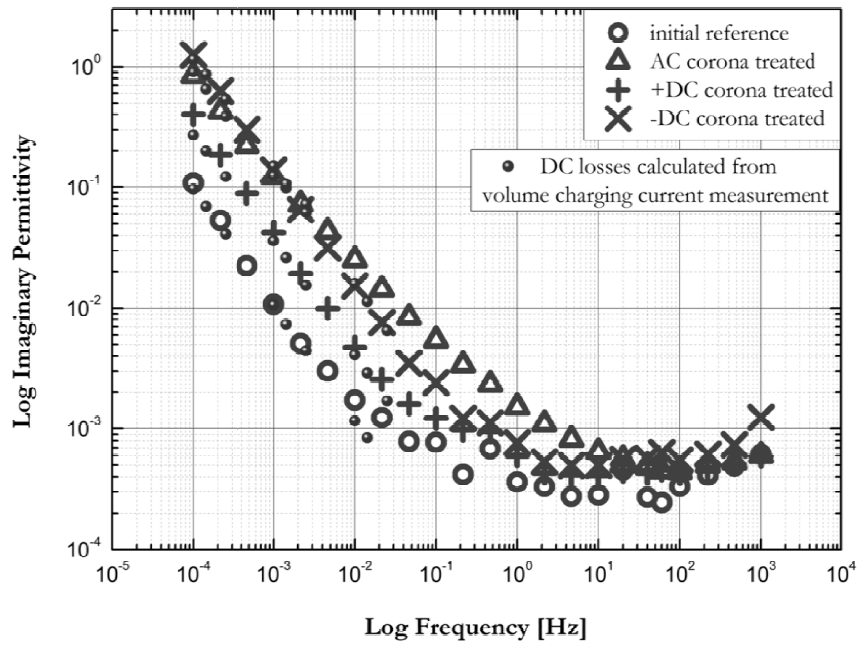
(b)

Figure 5.5: Real (a) and imaginary (b) parts of complex permittivity for the Powersil samples treated by AC and DC coronas.

5.3. Effects upon HTV silicone rubber properties



(a)



(b)

Figure 5.6: Real (a) and imaginary (b) parts of complex permittivity for the postcured Elastosil samples treated by AC and DC coronas.

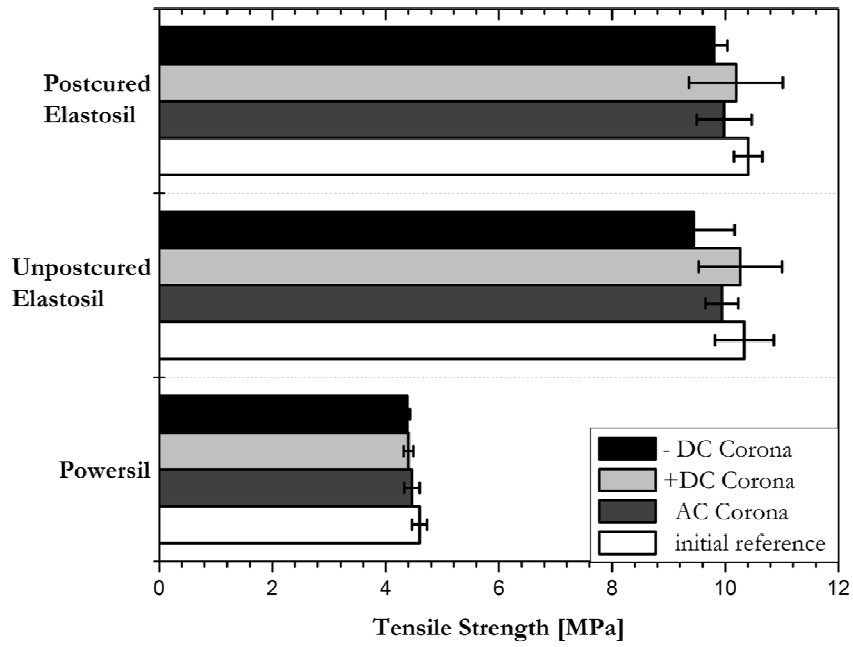
Table 5.1: Values of volume and surface resistivities of HTV silicone rubber samples treated by AC and DC corona, calculated for the time of current measurements equal to 3.6×10^4 s.

Batches	Volume resistivity (Ω m)		Effect of treatment (decades)	Surface resistivity (Ω /sq)		Effect of treatment (decades)	
	Initial	Treated		Initial	Treated		
Powersil	AC _{rms} (20 kV)	6.15×10^{13}	2.01×10^{13}	↓ 0.41	4.42×10^{17}	1.05×10^{14}	↓ 3.34
	DC (+28kV)	5.46×10^{13}	5.07×10^{13}	↓ 0.04	7.76×10^{17}	2.13×10^{16}	↓ 1.56
	DC (-28 kV)	6.30×10^{13}	5.72×10^{13}	↓ 0.06	6.95×10^{17}	6.60×10^{16}	↓ 1.04
Unpostcured Elastosil	AC _{rms} (20 kV)	8.49×10^{14}	4.44×10^{14}	↓ 0.40	2.15×10^{18}	1.94×10^{16}	↓ 2.02
	DC (+28kV)	1.04×10^{15}	1.09×10^{15}	↓ 0.01	1.07×10^{18}	4.51×10^{17}	↓ 0.66
	DC (-28 kV)	9.48×10^{14}	8.11×10^{14}	↓ 0.14	7.56×10^{17}	7.10×10^{17}	↓ 0.05
Postcured Elastosil	AC _{rms} (20 kV)	1.67×10^{15}	1.93×10^{14}	↓ 0.97	7.45×10^{18}	5.55×10^{15}	↓ 3.19
	DC (+28kV)	1.50×10^{15}	7.28×10^{14}	↓ 0.42	7.26×10^{17}	1.77×10^{15}	↓ 2.54
	DC (-28 kV)	1.69×10^{15}	2.31×10^{14}	↓ 0.94	8.29×10^{17}	1.26×10^{16}	↓ 1.70

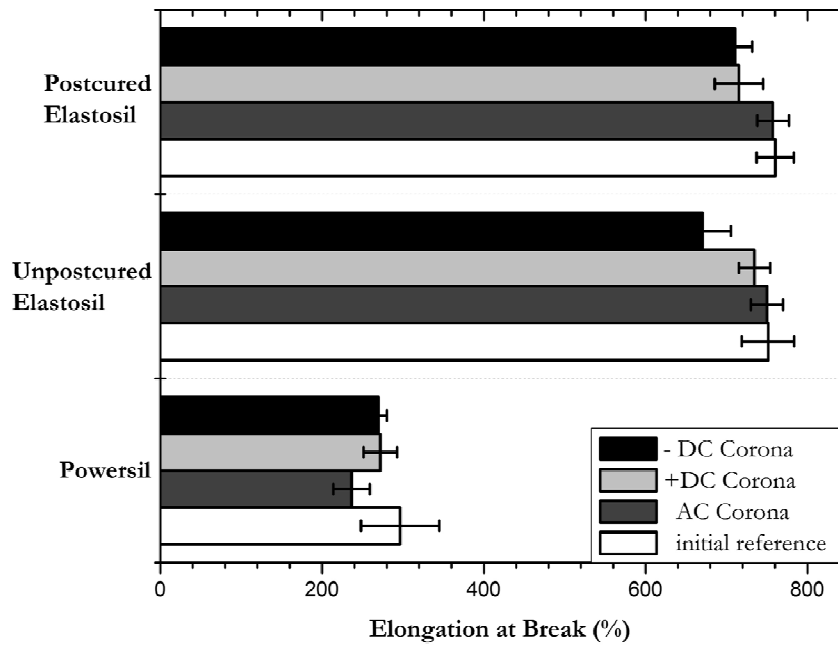
5.3.2 Mechanical properties

Since polymeric housing materials are expected to retain mechanical integrity under the influence of corona-ozone exposure the purpose of this investigation was to assess the arising changes of tensile strength and elongation at break. For obtaining statistically significant results, 6 specimens were cut out of each treated sample, as illustrated in Figure 5.1. Figure 5.7 shows that after the 100 h corona-ozone exposures, all of the tested samples exhibited some reduction of the tensile strength as well as the elongation at break. However, the variations in data were within experimental error even under the situation where the tested samples were cut in parallel to the pre-stressing direction during the treatment (dash lines refer to the parallel direction while the solid lines to the perpendicular one in Figure 5.8), although the reduction in elongation at break was observed a little bit higher as compared with the samples cut in the perpendicular direction. Both the parameters depend on crosslinking density of the polymer, filler type and its content and the observed changes could not unanimously be correlated with the corona discharge intensity or ozone concentration. However, it can be concluded that the post-curing step did not improve the mechanical properties of the Elastosil material further.

5.3. Effects upon HTV silicone rubber properties



(a)



(b)

Figure 5.7: Tensile strength (a) and elongation at break (b) of all the investigated material samples.

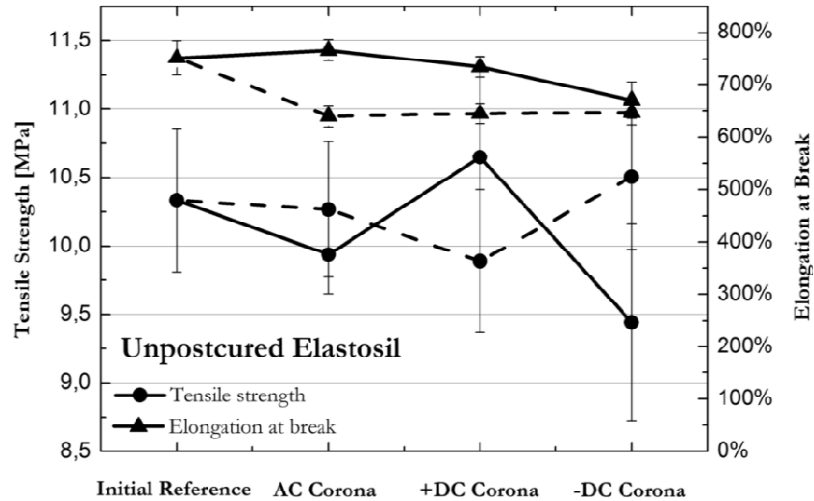


Figure 5.8: Tensile strength as well as elongation at break for the unpostcured Elastosil samples treated by corona discharges, with two mechanical pre-stressing directions.

5.3.3 FTIR studies

The IR spectra for AC and DC corona treated samples are shown in Figure 5.9. The following typical chemical bonds could be identified in the spectra of all the reference samples, i.e. C-H bonds in CH₃ groups at 2960 cm⁻¹, Si-CH₃ bonds at 1260 cm⁻¹ and Si-O-Si bonds at 1054 cm⁻¹. For the unpostcured Elastosil samples, a relatively high absorbance at ~3700-3200 cm⁻¹ was found after AC corona treatment, which was associated with increased content of hydroxyl (OH) groups. However, the same effect was not observed for the same material treated by DC corona. In addition, after the exposure, the Si-O-Si peak became broader and slightly displaced towards higher wave numbers. This broadening is a typical signature of oxidative crosslinking of the silicone rubber polymer matrix. The AC corona treated unpostcured Elastosil sample exhibited the largest shift. Besides, the ratio of Si-CH₃/Si-O-Si decreases from 0.57 to 0.3 (area ratio) after the corona treatment [96]. The increase in detected amount of Si-O-Si bonds is due to the formation of silica at the surface, which is the result of the condensation of Si-OH groups that are formed by the oxidation process of the PDMS [12].

In contrast both the broadening of Si-O-Si peak as well as higher absorbance of OH groups were much less pronounced in the postcured Elastosil samples, which is attributed to the relatively lower ozone concentration compared to unpostcured samples during AC corona exposures, see Figure 5.9. This difference could also be caused by a more complete crosslinking of the postcured samples compared to unpostcured ones, as revealed by the test results of swelling experiments in n-hexane. For the postcured and unpostcured Elastosil specimens the respective equilibrium swelling degrees were 126 wt.% and 144 wt.%. However, with comparable ozone

5.3. Effects upon HTV silicone rubber properties

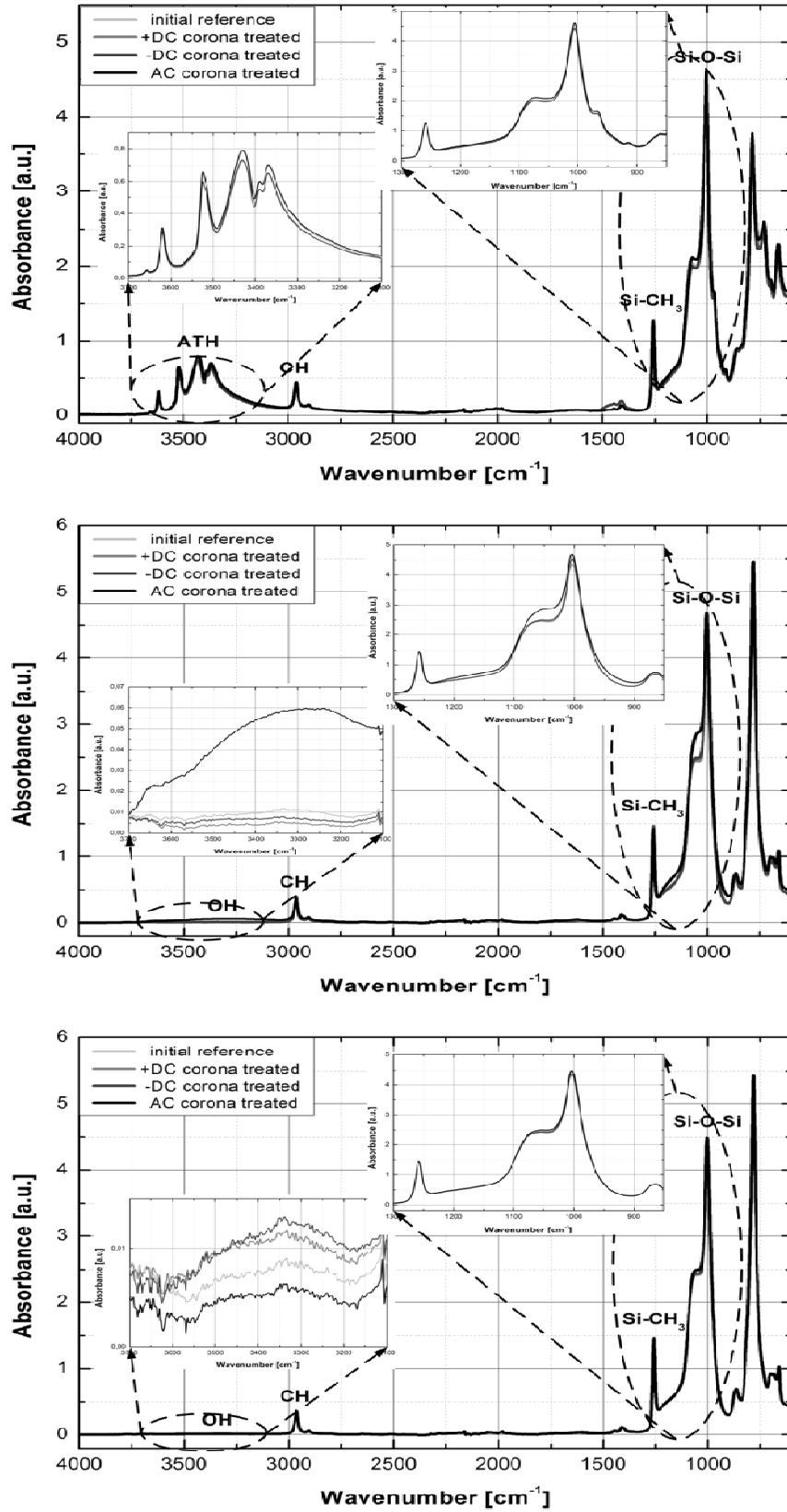


Figure 5.9: IR spectra for the AC and DC corona treated Powersil samples (top), the Elastosil unpostcured samples (middle) and the Elastosil postcured samples (bottom).

concentrations monitored during AC corona exposure, the Si-O-Si peak broadening was more distinguishable for the Powersil samples. It should be noticed that, since Powersil samples were ATH ($\text{Al}(\text{OH})_3$) filled, these OH groups obscure the weak absorption peak of surface-silanol groups observed for the Elastosil materials at $\sim 3700\text{-}3200\text{ cm}^{-1}$.

5.3.4 XPS studies

- **Atomic composition**

Table 5.2 presents the data of atomic compositions of the samples investigated. The estimated depth of penetration was $\sim 8\text{-}10\text{ nm}$. The angle between the direction of emitted photoelectrons to the analyzer and the surface normal was kept at 45° . Theoretically, the atomic composition of pure PDMS is 25 % Si, 50 % C as well as 25 % O. The three reference samples exhibited their atomic compositions different from the theoretical values, presumably due to carbon-rich contamination. For all three silicone rubbers investigated in this work, however, dramatic increases of oxygen and reduction of carbon contents after the AC corona-ozone exposure can be observed from the table, which indicates apparent surface oxidation.

Compared to the virgin state of Powersil, the carbon content of the sample treated by AC corona was reduced with 49 %, while the content of oxygen increased by 36 %. The degree of oxidation was similar to that of postcured Elastosil sample, both attributed to the comparable ozone concentration measured during the AC corona treatments (average 25.7 ppm for the Powersil sample and 25.5 ppm for the postcured Elastosil sample). For the latter the content of carbon atoms decreased by 45 % whereas oxygen increased by 40 % compared to the initial values. However, the surface oxidation for the unpostcured Elastosil sample was less pronounced, as demonstrated by an increase by 30 % in oxygen content and a 32 % reduction in carbon content, despite of the high ozone concentration measured (average 44.3 ppm). A possible reason for this effect could be a preventive action of residual decomposition products from the peroxide on the oxidative crosslinking process.

XPS analyses conducted on DC corona treated samples revealed less oxidation, compared AC corona. Variations of oxygen and carbon contents, as compared before and after DC corona treatments, a reduction of carbon content by 15.8 % and an increase of oxygen by 17.4 % were detected for the Powersil sample (average zone concentration of 4.9 ppm). A comparable ozone concentration, of average 2.4 ppm, was measured for the Elastosil postcured sample during the positive DC corona, and a comparable modification of the surface composition was observed. However, during the DC corona treatment of negative polarity a much higher ozone concentration was monitored, up to 19.1 ppm, which caused a relatively larger drop of carbon content by 24.6 % and an increase of oxygen content by 21.5 %. On the

Table 5.2: Atomic compositions on the surface layers of samples before and after AC and DC corona exposures.

Corona Treated Samples		C [%]		O [%]		Si [%]	Si _{2p} Peak Area [%]	
							102.1 eV	~103.5 eV
Powersil	Reference	58.2		21.9		19.9	91	9
	AC 20 kV _{rms}	29.6	↓ 49.1 %	34.2	↑ 36.0 %	36.2	37	63
	DC + 28 kV	49.0	↓ 15.8 %	26.5	↑ 17.4 %	24.5	94	6
	DC – 28 kV	43.9	↓ 24.6 %	27.9	↑ 21.5 %	28.2	92	8
Elastosil (unpostcured)	Reference	55.8		22.8		21.4	94	6
	AC 20 kV _{rms}	37.7	↓ 32.4 %	32.5	↑ 29.8 %	29.8	36	64
	DC + 28 kV	60.0	-	22.2	-	17.8	94	6
	DC – 28 kV	57.7	-	22.6	-	19.7	97	3
Elastosil (postcured)	Reference	57.9		22.8		19.3	92	8
	AC 20 kV _{rms}	31.8	↓ 45.1 %	38.1	↑ 40.2 %	30.1	36	64
	DC + 28 kV	49.3	↓ 14.9 %	27.4	↑ 16.8 %	23.3	95	5
	DC – 28 kV	48.5	↓ 16.2 %	26.5	↑ 14.0 %	25.0	97	3

other hand, for the postcured Elastosil sample, the ozone concentration during the negative DC corona treatment was low (average 2.5 ppm). Less pronounced effects in the variation of oxygen (increase by 14 %) and carbon contents (reduction by 16.2 %) were monitored, similarly as in the case of positive DC treatment. The content of oxygen as well as carbon for the DC treated (both of positive and negative polarity) unpostcured Elastosil samples remained practically unchanged, indicating a very weak surface oxidation happening due to the extremely low ozone concentration (lower than 1 ppm) measured in the corona chamber during the DC corona treatments.

- **High resolution scans on Si 2p**

High resolution spectra of Si 2p orbital peaks were further analyzed to investigate the changes in chemical surface composition. These are exemplified for the Powersil samples in Figure 5.10, exhibiting a peak broadening and a shift towards higher binding energy at ~103.5 eV after the AC corona treatment. This change represents a formation of an inorganic silica-like phase (SiO_x , $1 \leq x \leq 2$), i.e. a component with Si atoms bonded to more than two oxygen atoms, in the corona-treated surface region [89]. The Si 2p peak at 102.1 eV is assigned to an organic form of silicone polymer (PDMS). It is also presented in Table 5.2, as an increase of the inorganic silicone phase at ~103.5 eV from the initial state of 9 % up to 63 %. The initial small amount of silica (occupying 9 % of the integral Si 2p peak for the Powersil sample) can be attributed to the amorphous reinforcing silica filler added to the polymer. After the positive and negative DC corona treatments, no obvious shifts of the Si 2p peak position were observed.

Similar results were also obtained for the Elastosil samples (see Figure 5.11, 5.12), providing proofs of surface oxidation as well as build-up of the silica-like inorganic layer during the exposure to AC corona. On the other hand, under the DC corona treatments, surface oxidation could only be verified by an increased surface concentration of oxygen, and a reduction in carbon content, no significant broadening of the Si 2p was found.

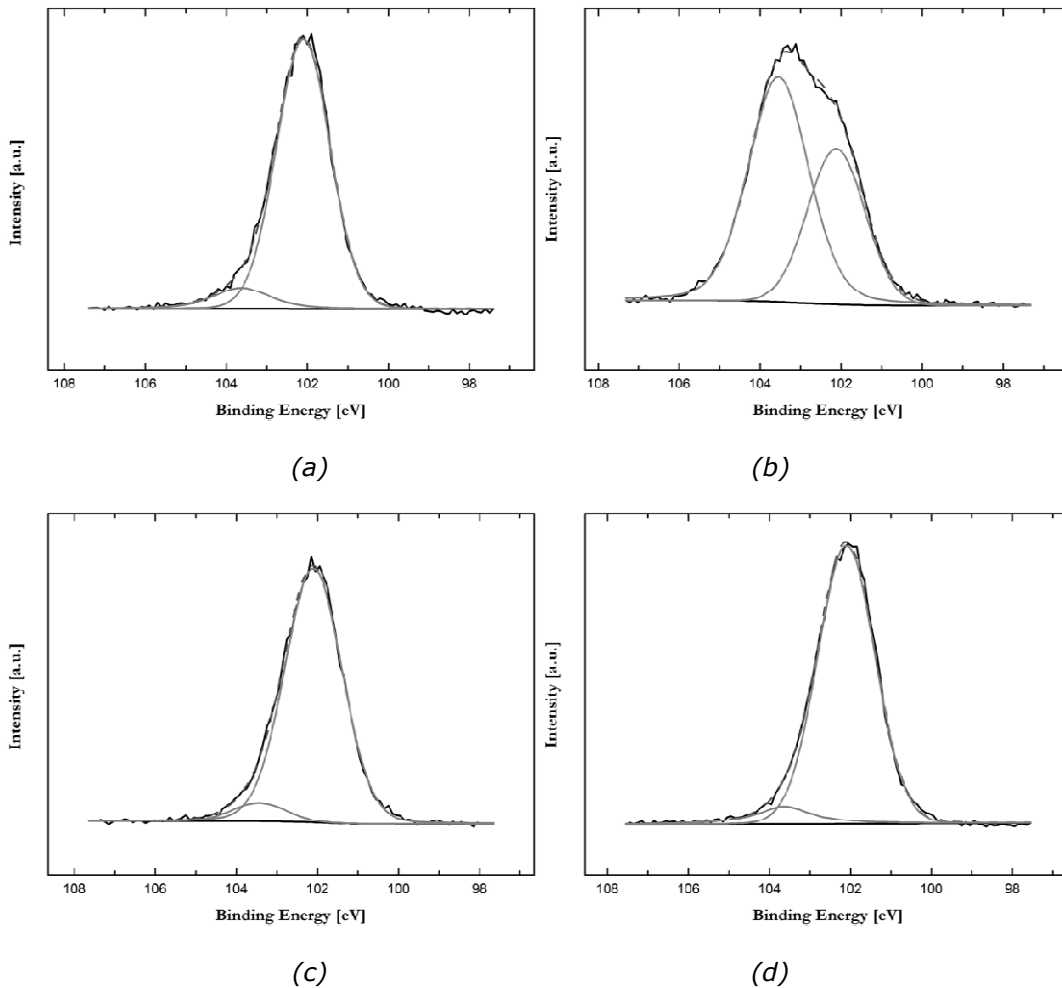


Figure 5.10: High resolution Si 2p spectra (XPS) of the Powersil samples exposed to different types of corona exposures: fresh sample as reference (a), treated by AC corona (b), by positive DC corona (c), and by negative DC corona (d), for 100 h respectively. The spectra are in arbitrary units and show relative intensities of the detected energy peaks.

5.3. Effects upon HTV silicone rubber properties

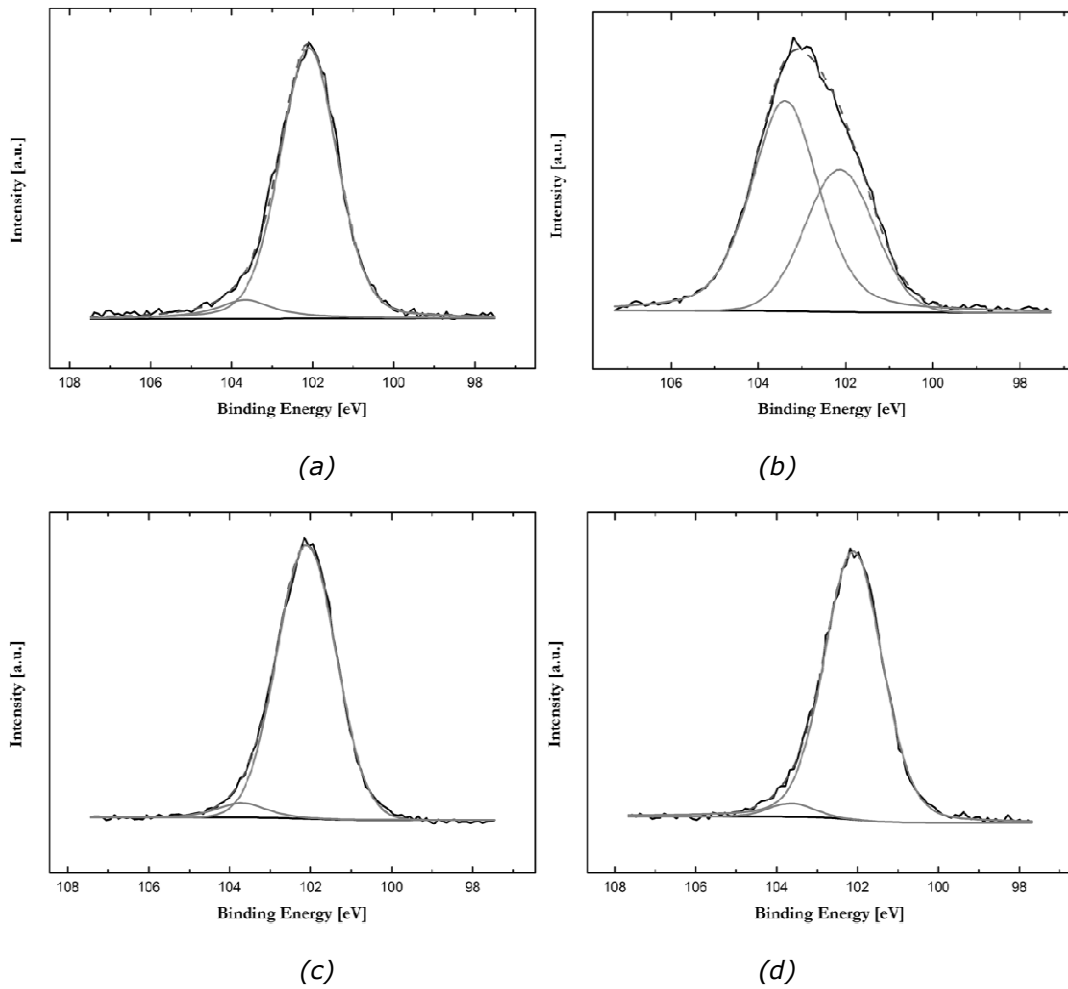


Figure 5.11: High resolution Si 2p spectra (XPS) of the postcured Elastosil samples: fresh sample as reference (a), treated by AC corona (b), by positive DC corona (c), and by negative DC corona (d), for 100 h respectively. The spectra are in arbitrary units and show relative intensities of the detected energy peaks.

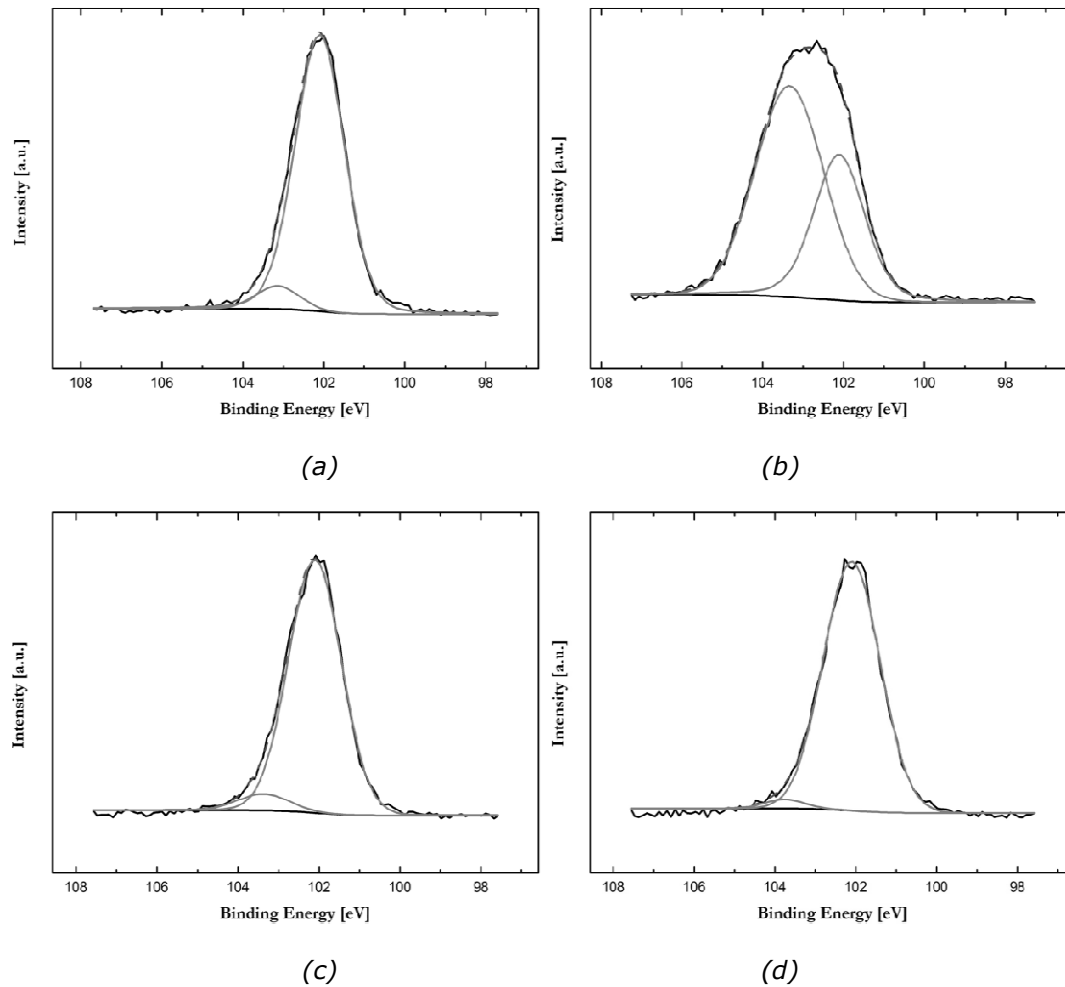


Figure 5.12: High resolution Si 2p spectra (XPS) of the unpostcured Elastosil samples: fresh sample as reference (a), treated by AC corona (b), by positive DC corona (c), and by negative DC corona (d), for 100 h respectively. The spectra are in arbitrary units and show relative intensities of the detected energy peaks.

5.3. Effects upon HTV silicone rubber properties

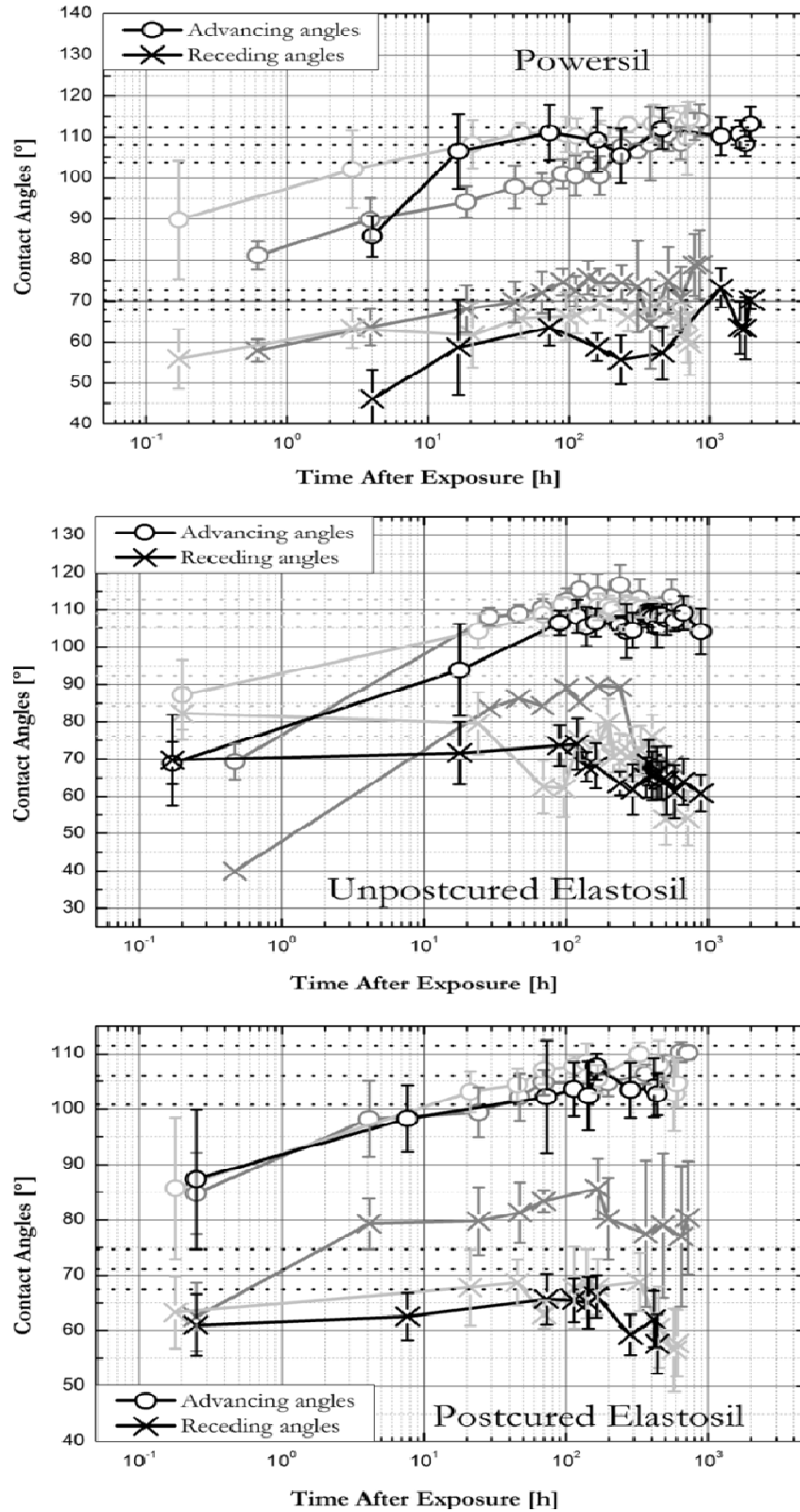


Figure 5.13: Contact angles for the Powersil (top), unpostcured Elastosil (middle), as well as postcured Elastosil (bottom) samples exposed to 100 h corona/ozone exposure plotted versus storage time at room ambient. (light gray - +DC corona, gray - AC corona, black - -DC corona).

5.3.5 Hydrophobicity variations

As indicated in Figure 5.13, the 100 h long corona/ozone exposure resulted in a decrease of advancing and receding angles, as compared to the virgin samples. The recovery of hydrophobicity was initiated directly after the end of corona exposure, when stored in ambient air. Most samples had recovered the hydrophobicity within the initial 100 h of resting. For the Powersil samples, the most pronounced reduction in hydrophobicity was found after negative DC corona, which correlates with the high amount of ozone generated; followed by the effects induced by AC and positive DC corona, respectively. For the unpostcured Elastosil samples, however, the largest hydrophobicity reduction was found for the specimen treated by AC corona, agreeing with the highest content of hydrophilic groups (e.g. OH) detected by FTIR analysis. The sample treated by negative corona took the second place followed by the one treated by positive corona. The scatter in hydrophobicity is lower for postcured Elastosil, no large variations are observed, with the exception of the specimen exposed to 100 h AC corona. Here the receding contact angle recovers to a value higher than the initial one. This could be caused by an increased surface roughness, caused by a spontaneous cracking of the oxidized silica like layer, which is revealed by the XPS data [99]. This observation is in line with the results provided by FTIR analysis (see Figure 5.9) where no substantial difference regarding the content of OH groups was found on the surfaces of postcured Elastosil samples treated by AC or DC corona.

5.4 Tests upon model nano-PDMS samples

5.4.1 Material description

Measurements of electrical properties (volume/surface resistivities/charging currents, frequency domain dielectric response) before and after AC/DC corona/ozone treatments were also performed on a batch of nano-filled silicone rubber samples. The matrix material in these specimens was polydimethylsiloxane (PDMS, ca. 10.000 mPas). The fillers used was SiO₂ with 15 nm particle diameter; the filler content was 0, 2, 5, 10 wt.% respectively. Four samples for each filler contents were available with the identical dimension of $\sim 100 \times 120 \times 2$ mm³.

5.4.2 Dielectric properties

The measurement system for the model nano-PDMS samples was modernized for precisely controlling ambient temperature (30 °C) as well as relative humidity (~43 % RH) by utilizing saturated potassium carbonate (K_2CO_3) solution. The volume resistivity of untreated samples increased with increasing concentration of nano-filler. A slight increase of the real part of dielectric permittivity can also be observed. There is also an increase of surface resistivity with increasing concentration of nano-filler, except for the 10 wt.% concentration, where it falls down below the initial level (for 0 wt.%).

As shown in Table 5.3, the changes in the surface resistivity imposed by the AC corona/ozone exposure of samples containing 0, 2 and 5 wt.% of nano-filler were at comparable levels – larger than 4 decades reduction, while the effect was found less pronounced for the 10 wt.% nano-filled sample. However, the influences on the surface resistivity induced by the DC corona/ozone treatments were less pronounced as compared to the AC case, though negative corona was found more influential than positive one, except for the PDMS samples without nano-filler. For volume resistivity, the overall effects of both AC and DC corona exposures remained less significant, though AC corona was more influential. One exception is 5 wt.% nano-filled samples, where the effect imposed by negative DC corona was instead stronger. When it comes to the dielectric response measurements, see Figure 5.15, higher dielectric losses were observed for all the samples treated by AC (also negative DC corona for the 5 wt.% nano-silica filled PDMS), and the corresponding frequency range depends on content of nano-fillers. However, no regularity can clearly be observed.

An attempt to evaluate the change in mechanical strength of the investigated samples before and after corona treatments was also undertaken. However, the samples appeared to be very brittle and because of that practically all of them were damaged while fixing in the test machine fixture arrangement.

Table 5.3: Values of volume and surface resistivities of the model nano-PDMS samples treated by AC and DC corona, calculated for the time of current measurements equal to 3.6×10^4 s.

Batches	Volume resistivity (Ω m)		Effect of treatment (decades)	Surface resistivity (Ω /sq)		Effect of treatment (decades)	
	Initial	Treated		Initial	Treated		
PDMS	AC _{rms} (20 kV)	7.72×10^{13}	1.99×10^{13}	↓ 0.57	4.72×10^{17}	2.96×10^{13}	↓ 4.18
	DC (+28kV)	8.28×10^{13}	5.40×10^{13}	↓ 0.29	2.30×10^{17}	3.04×10^{15}	↓ 1.93
	DC (-28 kV)	1.16×10^{14}	7.30×10^{13}	↓ 0.39	5.10×10^{17}	7.11×10^{15}	↓ 1.80
PDMS + 2 wt.% nano-silica	AC _{rms} (20 kV)	1.70×10^{14}	7.73×10^{13}	↓ 0.40	1.66×10^{18}	8.42×10^{13}	↓ 4.32
	DC (+28kV)	1.80×10^{14}	1.35×10^{14}	↓ 0.05	1.45×10^{18}	9.77×10^{18}	↑ 0.83
	DC (-28 kV)	2.03×10^{14}	1.48×10^{14}	↓ 0.06	5.56×10^{18}	8.40×10^{15}	↓ 2.72
PDMS + 5 wt.% nano-silica	AC _{rms} (20 kV)	3.55×10^{14}	3.40×10^{14}	↓ 0.02	1.18×10^{18}	1.01×10^{14}	↓ 4.02
	DC (+28kV)	3.69×10^{14}	2.64×10^{14}	↓ 0.11	4.70×10^{18}	2.70×10^{17}	↓ 1.20
	DC (-28 kV)	5.64×10^{14}	1.95×10^{14}	↓ 0.37	6.16×10^{18}	6.99×10^{14}	↓ 3.92
PDMS + 10 wt.% nano-silica	AC _{rms} (20 kV)	5.53×10^{14}	8.99×10^{13}	↓ 0.65	3.61×10^{17}	4.87×10^{14}	↓ 2.87
	DC (+28kV)	3.57×10^{14}	3.23×10^{14}	↓ 0.03	3.09×10^{17}	1.28×10^{18}	↑ 0.82
	DC (-28 kV)	7.11×10^{14}	3.30×10^{14}	↓ 0.38	3.29×10^{17}	3.01×10^{16}	↓ 1.03

5.4. Tests upon model nano-PDMS samples

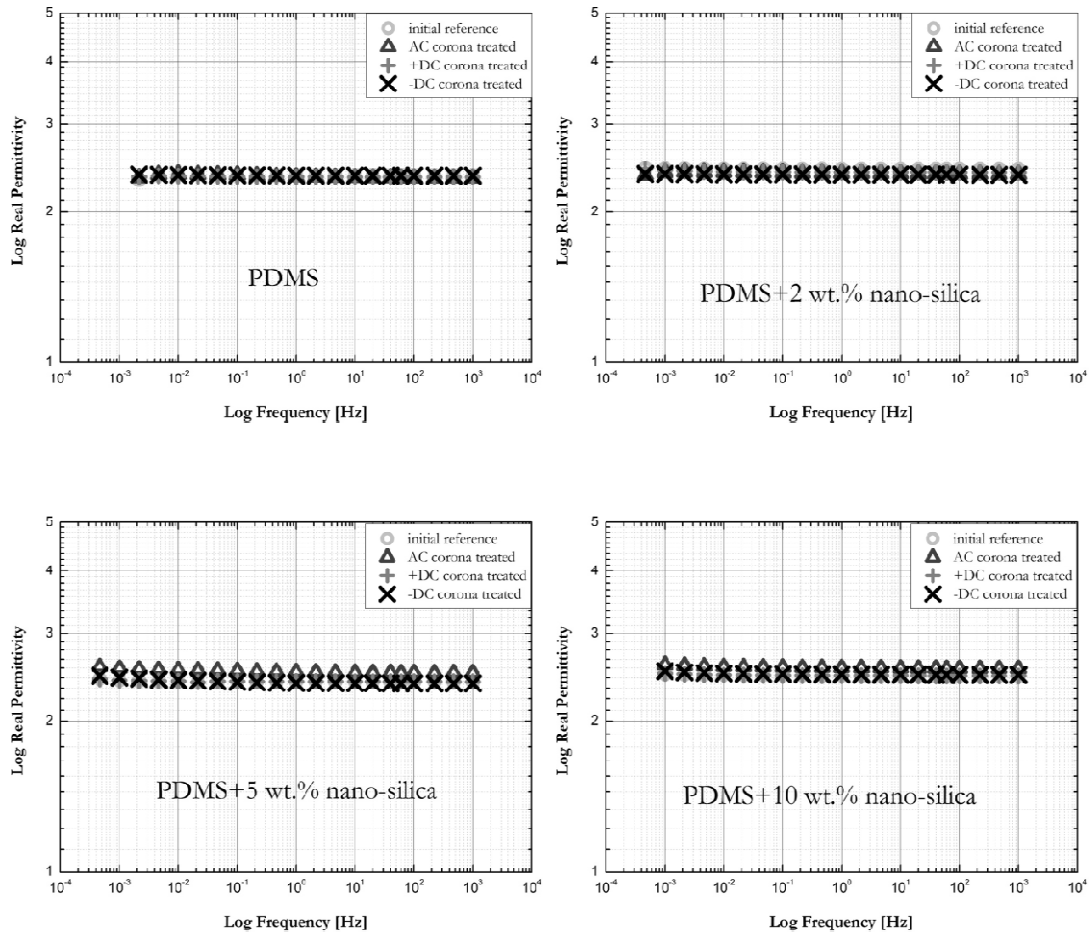


Figure 5.14: Real part of relative permittivity of the model nano-PDMS samples investigated before and after AC/DC corona treatments measured at 30 °C and ~43 % RH.

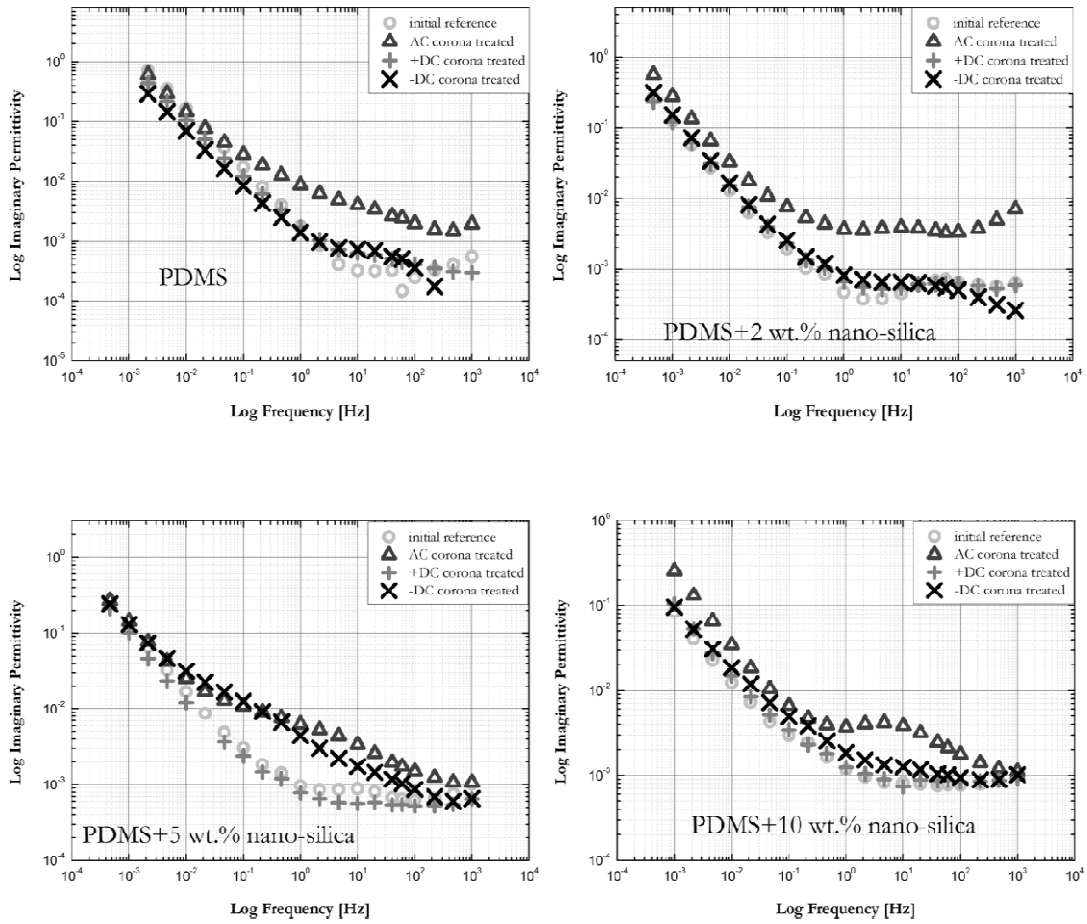


Figure 5.15: Imaginary part of relative permittivity of the model nano-PDMS samples investigated before and after AC/DC corona treatments measured at 30 °C and ~43 % RH.

5.5 Concluding remarks

An important step in securing reliable performance of polymeric insulators in HVDC applications is related to understanding the mechanisms of material degradation when exposed to corona activities. The impacts of AC and DC corona treatments on the properties of commercially available HTV silicone rubber materials are presented and discussed in this chapter.

For securing comparable test condition, the applied voltage level for DC corona treatments was set at ± 28 kV, which is the peak value of the recommended by CIGRE AC corona treatment at 20 kV_{rms}. By measuring the corona currents and the power released from the multi-needle electrode, the DC corona discharge intensity was found to be weaker than that of the AC case, which also yielded much lower ozone concentrations. Additionally, the results aiming at characterizing these corona sources showed that both the corona discharge intensities as well as the concentration of ozone generated by the discharges were dependent on the dielectric parameter of the materials treated.

Less pronounced effects on the electric properties were found during the DC treatments as compared to the AC ones, though surface resistivity was still the mostly affected parameter. In addition, the results of the tensile strength testing did not exhibit clear regularities in the observed weak reduction of mechanical performance. A reasonable explanation for this observation is that the corona-ozone treatment can cause deterioration of the surface, while the volume matrix of polymer remains practically untouched, even under stronger AC corona exposure doses. Finally, FTIR, associated with XPS analyses on the corona treated sample surfaces verified appearance of surface oxidation, which intensity could in turn be correlated with ozone concentration during the treatments. The AC corona exposure, with higher discharge intensity than under the DC treatment, yields higher doses of ozone and results in a more severe surface oxidation. One of the evidence of surface oxidation was the hydrophilic groups (e.g. OH) formed on the surface of the HTV rubber samples investigated during corona treatments confirmed by FTIR analysis, which determines the reduction of hydrophobicity as well as the recovery performance of it after corona exposures.

It seems likely that the observed reduction of the DC corona intensity, attributed to charging of polymeric materials and subsequent reduction of electric field distribution in the discharge regions may play an important role in impeding the degradation of polymeric insulators operating in HVDC installations.

Finally, the effects of AC/DC corona/ozone ageing on the model nano-PDMS samples followed similar regularities as those observed on the HTV elastomer

samples and the most influential corona type was AC corona as well as the mostly affected dielectric property was surface resistivity. In addition, the specific performance also relied on the content of nano-silica filler, as for example the sample filled with 10 wt.% nano-filler showed a more pronounced capability of maintaining the level of surface resistivity during corona treatments in contrast to the other formulations. AC corona treatments gave rise to obviously increased dielectric losses in all the formulations, the specific behaviors however were dependent on the nano-filler content and no clear regularities could so far be observed.

6 Conclusions

The work presented in this thesis concentrated on evaluating the resistance to the artificial AC/DC corona/ozone treatments of polymeric materials tailored for high voltage outdoor insulation applications, as well as investigating various material performance changes due to corona/ozone ageing.

6.1 Test methodology and conditions

For the purposes mentioned above, first and foremost, the corona/ozone ageing test arrangement was designed and thereafter the test conditions were fixed, which involved the careful analysis on both the adopted corona types and the test parameters. A multi-needle electrode system proposed by the CIGRE WG D1.14 was used as the corona source which can be energized by AC or DC high voltages. In the treatment chamber – a glass desiccators with a volume of $20 \times 10^{-3} \text{ m}^3$, a forced ventilation with dry air flowing at 5 L/min was set for maintaining a controlled concentration of humidity, ozone, and gaseous byproducts. By performing static electric field simulation with finite element method (FEM), the distance between the tip of innermost needle and the surface of the specimen to be treated was set at 40 mm to ensure a homogeneous electric field in the vicinity of the sample during the corona treatments. The duration of one round of the test was set at 100 h and the voltage applied to the corona electrode was 20 kV_{rms} for AC corona treatment as well as ± 28 kV, which are the peak values of the applied sinusoidal AC voltage, for DC corona treatments. The voltage level was determined based on measurements of released AC power of ~ 1.5 W from the multi-needle corona electrode. Elastomeric specimens were mechanically stretched by 3 % during the corona/ozone exposures. In addition, the erosion phenomenon of the electrode needles was monitored by means of measuring the corona current and the released power. It has therefore been recommended that for securing repeatability of test results, new set of needles should be used for each round of the 100 h lasting treatment.

6.2 Resistance to AC corona ageing

Associated with the testing methodology developed as well as the procedure proposed to the CIGRE WG D1.14, the first group of investigations in this project were within a international RRT procedure focusing on studying material property (dielectric, mechanical, and physical-chemical structure) changes imposed by the AC corona/ozone treatment of five commercially available polymeric materials (EP, LSR, HTV, EVA and EPDM). It has been observed that the mostly affected parameter on nearly all the materials investigated yielded by the 100 h corona/ozone treatment was surface resistivity. Besides, the mechanical properties, including breakdown strength and elongation at break, were also influenced. The observed changes could mainly be attributed to the surface oxidation as revealed by the performed SEM as well as FTIR analysis. However, the effects of the treatment on volume resistivity, dielectric permittivity as well as dissipation factor (dielectric losses), all being the properties of the materials bulk, did not exhibit high sensitivity to the ageing test. As a consequence of the observed surface cracking and reduction of mechanical strength, it is believed that the presence of corona and ozone in the vicinity of polymeric materials may especially influence materials' mechanical integrity, especially when the materials remain under continuous tension, and thereafter may negatively influence its resistance to tracking and erosion. On the other hand, in respect of dielectric parameters, the influence of corona/ozone does not seem to be too critical despite the relatively strong variations imposed on the surface resistivity.

6.3 Performance changes induced by AC/DC coronas

The project proceeded thereafter to the second group of investigations on the impacts of AC and DC corona treatments on the properties of commercially available HTV silicone rubber materials. Firstly, AC/DC corona discharge intensities were characterized by measuring the corona currents as well as the power released from the multi-needle electrode; the DC corona discharge intensity was found to be weaker than that of the AC case, which also yielded much lower ozone concentrations. Additionally, it was observed that both the corona discharge intensities as well as the concentration of ozone generated by the discharges were dependent on the dielectric parameter of the materials treated.

When comparing the effects on the dielectric properties induced by AC and DC corona treatments, less pronounced effects were found during the DC case, though surface resistivity was still the mostly affected parameter. However, the results

6.4. Performance of nanocomposites under corona ageing

obtained from the tensile tests did not exhibit clear regularities in the observed weak reduction of mechanical performance. Therefore, it was elucidated for this observation that the corona/ozone treatment can cause deterioration of the specimen surface, while the volume matrix of polymer remains practically untouched, even under stronger doses of AC corona exposures. Furthermore, deterioration of the material surface treated by corona discharges were typically reflected by surface oxidation revealed by FTIR, associated with XPS analysis, the intensity of which could in turn be correlated with ozone concentration during the treatments. The AC corona exposure, with higher discharge intensity than under the DC treatment, yields higher doses of ozone and results in a more severe surface oxidation. The hydrophilic groups (e.g. OH) formed on the surface of the HTV silicone rubber samples investigated during corona treatments confirmed by FTIR analysis, determining the reduction of hydrophobicity as well as the recovery performance of it after corona exposures, was one of the evidence for the occurrence of surface oxidation.

An important conclusion one could draw from this part of investigations is that, the observed reduction of the DC corona intensity, attributed to charging of polymeric materials and subsequent reduction of electric field distribution in the discharge regions may play an important role in impeding the degradation of polymeric insulators operating in HVDC installations.

6.4 Performance of nanocomposites under corona ageing

On top of the investigations on the commercially available polymeric material specimens, two extra batches of model nanocomposites were involved in this project. As for the resistance to AC corona/ozone treatment of the model epoxy compositions filled with micro- and nano-fillers at different proportions, similarly to the commercial materials, the 100 h long corona/ozone exposure had obvious effect on the surface properties for all the compositions investigated and the presence of the nano-filler has a significant role in retarding further degradation on the surface of the epoxy compositions. In addition, increase of the nano-filler content yielded an incremental tendency in the activation energy value, while the effect was reduced by adding micro-fillers. As regards the performance of the nano-PDMS specimens under the AC/DC corona ageing tests, it was observed that the most influential corona type was AC corona as well as the mostly affected dielectric property was surface resistivity, similarly to those observed on the HTV rubber samples. In addition, the specific performance under corona ageing also relied on the content of nano-silica filler, as for example the sample filled with 10 wt.% nano-filler showed a more remarkable capability of maintaining the level of surface resistivity during corona treatments in

Chapter 6. Conclusions

contrast to the other formulations. Finally, obviously increased dielectric losses induced by AC corona treatments were observed in all the formulations, the specific behaviors however were dependent on the nano-filler content and no clear regularities could so far be observed.

7 Future work

On the way of making efforts to standardize the selection of polymeric materials for high voltage outdoor environments, the investigations reported in this thesis play a role of proposing a new methodology for testing the resistance to AC/DC corona/ozone ageing as well as for providing a reference for international standardization and definition of material minimum requirements.

Before considering standardization of the proposed procedure, it must still be evaluated by different laboratories, in a round robin test procedure, for checking if repeatable of the results is on an acceptable level. In addition, the influence of air humidity in the test chamber, possibly being a strongly influencing factor, should also be elucidated in the future.

Though the changes observed on the tested materials seem to still lie above the levels that might be considered as dangerous, the limits (minimum requirements) are not agreed today among material suppliers, insulators manufacturers and insulator users. Furthermore, the tested materials show different characteristic features, dependent on polymer type as well as type and amount of fillers. Actions and discussions are therefore necessary on international forum for defining these limits. In case of the tensile strength and the elongation at break the procedure should rather be used for ranking materials of similar type and eliminating the weakest. Perhaps, a reduction of the mechanical parameters by, say, 50 % in reference to the initial values should be considered as a warning point.

Last but not least, some phenomena were repeatedly observed during tests, like the ozone concentration measured during DC corona treatments was not proportional to the power released from the multi-needle corona source as compared to the one behaving under AC case as well as the ozone production depended on the material dielectric parameters during DC corona treatments. Attempts to elucidate these phenomena were provided, however, more investigations, which might be outside the scope of this thesis, are still needed in the future for an even better understanding on the performance of polymeric materials during corona/ozone exposures.

Bibliography

- [1] J. S. T. Looms, *Insulators for High Voltages*. Peter Peregrinus Ltd., UK, 1988.
- [2] R. Hackam, "Outdoor HV composite polymeric insulators", IEEE Trans. Dielectr. Electr. Insul., vol. 6, pp. 557-585, 1999.
- [3] X. Liang, S. Wang, J. Fan, and Z. Guan, "Development of composite insulators in China", IEEE Trans. Dielectr. Electr. Insul., vol. 6, pp. 586-594, 1999.
- [4] X. Liang, J. Wang, Q. Shen, Y. Zhang, and Y. Li, "Methods used in China to assess composite insulators after years in service", Proc. INMR World Insulator Congress & Exhibition, paper B-4, Crete, Greece, 2009.
- [5] S. Vittorio and G. James, "40 years of Dow Corning technology for transmission & distribution applications", Proc. INMR World Insulator Congress & Exhibition, Rio de Janeiro, Brazil, 2007.
- [6] CIGRE WG D1.14, "Material properties for non-ceramic outdoor insulation: State of the art", CIGRE Technical Brochure No. 255, 2004.
- [7] J. Andersson, B. Sonnerud, Y. V. Serdyuk, S. M. Gubanski, and H. Hillborg, "Evaluation of polymeric materials resistance to corona and ozone", Proc. Int. Symp. High Voltage Eng. (ISH), pp. 161-166, Ljubljana, Slovenia, 2007.
- [8] R. S. Gorur, E. A. Cherney, and J. T. Burnham, *Outdoor Insulators*. Ravi S. Gorur Inc., 1999.
- [9] S. Kumagai and N. Yoshimura, "Tracking and erosion of HTV silicone rubber and suppression mechanism of ATH", IEEE Trans. Dielectr. Electr. Insul., vol. 8, pp. 203-211, 2001.
- [10] E. A. Cherney, "Non-ceramic insulators - a simple design that requires careful analysis", IEEE Electr. Insul. Mag., vol. 12, pp. 7-15, 1996.
- [11] S. J. Clarson and J. A. Semlyen, *Siloxane Polymers*. PTR Prentice Hall Inc., 1993.

Bibliography

- [12] H. Hillborg and U. W. Gedde, "Hydrophobicity changes in silicone rubbers", *IEEE Trans. Dielectr. Electr. Insul.*, vol. 6, pp. 703-715, 1999.
- [13] C. A. Spellman, H. M. Young, A. Haddad, A. R. Rowlands, and R. T. Waters, "Survey of polymeric insulator ageing factors", *Proc. Int. Symp. High Voltage Eng. (ISH)*, vol. 4, pp. 160-163, London, UK, 1999.
- [14] R. G. Houlgate and D. A. Swift, "Composite rod insulators for AC power lines: electrical performance of various designs at a coastal testing station", *IEEE Trans. Power Del.*, vol. 5, pp. 1944-1955, 1990.
- [15] T. Sörqvist and A. E. Vlastos, "Outdoor polymeric insulators long-term exposed to HVDC", *IEEE Trans. Power Del.*, vol. 12, pp. 1041-1048, 1997.
- [16] M. A. R. M. Fernando, "Performance of non-ceramic insulators in tropical environments", Ph.D. thesis, Department of Electric Power Engineering, Chalmers University of Technology, Gothenburg Sweden, 1999.
- [17] T. Sörqvist, "Polymeric outdoor insulators - a long term study", Ph.D. thesis, Department of Electric Power Engineering, Chalmers University of Technology, Gothenburg Sweden, 1997.
- [18] A. E. Vlastos and S. M. Gubanski, "Surface structural changes of naturally aged silicone and EPDM composite insulators", *IEEE Trans. Power Del.*, vol. 6, pp. 888-900, 1991.
- [19] T. Sörqvist and A. E. Vlastos, "Performance and aging of polymeric insulators", *IEEE Trans. Power Del.*, vol. 12, pp. 1657-1665, 1997.
- [20] C. N. Ravera, P. J. Olivier, A. C. Britten, and D. A. Swift, "Silicone rubber insulators on Eskom's AC transmission lines", *Proc. Int. Conf. AC-DC Power Transmiss.*, pp. 70-75, 1996.
- [21] T. Sörqvist, U. Karlsson, and A. E. Vlastos, "Surface aging and its impact on the performance of polymeric insulators", *Proc. Int. Symp. High Voltage Eng. (ISH)*, pp. 3234-1 -3234-4, Graz, Austria, 1995.
- [22] R. S. Gorur, J. Mishra, R. Tay, and R. McAfee, "Electrical performance of RTV silicone rubber coatings", *IEEE Trans. Dielectr. Electr. Insul.*, vol. 3, pp. 299-306, 1996.
- [23] A. E. Vlastos and E. Sherif, "Experience from insulators with RTV silicon rubber sheds and shed coatings", *IEEE Trans. Power Del.*, vol. 5, pp. 2030-2038, 1990.
- [24] S. H. Kim, E. A. Cherney, and R. Hackam, "Suppression mechanism of leakage current on RTV coated porcelain and silicone rubber insulators", *IEEE Trans. Power Del.*, vol. 6, pp. 1549-1556, 1991.

- [25] G. G. Karady, M. Shah, and R. L. Brown, "Flashover mechanism of silicone rubber insulators used for outdoor insulation-I", *IEEE Trans. Power Del.*, vol. 10, pp. 1965-1971, 1995.
- [26] A. Eriksson and D. Wikstrom, "Influence of the hydrophobicity of outdoor insulators on the flashover voltage", *Proc. Nordic Insul. Symp. (NORD-IS)*, pp. 39-51, Vaasa, Finland, 1994.
- [27] J. Mackevich and M. Shah, "Polymer outdoor insulating materials. Part I: Comparison of porcelain and polymer electrical insulation", *IEEE Electr. Insul. Mag.*, vol. 13, pp. 5-12, 1997.
- [28] S. M. Gubanski and A. E. Vlastos, "Wettability of naturally aged silicon and EPDM composite insulators", *IEEE Trans. Power Del.*, vol. 5, pp. 1527-1535, 1990.
- [29] A. Tóth, I. Bertóti, M. Blazsó, G. Bánhegyi, A. Bogнар, and P. Szaplóczay, "Oxidative damage and recovery of silicone rubber surfaces. I. X-ray photoelectron spectroscopic study", *J. Appl. Polym. Sci.*, vol. 52, pp. 1293-1307, 1994.
- [30] P. J. Smith, M. J. Owen, P. H. Holm, and G. A. Toskey, "Surface studies of corona-treated silicone rubber high-voltage insulation", *Proc. IEEE Conf. Electr. Insul. Dielectr. Phenom. (CEIDP)*, pp. 829-836, Victoria, BC, Canada, 1992.
- [31] J. Kindersberger and M. Kuhl, "Effect of Hydrophobicity on Insulator Performance", *Proc. Int. Symp. High Voltage Eng. (ISH)*, paper no. 12. 01, New Orleans, Louisiana, USA, 1989.
- [32] J. G. Wankowicz, S. M. Gubanski, and W. D. Lampe, "Loss and recovery of hydrophobicity on RTV coating surfaces", *IEEE Trans. Dielectr. Electr. Insul.*, vol. 1, pp. 604-614, 1994.
- [33] R. Bärsch, J. Lambrecht, and H. J. Winter, "On the evaluation of influences on the hydrophobicity of silicone rubber surface", *Proc. Int. Symp. High Voltage Eng. (ISH)*, paper no. 3220, Montreal, Canada, 1997.
- [34] J. W. Chang and R. S. Gorur, "Surface recovery of silicone rubber used for HV outdoor insulation", *IEEE Trans. Dielectr. Electr. Insul.*, vol. 1, pp. 1039-1046, 1994.
- [35] K. O. Papailiou, "Composite insulators are gaining ground-25 years of Swiss experience", *Proc. IEEE Trans. Distrib. Syst.*, vol. 2, pp. 827-833, 1999.
- [36] T. Kikuchi, S. Nishimura, M. Nagao, K. Izumi, Y. Kubota, and M. Sakata, "Survey on the use of non-ceramic composite insulators", *IEEE Trans. Dielectr. Electr. Insul.*, vol. 6, pp. 548-556, 1999.

Bibliography

- [37] C. de Turreil, G. Riquel, G. Beszrercey, R. Hartings, S. W. Hodgkinson, M. Ishiwari, R. Joulie, B. Kahl, R. Macey, R. Matsuoka, K. Naito, K. O. Papailiou, T. Pinkham, G. Pirovano, M. Portillo, H. Schneider, R. de Oliveira, B. Staub, and R. Stone, "Worldwide service experience with HV composite insulators," *Electra*, Iss. 191, pp. 26-43, 2000.
- [38] M. Zimmerman, "Innovative compact line design at Energie Ouest Suisse", *Insulator News and Market Report (INMR)*, pp. 20-28, March/April, 1999.
- [39] D. Dumora, "New compact composite insulation for environmental, economic and safety considerations", *Proc. INMR World Insulator Congress & Exhibition*, pp. 168-181, Shanghai, China, 2001.
- [40] L. H. Meyer, E. A. Cherney, and S. H. Jayaram, "The role of inorganic fillers in silicone rubber for outdoor insulation alumina tri-hydrate or silica", *IEEE Electr. Insul. Mag.*, vol. 20, pp. 13-21, 2004.
- [41] Y. Koshino, I. Nakajima, and I. Umeda, "Effect on the electrical properties of fillers in silicone rubber for outdoor insulation", *Proc. Int. Symp. Electr. Insul. Mater. (ISEIM)*, pp. 465-468, Toyohashi, Japan, 1998.
- [42] Y. Koshino, I. Umeda, and M. Ishiwari, "Deterioration of silicone rubber for polymer insulators by corona discharge and effect of fillers", *Proc. IEEE Conf. Electr. Insul. Dielectr. Phenom. (CEIDP)*, pp. 72-79, Atlanta, Georgia, USA, 1998.
- [43] H. Janssen, A. Herden, and H. C. Karner, "The loss and recovery of hydrophobicity on silicone rubber surfaces", *Proc. Int. Symp. High Voltage Eng. (ISH)*, pp. 145-148, Montreal, Canada, 1997.
- [44] L. Lan and X. Wen, "Investigation to the influence of nanomaterial on the resistance to tracking and erosion of RTV coatings", *Proc. IEEE Int. Conf. Power Syst. Tech. (PowerCon)*, pp. 1881-1883, Kunming, China, 2002.
- [45] D. Cai, J. Yu, X. Wen, and L. Lan, "Research on characterization of RTV silicone rubber/LS(layered silicate) electrical insulation nanocomposites", *Proc. IEEE Int. Conf. Solid Dielectr. (ICSD)*, pp. 796-799, Toulouse, France, 2004.
- [46] L. Lan, X. Wen, and D. Cai, "Corona aging tests of RTV and RTV nanocomposite materials", *Proc. IEEE Int. Conf. Solid Dielectr. (ICSD)*, pp. 804-807, Toulouse, France, 2004.
- [47] B. Venkatesulu and M. J. Thomas, "Corona aging studies on silicone rubber nanocomposites," *IEEE Trans. Dielectr. Electr. Insul.*, vol. 17, pp. 625-634, 2010.

- [48] M. Kozako, S. Kuge, T. Imai, T. Ozaki, T. Shimizu, and T. Tanaka, "Surface erosion due to partial discharges on several kinds of epoxy nanocomposites", Proc. IEEE Conf. Electr. Insul. Dielectr. Phenom. (CEIDP), pp. 162-165, Nashville, Tennessee, USA, 2005.
- [49] B. Venkatesulu, "Studies on polymeric micro/nanocomposites for outdoor high voltage insulation", Ph.D. thesis, Department of Electrical Engineering, Indian Institute of Science, Bangalore, India, 2010.
- [50] I. R. Vazquez, "A study of nanofilled silicone dielectrics for outdoor insulation", Ph.D. thesis, Department of Electrical and Computer Engineering, University of Waterloo, Waterloo, Ontario, Canada, 2009.
- [51] S. Rätzke and J. Kindersberger, "Erosion behavior of nanofilled silicone elastomers", Proc. Int. Symp. High Voltage Eng. (ISH), pp. C09 1-6, Beijing, China, 2005.
- [52] A. H. El-Hag, S. H. Jayaram, and E. A. Cherney, "Comparison between silicone rubber containing micro- and nano- size silica fillers [insulating material applications]", Proc. IEEE Conf. Electr. Insul. Dielectr. Phenom. (CEIDP), pp. 385-388, Boulder, Colorado, USA, 2004.
- [53] L. H. Meyer, S. H. L. Cabral, E. Araujo, G. Cardoso, and N. Liesenfeld, "Use of nano-silica in silicone rubber for ceramic insulators coatings in coastal areas", Proc. IEEE Int. Symp. Electr. Insul. (ISEI), pp. 474-477, Toronto, Ont., Canada, 2006.
- [54] I. Ramirez, E. A. Cherney, S. Jayaram, and M. Gauthier, "Silicone rubber nanocomposites for outdoor insulation applications", Proc. IEEE Conf. Electr. Insul. Dielectr. Phenom. (CEIDP), pp. 384-387, Vancouver, BC, Canada, 2007.
- [55] I. Ramirez, E. A. Cherney, S. Jayaram, and M. Gauthier, "Nanofilled silicone dielectrics prepared with surfactant for outdoor insulation applications", IEEE Trans. Dielectr. Electr. Insul., vol. 15, pp. 228-235, 2008.
- [56] T. Tanaka, Y. Ohki, M. Ochi, M. Harada, and T. Imai, "Enhanced partial discharge resistance of epoxy/clay nanocomposite prepared by newly developed organic modification and solubilization methods", IEEE Trans. Dielectr. Electr. Insul., vol. 15, pp. 81-89, 2008.
- [57] T. Imai, F. Sawa, T. Nakano, T. Ozaki, T. Shimizu, M. Kozako, and T. Tanaka, "Effects of nano- and micro-filler mixture on electrical insulation properties of epoxy based composites", IEEE Trans. Dielectr. Electr. Insul., vol. 13, pp. 319-326, 2006.
- [58] T. Imai, F. Sawa, T. Nakano, T. Ozaki, T. Shimizu, S. Kuge, M. Kozako, and T. Tanaka, "Insulation properties of nano- and micro-filler mixture

Bibliography

- composite," Proc. IEEE Conf. Electr. Insul. Dielectr. Phenom. (CEIDP), pp. 171-174, Nashville, Tennessee, USA, 2005.
- [59] N. Fuse, M. Kozako, T. Tanaka, and Y. Ohki, "Effects of mica fillers on dielectric properties of polyamide nanocomposites", Proc. IEEE Conf. Electr. Insul. Dielectr. Phenom. (CEIDP), pp. 148-151, Nashville, Tennessee, USA, 2005.
- [60] S. Singha and M. J. Thomas, "Polymer composite/nanocomposite processing and its effect on the electrical properties", Proc. IEEE Conf. Electr. Insul. Dielectr. Phenom. (CEIDP), pp. 557-560, Kansas City, Missouri, USA, 2006.
- [61] M. Kurimoto, H. Watanabe, K. Kato, M. Hanai, Y. Hoshina, M. Takei, and H. Okubo, "Dielectric properties of epoxy/alumina nanocomposite influenced by particle dispersibility," Proc. IEEE Conf. Electr. Insul. Dielectr. Phenom. (CEIDP), pp. 706-709, Quebec City, Canada, 2008.
- [62] A. H. El-Hag, L. C. Simon, S. H. Jayaram, and E. A. Cherney, "Erosion resistance of nano-filled silicone rubber", IEEE Trans. Dielectr. Electr. Insul., vol. 13, pp. 122-128, 2006.
- [63] F. W. Peek, *Dielectric Phenomena in High-Voltage Engineering*. 3rd ed., McGraw-Hill, New York, 1929.
- [64] I. W. McAllister, G. C. Crichton, and E. Bregnsbo, "Experimental study on the onset of positive corona in atmospheric air", J. Appl. Phys., vol. 50, pp. 6797-6805, 1979.
- [65] J. B. Whitehead, "High-voltage corona", Int. Crit. Tab., McGraw-Hill, 1929.
- [66] J. Brady, "Corona and tracking conditions in metal-clad switchgear case studies", Brady Infrared Inspections, Inc., pp. 1-16, 2005.
- [67] J. H. Chen, "Direct current corona-enhanced chemical reactions", Ph.D. thesis, Department of Mechanical Engineering, University of Minnesota, Minneapolis, Minnesota, USA, 2002.
- [68] I. A. Kossyi, A. Yu Kostinsky, A. A. Matveyev, and V. P. Silakov, "Kinetic scheme of the non-equilibrium discharge in nitrogen-oxygen mixtures", Plasma Sources Sci. Technol., vol. 1, pp. 207-220, 1992.
- [69] R. S. Sigmond, *Electric breakdown of gases*. Wiley, New York, 1978.
- [70] L. B. Loeb, *Fundamental Processes of Electrical Discharge in Gases*. John Wiley & Sons, Inc., New York, 1947.
- [71] R. Morrow, "Theory of negative corona in oxygen", Phys. Review A, vol. 32, pp. 1799-1809, 1985.
- [72] Y. P. Raizer, *Gas Discharge Physics*. Springer, New York, 1997.

- [73] Carl Nordling and Jonny Österman, *Physics Handbook for Science and Engineering*. 8th ed., Studentlitteratur, Lund, Sweden, 2006.
- [74] J. H. Chen and J. H. Davidson, "Ozone production in the negative DC corona: the dependence of discharge polarity", *Plasma Chem. Plasma Process.*, vol. 23, pp. 501-518, Sep 2003.
- [75] K. Takaki, H. Akiyama, and S. Maeda, "Characteristics of discharge for a point-to-plane gap in gas flow", *Trans. Inst. Electr. Eng. Japan, Part A*, vol. 110-A, pp. 119-125, 1990.
- [76] S. Chapman, "Corona point current in wind", *J. Geophys. Res.*, vol. 75, pp. 2165-2169, 1970.
- [77] J. A. Chalmers, "Effect of wind on point-discharge pulses", *J. Atm. Terr. Phys.*, vol. 27, pp. 1037-1038, 1965.
- [78] K. J. Nygaard, "Frequency of corona discharge trichel pulses in air flows", *J. Appl. Phys.*, vol. 37, pp. 2850-2852, 1966.
- [79] T. Yamamoto, P. A. Lawless, and L. A. Sparks, "Narrow-gap point-to-plane corona with high velocity flows", *IEEE Trans. Ind. Appl.*, vol. 24, pp. 934-939, 1988.
- [80] W. L. Lama and C. F. Gallo, "Interaction of trichel current pulses of a pair of negative coronas", *J. Phys. D: Appl. Phys.*, vol. 6, pp. 1963-1972, 1973.
- [81] M. Abdel-Salam, A. A. Fattah, M. M. Saied, and M. Tharwat-El-Mohandes, "Positive corona pulse characteristics from two interacting needles in air", *IEEE Trans. Ind. Appl.*, vol. IA-21, pp. 912-918, 1985.
- [82] L. C. Thanh, "Negative corona in a multiple interacting point-to-plane gap in air", *IEEE Trans. Ind. Appl.*, vol. IA-21, pp. 518-522, 1985.
- [83] P. J. McKinney, J. H. Davidson, and D. M. Leone, "Current distributions for barbed plate-to-plane coronas", *IEEE Trans. Ind. Appl.*, vol. 28, pp. 1424-1431, 1992.
- [84] A. Jaworek and A. Krupa, "Electrical characteristics of a corona discharge reactor of multipoint-to-plane geometry", *Czechoslovak J. Phys.*, vol. 45, pp. 1035-1047, 1995.
- [85] Y. S. Akishev, A. A. Deryugin, I. V. Kochetov, A. P. Napartovich, and N. I. Trushkin, "DC glow-discharge in air-flow at atmospheric-pressure in connection with waste gases treatment", *J. Phys. D: Appl. Phys.*, vol. 26, pp. 1630-1637, Oct 1993.
- [86] M. T. El-Mohandes, S. Ushiroda, S. Kajita, Y. Kondo, and K. Horii, "Ozone production in corona discharges in air in a multi-needle to plane

Bibliography

- configuration", IEEE Ind. Appl. Soc. Annu. Meet., pp. 1567-1569, Houston, Texas, USA, 1992.
- [87] M. Horvath, *Ozone*. Amsterdam, The Netherlands: Elsevier Science, 1980.
- [88] R. Feng, G. S. P. Castle, and S. Jayaram, "Automated system for power measurement in the silent discharge", IEEE Trans. Ind. Appl., vol. 34, pp. 563-570, 1998.
- [89] H. Hillborg and U. W. Gedde, "Hydrophobicity recovery of polydimethylsiloxane after exposure to corona discharges", Polymer, vol. 39, pp. 1991-1998, 1998.
- [90] Y. Nomoto, T. Ohkubo, S. Kanazawa, and T. Adachi, "Improvement of ozone yield by a silent-surface hybrid discharge ozonizer", IEEE Trans. Ind. Appl., vol. 31, pp. 1458-1462, 1995.
- [91] J. S. Chang and S. Masuda, "Mechanism of the ozone formations in a near liquid nitrogen temperature medium pressure glow discharge positive column", Pure Appl. Chem., vol. 60, No. 5, pp. 645-650, 1980.
- [92] K. Nashimoto, "The effect of electrode materials on O₃ and NO_x emissions by corona discharging", J. Imaging Sci., vol. 32, pp. 205-210, 1988.
- [93] S. Okazaki, H. Sugimitsu, H. Niwa, M. Kogoma, T. Moriwaki, and T. Inomata, "Ozone formation from the reaction of O₂-activated N₂ molecules and a new type of ozone generator with fine wire electrode", Oz. Sci. Eng. vol. 10, pp. 137-151, 1988.
- [94] B. Held and R. Peyrous, "Physical and chemical studies of corona discharges in air", Czechoslovak J. Phys., vol. 49, pp. 301-320, 1999.
- [95] R. J. Hollahan and L. G. Carlson, "Hydroxylation of polymethylsiloxane surfaces by oxidizing plasmas", J. Appl. Polym. Sci., vol. 14, pp. 2499-2508, 1970.
- [96] Y. Zhu, M. Otsubo, C. Honda, and S. Tanaka, "Loss and recovery in hydrophobicity of silicone rubber exposed to corona discharge", Polym. Degrad. Stabl., vol. 91, pp. 1448-1454, 2006.
- [97] M. Morra, E. Occhiello, R. Marola, F. Garbassi, P. Humphrey, and D. Johnson, "On the aging of oxygen plasma-treated polydimethylsiloxane surfaces", J. Coll. Interf. Sci., vol. 137, pp. 11-24, 1990.
- [98] A. D. Delman, M. landy, and B. B. Simms, "Photodecomposition of polymethylsiloxane", J. Polym. Sci., vol. 7, pp. 3375-3386, 1969.

- [99] H. Hillborg, "Loss and recovery of hydrophobicity of polydimethyl-siloxane after exposure to electrical discharges", Ph.D. thesis, Department of Polymer Technology, Royal Institute of Technology, Stockholm Sweden, 2001.
- [100] J. Lacoste, Y. Israeli, Y. Lemaire, in *Polymer Durability, Degradation Stabilisation and Lifetime Prediction*, Eds. L. R. Clough, C. N. Billingham, and T. K. Gillen, *Advances in Chemistry Series 249*, American Chemical Soc., Washington DC, 1996.
- [101] S.-H. Kim, E. A. Cherney, R. Hackam, and K. G. Rutherford, "Chemical changes at the surface of RTV silicone rubber coatings on insulators during dry-band arcing", *IEEE Trans. Dielectr. Electr. Insul.*, vol. 1, pp. 106-123, 1994.
- [102] T. G. Gustavsson, S. M. Gubanski, H. Hillborg, S. Karlsson, and U. W. Gedde, "Aging of silicone rubber under AC or DC voltages in a coastal environment", *IEEE Trans. Dielectr. Electr. Insul.*, vol. 8, pp. 1029-1039, 2001.
- [103] H. Hillborg, S. Karlsson, and U. W. Gedde, "Characterisation of low molar mass siloxanes extracted from crosslinked polydimethylsiloxanes exposed to corona discharges", *Polymer*, vol. 42, pp. 8883-8889, 2001.
- [104] J. Kim, M. K. Chaudhury, and M. J. Owen, "Hydrophobicity loss and recovery of silicone HV insulation", *IEEE Trans. Dielectr. Electr. Insul.*, vol. 6, pp. 695-702, 1999.
- [105] S. Kumagai and N. Yoshimura, "Hydrophobic transfer of RTV silicone rubber aged in single and multiple environmental stresses and the behavior of LMW silicone fluid", *IEEE Trans. Power Del.*, vol. 18, pp. 506-516, 2003.
- [106] T. Gustavsson, "Silicone rubber insulators - impacts of material formulation in coastal environment", Ph.D. thesis, Department of electric power engineering, Chalmers university of technology, Gothenburg Sweden, 2002.
- [107] A. J. Phillips, D. J. Childs, and H. M. Schneider, "Water drop corona effects on full-scale 500 kV non-ceramic insulators", *IEEE Trans. Power Del.*, vol. 14, pp. 258-265, 1999.
- [108] A. J. Phillips, D. J. Childs, and H. M. Schneider, "Aging of nonceramic insulators due to corona from water drops", *IEEE Trans. Power Del.*, vol. 14, pp. 1081-1089, 1999.
- [109] J. P. Reynders, I. R. Jandrell, and S. M. Reynders, "Surface ageing mechanisms and their relationship to service performance of silicone rubber insulation", *Proc. Int. Symp. High Voltage Eng. (ISH)*, pp. 54-58, London, UK, 1999.

Bibliography

- [110] M. Kumosa, L. Kumosa, and D. Armentrout, "Failure analyses of nonceramic insulators: part II - the brittle fracture model and failure prevention", *IEEE Electr. Insul. Mag.* vol. 21, pp. 28-41, 2005.
- [111] M. Kumosa, L. Kumosa, and D. Armentrout, "Causes and potential remedies of brittle fracture failure of composite (nonceramic) insulators", *IEEE Trans. Dielectr. Electr. Insul.*, vol. 11, pp. 1037-1048, 2004.
- [112] A. R. Chughtai, D. M. Smith, L. S. Kumosa, and M. Kumosa, "FTIR analysis of non-ceramic composite insulators", *IEEE Trans. Dielectr. Electr. Insul.*, vol. 11, pp. 585-596, 2004.
- [113] K. Katada, Y. Takada, M. Takano, T. Nakanishi, Y. Hayashi, and R. Matsuoka, "Corona discharge characteristics of water droplets on hydrophobic polymer insulator surface", *Proc. IEEE Int. Conf. Prop. Appl. Dielectr. Mater. (ICPADM)*, pp. 781-784, Xi'an, China, 2000.
- [114] I. J. S. Lopes, S. H. Jayaram, and E. A. Cherney, "A study of partial discharges from water droplets on a silicone rubber insulating surface", *IEEE Trans. Dielectr. Electr. Insul.*, vol. 8, pp. 262-268, 2001.
- [115] Y. Higashiyama, S. Yanase, and T. Sugimoto, "DC corona discharge from water droplets on a hydrophobic surface", *J. Electrostat.*, vol. 55, pp. 351-360, 2002.
- [116] T. Braunsberger, A. Dziubek, and M. Kurrat, "Water drop corona on hydrophobic epoxy", *Proc. IEEE Int. Conf. Solid Dielectr. (ICSD)*, pp. 439-442, Toulouse, France, 2004.
- [117] Y. Zhu, S. Yamashita, N. Anami, M. Otsubo, C. Honda, and Y. Hashimoto, "Corona discharge phenomenon and behavior of water droplets on the surface of polymer in the AC electric field", *Proc. IEEE Int. Conf. Prop. Appl. Dielectr. Mater. (ICPADM)*, pp. 638-641, Nagoya, Japan, 2003.
- [118] Z. Yong, M. Otsubo, and C. Honda, "Behavior of water droplet on electrically stressed polymeric coating surface", *Surf. Coat. Tech.*, vol. 201, pp. 5541-5546, 2007.
- [119] V. M. Moreno and R. S. Goror, "An experimental approach to the estimation of the long term corona performance of non-ceramic insulator housings", *Proc. IEEE Int. Symp. Electr. Insul. (ISEI)*, pp. 193-196, Anaheim, California, USA, 2000.
- [120] V. M. Moreno and R. S. Gorur, "Effect of long-term corona on non-ceramic outdoor insulator housing materials", *IEEE Trans. Dielectr. Electr. Insul.*, vol. 8, pp. 117-128, 2001.

- [121] Ohio Brass, "Applying technology for better reliability; Materials testing and evaluation", Proc. INMR World Insulator Congress & Exhibition, pp. 245-253, Shanghai, China, 2001.
- [122] C. Beisele, "Hydrophobic Cycloaliphatic epoxy - latest findings and future developments", Proc. INMR World Insulator Congress & Exhibition, pp. 141-153, Shanghai, China, 2001.
- [123] N. M. Ijumba, A. C. Britten, and J. P. Swartz, "The hydrophobicity of silicone rubber insulators subjected to water droplet corona under HVDC potential", Proc. IEEE Int. Conf. Power Syst. Tech. (PowerCon), pp. 1884-1889, Kunming, China, 2002.
- [124] P. E. Mallon, C. J. Greyling, W. Vosloo, and Y. C. Jean, "Positron annihilation spectroscopy study of high-voltage polydimethylsiloxane (PDMS) insulators", Rad. Phys. Chem., vol. 68, pp. 453-456, 2003.
- [125] M. Meincken, T. A. Berhane, and P. E. Mallon, "Tracking the hydrophobicity recovery of PDMS compounds using the adhesive force determined by AFM force distance measurements", Polymer, vol. 46, pp. 203-208, 2005.
- [126] V. M. Moreno and R. S. Gorur, "Impact of corona on the long-term performance of nonceramic insulators", IEEE Trans. Dielectr. Electr. Insul., vol. 10, pp. 80-95, 2003.
- [127] M. Goldman, A. Goldman, and J. Gatellet, "Physical and chemical aspects of partial discharges and their effects on materials", IEE Proc. Sci. Meas. Tech., vol. 142, pp. 11-16, 1995.
- [128] K. Fateh-Alavi, "Stabilizers in crosslinked polydimethylsiloxane - the effect of stabilizers on the discharge-induced oxidation of crosslinked polydimethylsiloxane", Ph.D. thesis, Department of Fiber and Polymer Technology, School of Chemical Science and Engineering, KTH Royal Institute of Technology, Stockholm, Sweden, 2003.
- [129] International Electrotechnical Commission, Recommended test methods for determining the relative resistance of insulating materials to breakdown by surface discharges (IEC 60343), 1992.
- [130] V. M. Moreno and R. S. Gorur, "Accelerated corona discharge performance of polymer compounds used in high voltage outdoor insulators", Proc. IEEE Conf. Electr. Insul. Dielectr. Phenom. (CEIDP), pp. 731-734, Austin, Texas, USA, 1999.
- [131] V. M. Moreno and R. S. Gorur, "Corona-induced degradation of nonceramic insulator housing materials", Proc. IEEE Conf. Electr. Insul. Dielectr. Phenom. (CEIDP), pp. 640-643, Kitchener, Ontario, Canada, 2001.

Bibliography

- [132] A. Olah, H. Hillborg, and G. J. Vancso, "Hydrophobic recovery of UV/ozone treated poly(dimethylsiloxane): adhesion studies by contact mechanics and mechanism of surface modification", *Appl. Surf. Sci.*, vol. 239, pp. 410-423, 2005.
- [133] M. P. Panaget, A. Goldman, and M. Goldman, "Ozone in wire-to-plane electrode systems", *Proc. IEEE Int. Symp. Electr. Insul. (ISEI)*, pp. 428-431, Montreal, Quebec., Canada, 1996.
- [134] K. Fateh-Alavi, M. Gällstedt, and U. W. Gedde, "The effect of antioxidants on the surface oxidation and surface cracking of crosslinked polydimethylsiloxane", *Polym. Degrad. Stabl.*, vol. 74, pp. 49-57, 2001.
- [135] K. Fateh-Alavi, M. E. Núñez, S. Karlsson, and U. W. Gedde, "The effect of stabilizer concentration on the air-plasma-induced surface oxidation of crosslinked polydimethylsiloxane", *Polym. Degrad. Stabl.*, vol. 78, pp. 17-25, 2002.
- [136] K. Fateh-Alavi and U. W. Gedde, "Effect of stabilizers on surface oxidation of silicone rubber by corona discharge", *Polym. Degrad. Stabl.*, vol. 84, pp. 469-474, 2004.
- [137] B. X. Du, L. Yong, and R. L. Wang, "Effects of corona discharge on surface deterioration of silicone rubber insulator under reduced pressures", *Proc. Int. Symp. Electr. Insul. Mater. (ISEIM)*, pp. 271-274, Piscataway, New Jersey, USA, 2008.
- [138] Z. Yong, M. Otsubo, and C. Honda, "Degradation of polymeric materials exposed to corona discharges", *Polym. Test.*, vol. 25, pp. 313-317, 2006.
- [139] Z. Yong, K. Haji, M. Otsubo, and C. Honda, "Surface degradation of silicone rubber exposed to corona discharge", *IEEE Trans. Plasma Sci.*, vol. 34, pp. 1094-1098, 2006.
- [140] M. A. Handala and O. Lamrous, "Surface degradation of styrene acrylonitrile exposed to corona discharge", *Europe. Trans. Electr. Power*, vol. 18, pp. 494-505, 2008.
- [141] Y. Liang, L. J. Ding, C. R. Li, K. Yang, and Y. P. Tu, "A method to detect the deterioration of HTV silicone rubber under corona discharge", *Proc. IEEE Conf. Electr. Insul. Dielectr. Phenom. (CEIDP)*, pp. 509-512, Piscataway, New Jersey, USA, 2006.
- [142] American Society for Testing and Materials, Standard test method for rubber deterioration - surface ozone cracking in a chamber (ASTM D1149-99).
- [143] Deutsches Institut für Normung, Prüfung von kautschuk und elastomerenbestimmung der beständigkeit gegen rissbildung unter ozonwirkung-

- teil 2: Referenz- verfahren zur bestimmung der ozonkonzentration in prüfkammern (DIN 53509-2, in German), 1994.
- [144] Deutsches Institut für Normung, Prüfung von kautschuk und elastomeren- bestimmung der beständigkeit gegen rissbildung unter ozoneinwirkung- teil 1: statische beanspruchung (DIN 53509-1, in German), 2001.
- [145] International Organization for Standardization, Rubber, vulcanized or thermoplastic - Resistance to ozone cracking - Part 1: Static strain test (ISO 1431-1), 1989.
- [146] International Organization for Standardization, Rubber, vulcanized or thermoplastic - Resistance to ozone cracking - Part 2: Dynamic strain test (ISO 1431-2), 1994.
- [147] International Organization for Standardization, Rubber, vulcanized or thermoplastic - Resistance to ozone cracking - Part 3: Reference and alternative methods for determining the ozone concentration in laboratory test chambers (ISO 1431-3), 2000.
- [148] Druzik, J. R., "Ozone: the intractable problem", Waac News Letter, pp. 3-9, 1985.
- [149] R. P. Brown, T. Butler and S. W. Hawley, *Ageing of rubber- accelerated weathering and ozone test results*. Rapra Technology Limited, United Kingdom, 2001.
- [150] *KITAGAWA Gas Detector Tube System Handbook*. Tokyo Japan: Komyo Rikagaku Kogyo K. K., 2008.
- [151] N. G. Trinh, "Partial discharge XX. Partial discharges in air. II. Selection of line conductors", IEEE Electr. Insul. Mag., vol. 11, No. 3, pp. 5-11, 1995.
- [152] W. S. Zaengl, "Dielectric spectroscopy in time and frequency domain for HV power equipment. I. Theoretical considerations", IEEE Electr. Insul. Mag., vol. 19, pp. 5-19, 2003.
- [153] W. S. Zaengl, "Applications of dielectric spectroscopy in time and frequency domain for HV power equipment," IEEE Electr. Insul. Mag., vol. 19, pp. 9-22, 2003.
- [154] A. Rakowska and K. Hajdrowski, "Influence of different test conditions on volume resistivity of polymeric insulated cables and polyethylene samples", Proc. Int. Conf. Dielectr. Mater. Meas. Appl., pp. 281-284, Edinburgh, UK, 2000.
- [155] A. K. Jonscher, *Dielectric Relaxation in Solids*. 2nd ed., Chelsea Dielectrics Press Limited, London, UK, 1996.

Bibliography

- [156] J. L. Koenig, *Spectroscopy of Polymers*. 2nd ed., Elsevier Science Inc., New York, USA, 1999.
- [157] R. S. Gorur, G. G. Karady, A. Jagota, M. Shah, and A. M. Yates, "Aging in silicone rubber used for outdoor insulation", *IEEE Trans. Power Del.*, vol. 7, pp. 525-538, 1992.
- [158] S. H. Kim, E. A. Cherney, and R. Hackam, "Effect of dry band arcing on the surface of RTV silicone rubber coatings", *Proc. IEEE Int. Symp. Electr. Insul. (ISEI)*, pp. 237-240, Baltimore, Maryland, USA, 1992.
- [159] F. Garbassi, M. Morra, and E. Occhiello, *Polymer surfaces, from physics to technology*. J. Wiley & Sons, West Sussex, England, 1998.
- [160] G. Beamson and D. Briggs, *High Resolution XPS of Organic Polymers: The Scienta ESCA300 Database*. Wiley, Chichester, 1992.
- [161] C. E. Carraher, *Polymer Chemistry*. 6th ed., Marcel Dekker Inc, New York, USA, 2003.
- [162] S. Wu, *Polymer Interface and Adhesion*. M. Dekker Inc., 1982.
- [163] C. L. Kahongo, D. Banda, "Testing resistance to corona – effect of corona discharges on silicone rubber and ethylene vinyl acetate", M.S. thesis, Department of Materials and Manufacturing Technology, Chalmers University of Technology, Gothenburg, Sweden, 2006.
- [164] M. J. Owen, "Hydrophobicity and recovery of silicone high voltage insulation", *Proc. INMR World Insulator Congress & Exhibition*, pp. 13-24, Barcelona, Spain, 1999.
- [165] C. Pusineri, A. Pouchelon, B. Jung, J. Heiman, C. Basire, and P. Peccoux, "LSR-RTV2 what is the difference?" *Proc. INMR World Insulator Congress & Exhibition*, Shanghai, China, 2001.
- [166] H. Hillborg, M. Sandelin, and U. W. Gedde, "Hydrophobic recovery of polydimethylsiloxane after exposure to partial discharges as a function of crosslink density", *Polymer*, vol. 42, pp. 7349-7362, 2001.
- [167] Bin Ma, Stanislaw M. Gubanski, Andrej Krivda, Lars E. Schmidt, and Rebecca Hollertz, "Dielectric properties and resistance to corona and ozone of epoxy compositions filled with micro- and nano-fillers", *Proc. IEEE Conf. Electr. Insul. Dielectr. Phenom. (CEIDP)*, paper 7B-4, Virginia Beach, USA, 2009.
- [168] R. Sanctuary, J. Baller, J. K. Krüger, D. Schaefer, R. Bactavatchalou, B. Wetzel, W. Possart, and P. Alnot, "Complex specific heat capacity of two nanocomposite systems", *Thermochimica Acta*, vol. 445, pp. 111-115, 2006.

Appendix A: Abbreviations

Abbreviations appeared in the *Bibliography* are not included in the list below.

- Conferences and organizations

ASTM American Society for Testing and Materials

CEIDP Conference on Electrical Insulation and Dielectric Phenomena

INMR Insulator News and Market Report

ISH International Symposium on High Voltage Engineering

ISO International Standards Organization

NORD-IS Nordic Insulation Symposium

- Relevant to high voltage techniques

DAQ Data Acquisition

FEM Finite Element Method

HVDC High Voltage Direct Current

LI Lightning Impulse

PD Partial Discharge

RRT Round Robin Test

UHV Ultra High Voltage

UV Ultraviolet

- Relevant to materials

ATH Aluminum Trihydrate

EP Epoxy

Appendix A: Abbreviations

EPDM	Ethylene Propylene Diene Monomer
EPR	Ethylene Propylene Rubber
ESP	Mixture of Ethylene Propylene and Silicone Polymers
EVA	Ethylene Vinyl Acetate
FRP	Fiberglass Reinforced Plastic
HTV	High Temperature Vulcanized
LS	Layered Silicate
LMW	Low Molecular Weight
LSR	Liquid Silicone Rubber
NCI	Non-ceramic Insulator
NMMC	Nano- and Micro-filler Mixture Composite
ODMS	Oligomeric Dimethylsiloxane
PDMS	Polydimethylsiloxane
PTFE	Polytetrafluoroethylene/Teflon
RTV	Room Temperature Vulcanized
SIR	Silicone Rubber

- Relevant to material characterization methodologies

ATR	Attenuated Total Reflection
CCD	Charge Coupled Device
DR	Dielectric Response
EDX	Energy Disperse X-ray Analyses
ESCA	Electron Spectroscopy for Chemical Analyses
FTIR	Fourier Transform Infrared Spectroscopy
SEM	Scanning Electron Microscopy
TSC	Thermally Stimulated Current
XPS	X-ray Photoelectron Spectroscopy

Appendix B: Charging currents for nano-PDMS samples

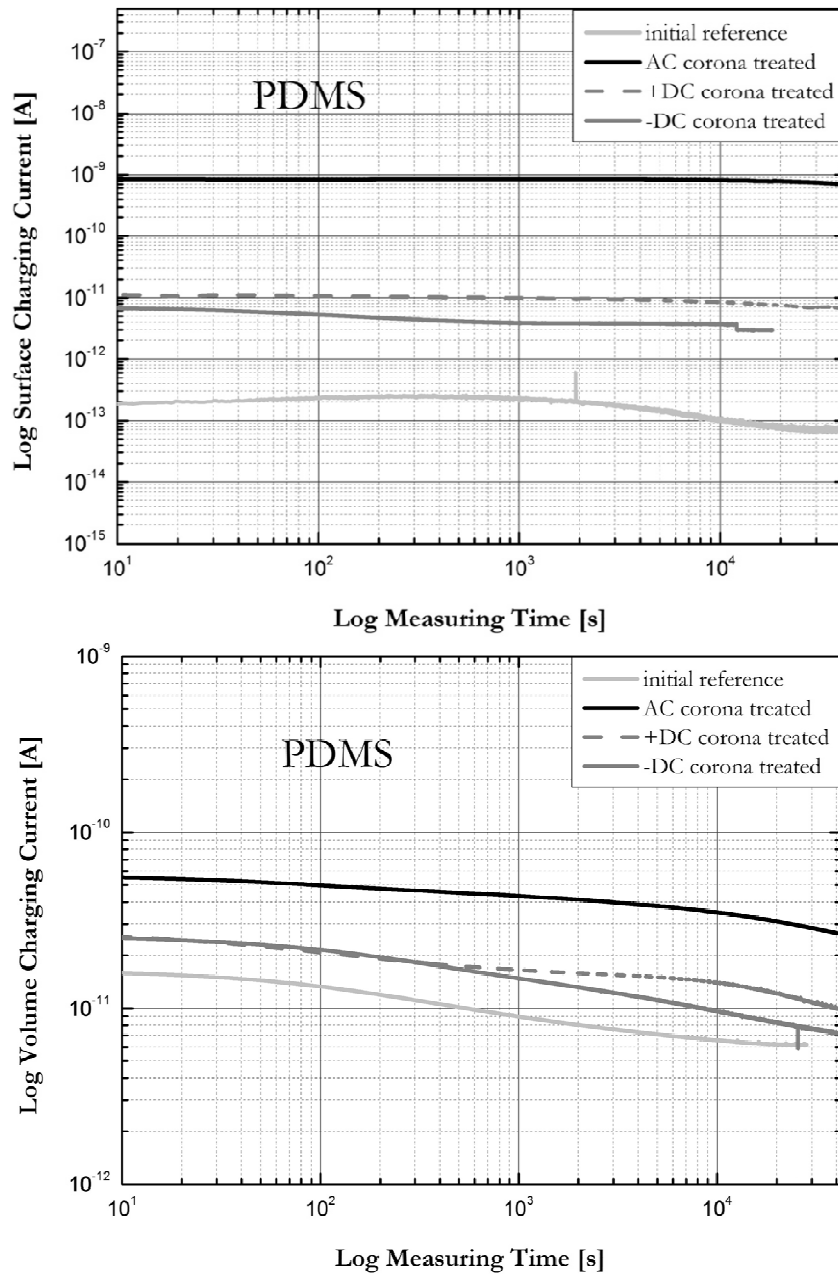


Figure 1: Surface (top) and volume (below) charging currents for the model PDMS samples without nano-silica filled before and after 100 h lasting AC/DC corona/ozone treatments.

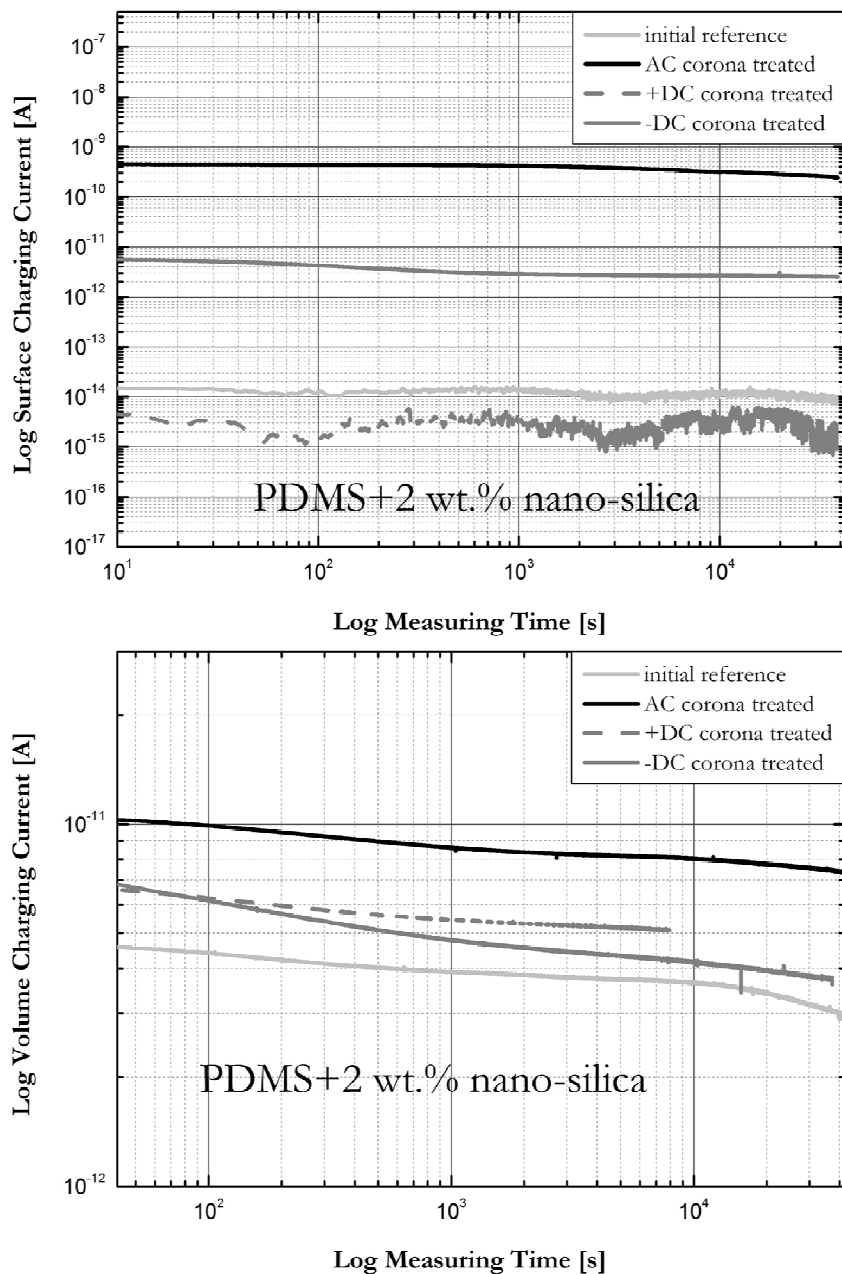


Figure 2: Surface (top) and volume (below) charging currents for the model PDMS samples filled with 2 wt.% nano-silica before and after 100 h lasting AC/DC corona/ozone treatments.

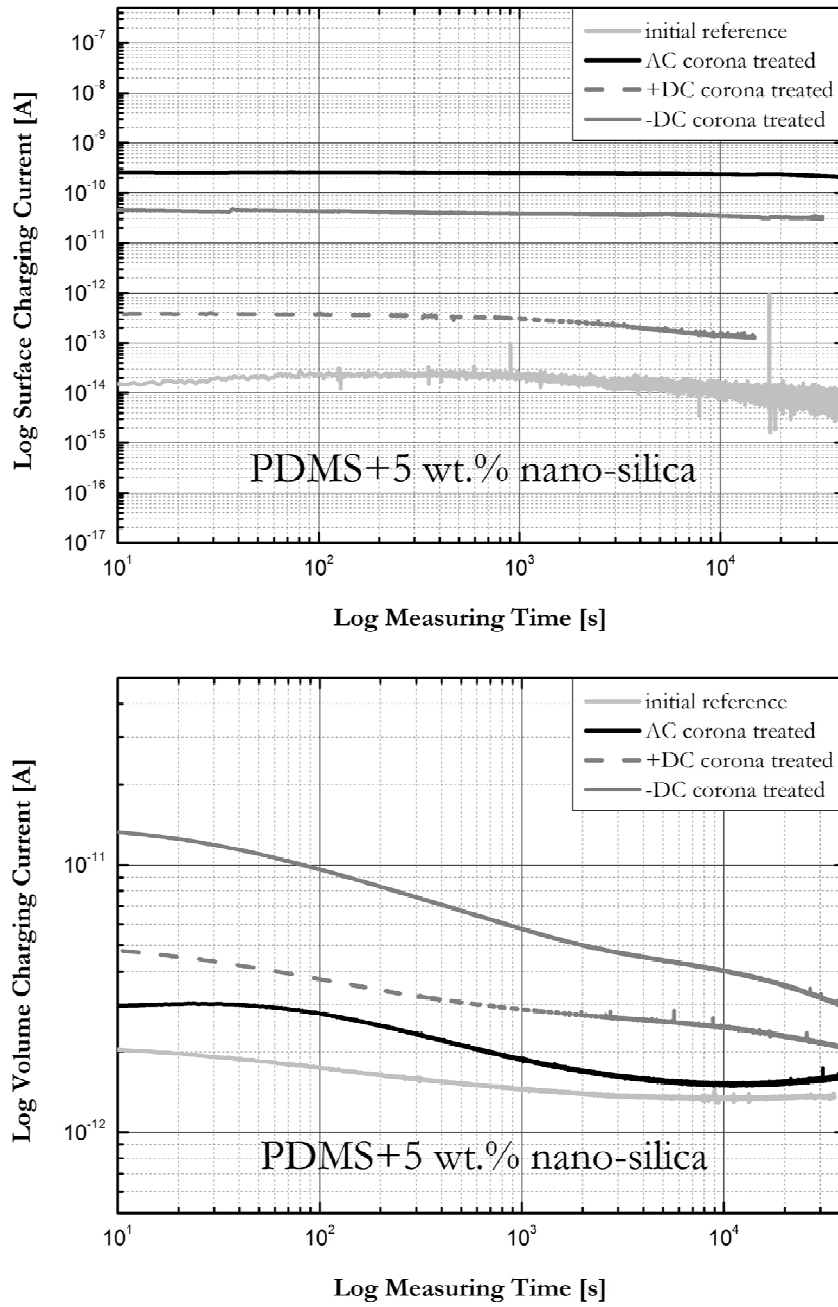


Figure 3: Surface (top) and volume (below) charging currents for the model PDMS samples filled with 5 wt.% nano-silica before and after 100 h lasting AC/DC corona/ozone treatments.

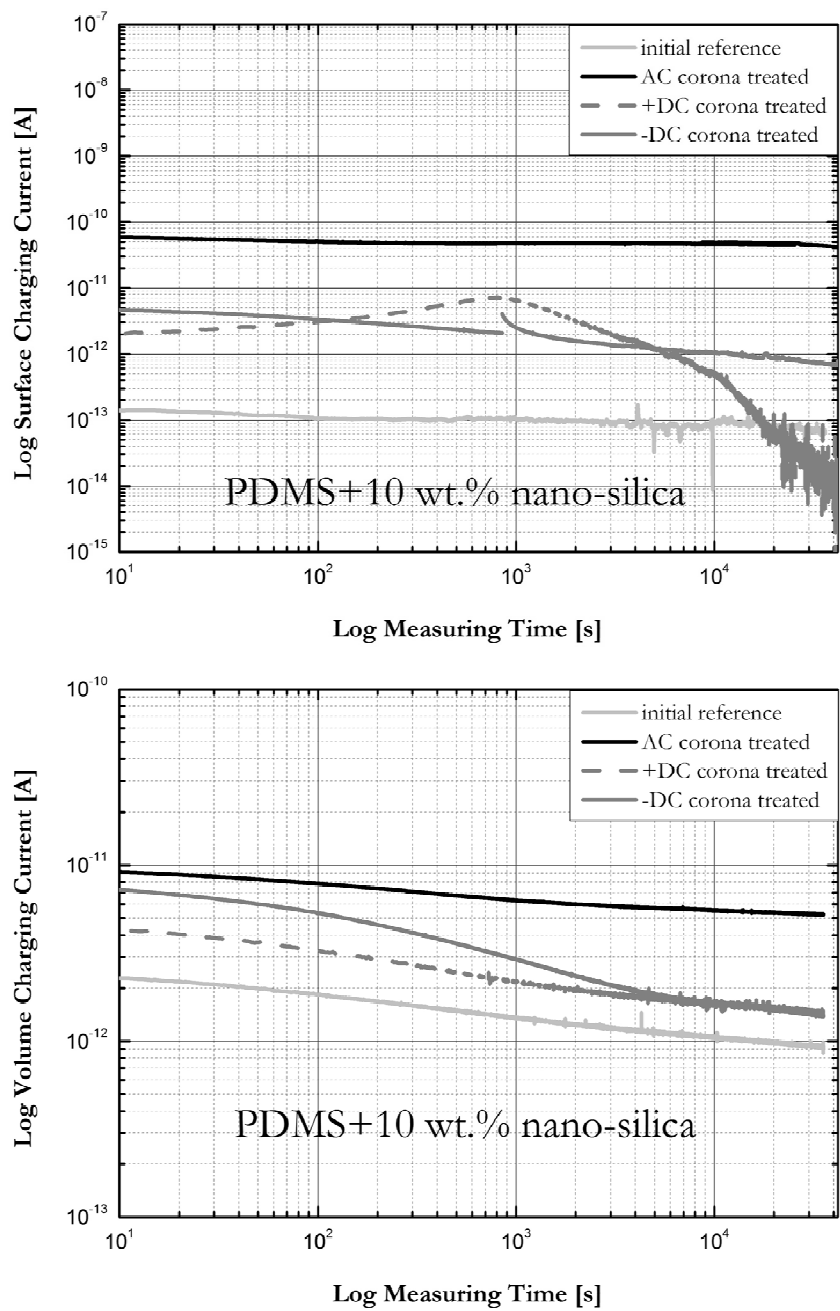


Figure 4: Surface (top) and volume (below) charging currents for the model PDMS samples filled with 10 wt.% nano-silica before and after 100 h lasting AC/DC corona/ozone treatments.

